ABSTRACT

Title of Dissertation:	TISSUE ADHESIVE, SPRAYABLE POLYMER BLENDS AS ADJUVANT SURGICAL TOOLS
	Metecan Erdi, Doctor of Philosophy, 2022
Dissertation directed by:	Professor Peter Kofinas, Chemical and Biomolecular Engineering

Commercial materials deployed in surgery for treatment of high-impact clinical pathologies suffer from shortcomings stemming from a combination of poor mechanical properties, difficulty in precise application, and non-specific prevention mechanisms. Work in this dissertation seeks to counteract these concerns through a multitude of blending approaches with biodegradable polymers and therapeutic agents for improved outcomes following traumatic tissue injury. The polymer blends were spray deposited using solution blow spinning, a method of fiber production where material rapidly accumulates onto target tissue substrate and forms a stable interface.

The first thrust of this dissertation hones on deposition of a biocompatible, wet tissue adhesive. These tissue adhesives were fabricated through molecular weight ratio blends of poly(lactide-co-caprolactone) (PLCL), a synthetic, biodegradable copolymer with viscoelastic properties fostering pressure-dependent adhesion. High molecular weight PLCL endowed the composite material with rigidity and inherent cohesive strength, while low molecular weight PLCL induced spreadability

and adhesive strength. Such optimized material behavior presented an ability to not only adhere to hydrophilic surfaces, but also demonstrated an ability to act as a media for biocompatible and complete wound healing. Efficacy as an adhesive in wound dressings was exhibited through spray deposition of blend adhesives to bandage substrates in a porcine partial thickness burn wound model and comparison with a poly(urethane)-based clinical control material.

The second thrust of this dissertation focuses on development of an effectively applied barrier material for prevention of post-operative fibrotic scar tissue termed as adhesions. Rapid generation of tissue-conformal polymer fibers through solution blow spinning yields a material that is inherently flexible, thereby counteracting the brittle architecture of a sheet-like film currently deployed in surgery. Prevention of asymmetric fibrosis was accomplished through tuned surface biodegradation via high and low molecular weight PLCL blends. This strategy seeks to physically prevent prolonged retention of adhesion-generating molecules at the site of injury, as well as biologically counteract underlying inflammatory processes through controlled release of a therapeutic, apolipoprotein mimetic peptide from composite PLCL fiber mat. Adhesion prevention efficacy was qualified in high impact pre-clinical mouse models of cecal ligation and cecal anastomosis, and compared to pre-fabricated, dried hydrogel barrier and aqueous therapeutic suspension controls. Both adhesion severity and resultant wound healing response were significantly improved versus no treatment and clinically adopted controls.

TISSUE ADHESIVE, SPRAYABLE POLYMER BLENDS AS ADJUVANT SURGICAL TOOLS

by

Metecan Erdi

Dissertation submitted to the Faculty of the Graduate School of the
University of Maryland, College Park, in partial fulfillment
of the requirements for the degree of
Doctor of Philosophy
2022

Advisory Committee:
Professor Peter Kofinas, Chair
Associate Professor Giuliano Scarcelli, Dean's Representative
Professor Srinivasa Raghavan
Associate Professor Amy Karlsson
Assistant Professor Hannah Zierden

Dedication

To my parents and family, thank you for always supporting me regardless of time and place.

To my friends from UMD, from fantasy football, from BIOE basketball, I would not have been able to do this without you.

To Jennifer, thank you for always being my rock and knowing all there is about adhesions.

Acknowledgements

Peter’s guidance and never-ending support over the past 7 years has been nothing short of the best. He has placed a great deal of trust in me and instilled a sense of confident research independence in his mentorship, one that I hope to carry in my pursuit of an academic career. Without him, I would not have become the researcher and person I am today and will be in the years to come. The Kofinas Lab has provided me with tremendous graduate student mentors in John, Leo, and Matthew when I was an undergraduate student working in the lab, who have each excelled in their careers. I have immense gratitude for John’s work on solution blow spinning and help in passing on the torch and guiding my research visions. I am grateful to call him not only my workplace proximity associate, but also lifelong friend.

I have been supported by amazing members of the Kofinas Lab in Kyle and Rebecca through hours of help and collaborative discussions. I had the fortune of working with Manogna and Chris, I am immensely grateful for the significant contributions they made to my dissertation.

None of the work in my Ph.D. would be possible without the never-ending levels of support from our longstanding collaborators at Sheikh Zayed Institute for Pediatric Surgical Innovation in the Children's National Medical Center in Washington, D.C. Dr. Anthony D. Sandler has provided me with the best mentorship and clinical insight that anyone could have asked for. Without him and the collaborative effort from those in Dr. Selim Rozyyev and Dr. Michele S. Saruwatari, translating a material vision to a

clinically impactful product would not be possible. The assistance of those in the Sandler Lab in Dr. Priya Srinivasan and Dr. Lung W. Lau was something I will never cease to be grateful for.

I would also like to thank and acknowledge the support of my committee members in providing feedback on the work in my Ph.D.

Manuscript Collaborator Contributions

Research is an endeavor of continued collaboration rather than individual effort. I am forever indebted to those who made these manuscripts possible. My advisor Dr. Peter Kofinas guided my research visions and consistently taught me the value in eruditely conveying all aspects of my Ph.D. work in both written and oral format. Dr. John L. Daristotle provided me with never-ending teachings on all aspects of blow spinning polymer fiber mats and subsequent material characterization techniques, and mentorship on manuscript publishing.

Shadden T. Zaki and Manogna Balabhadrapatruni performed mass loss degradation and mechanical testing experiments in Chapter 3 and Chapter 4. Christopher Acha performed burst pressure and drug release experiments in Chapter 5. Rheology data in Chapter 5 was made by possible by Dr. Srinivasa R. Raghavan, who graciously allowed us to use his rheometer, and initial training on the instrument supervised by Dr. Sai Nikhil Subraveti.

Our collaborators at Children's National Medical Center in Dr. Anthony D. Sandler, Dr. Selim Rozyyev, Dr. Michele S. Saruwatari, and Dr. Lung W. Lau made this work clinically relevant and impactful through porcine wound healing and mouse peritoneal adhesion models studied in Chapter 3, Chapter 4, and Chapter 5.

Chapter 2

Title:

"Polymer nanomaterials for use as adjuvant surgical tools"

Authors:

Metecan Erdi, Anthony D. Sandler, Peter Kofinas

Journal:

WIREs Nanomedicine and Nanobiotechnology

Status:

Under Review

Contributions:

Writing – original draft (M.E.)
Writing – review and editing (M.E., A.D.S., P.K.)
Conceptualization (M.E., A.D.S., P.K.)
Investigation (M.E.)
Supervision (A.D.S., P.K.)

Chapter 3

Title:

"Biodegradable, Tissue Adhesive Polyester Blends for Safe, Complete Wound Healing"

Authors:

John L. Daristotle*, Metecan Erdi*, Lung W. Lau, Shadden T. Zaki, Priya Srinivasan, Manogna Balabhadrapatruni, Omar B. Ayyub, Anthony D. Sandler, Peter Kofinas

Journal:

ACS Biomaterials Science and Engineering

Status:

Published (7 (8), 3908-3916. DOI: 10.1021/acsbiomaterials.1c00865)

Contributions:

Writing – original draft (J.L.D., M.E.)
Writing – review and editing (J.L.D., M.E., A.D.S., P.K.)
Conceptualization (J.L.D., L.W.L., O.B.A, A.D.S., P.K.)
Data curation (J.L.D., M.E.)
Formal analysis (J.L.D., M.E.)
Validation (J.L.D., L.W.L.)
Visualization (J.L.D., M.E., O.B.A.)
Investigation (J.L.D., M.E., L.W.L., S.T.Z., P.S., M.B.)
Methodology (J.L.D., M.E., L.W.L., O.B.A., A.D.S., P.K.)
Resources (A.D.S., P.K.)
Supervision (A.D.S., P.K.)
Funding acquisition (J.L.D., A.D.S., P.K.)
Project administration (A.D.S., P.K.)

Adapted Acknowledgements[1]:

The authors acknowledge the support of the Maryland NanoCenter, the AIMLab, the Functional Macromolecular Laboratory, and the Sheikh Zayed Institute for Pediatric Surgical Innovation. Research reported in this publication was supported by the National Institute of Biomedical Imaging and Bioengineering of the National Institutes of Health under Award Number R01EB019963. J.L.D. was supported by the National Institute of Biomedical Imaging and Bioengineering of the National Institutes of Health under Award Number F31EB025735. The content is solely the responsibility of the authors and does not necessarily represent the official views of the National Institutes of Health. S.T.Z. received support from the UMD ASPIRE program.

Chapter 4

Title:

"Sprayable tissue adhesive with biodegradation tuned for prevention of postoperative abdominal adhesions"

Authors:

Metecan Erdi, Selim Rozyyev, Manogna Balabhadrapatruni, Michele S. Saruwatari, John L. Daristotle, Omar B. Ayyub, Anthony D. Sandler, Peter Kofinas

Journal:

Bioengineering and Translational Medicine

Status:

Published (e10335. DOI:10.1002/btm2.10335)

Contributions:

Writing – original draft (M.E.)
Writing – review and editing (M.E., M.S.S., J.L.D., A.D.S., P.K.)
Conceptualization (M.E., S.R., J.L.D., O.B.A, A.D.S., P.K.)
Data curation (M.E., S.R., O.B.A., A.D.S., P.K.)
Formal analysis (M.E., S.R., M.B., M.S.S.)
Validation (M.E., S.R., M.S.S., A.D.S, P.K.)
Visualization (M.E., S.R., M.S.S., J.L.D., O.B.A., A.D.S., P.K.)
Investigation (M.E., S.R., M.B., M.S.S.)
Methodology (M.E., S.R., M.B., A.D.S., P.K.)
Resources (A.D.S., P.K.)
Supervision (A.D.S., P.K.)
Funding acquisition (A.D.S., P.K.)
Project administration (O.B.A., A.D.S., P.K.)

Adapted Acknowledgements[2]:

We acknowledge the support of the Maryland NanoCenter, the Robert E. Fischell Institute for Biomedical Devices, the Functional Macromolecular Laboratory, and the Sheikh Zayed Institute for Pediatric Surgical Innovation. The authors would also like to thank Dr. Leopoldo Torres Jr. for their insight and thoughtful discussions into this work. Research reported in this publication was supported by the National Institute of Biomedical Imaging and

Bioengineering of the National Institutes of Health under Award Number R01EB019963. The content is solely the responsibility of the authors and does not necessarily represent the official views of the National Institutes of Health.

Chapter 5

Title:

"Biodegradation Driven Release of a Therapeutic Peptide in Sprayable Surgical Sealant for Prevention of Postoperative Abdominal Adhesions"

Authors:

Metecan Erdi, Michele S. Saruwatari, Selim Rozyyev, Christopher Acha, Omar B. Ayyub, Anthony D. Sandler, Peter Kofinas

Journal:

Advanced Healthcare Materials

Status:

Under Review

Contributions:

Writing – original draft (M.E.)
Writing – review and editing (M.E., M.S.S., A.D.S., P.K.)
Conceptualization (M.E., O.B.A, A.D.S., P.K.)
Data curation (M.E., M.S.S., C.A., O.B.A., A.D.S., P.K.)
Formal analysis (M.E., M.S.S., S.R.)
Validation (M.E., M.S.S., S.R.)
Visualization (M.E., M.S.S., S.R., C.A., O.B.A., A.D.S., P.K.)
Investigation (M.E., M.S.S., C.A., S.R.)
Methodology (M.E., M.S.S., C.A., A.D.S., P.K.)
Resources (A.D.S., P.K.)
Supervision (A.D.S., P.K.)
Funding acquisition (M.E., A.D.S., P.K.)
Project administration (O.B.A., A.D.S., P.K.)

Acknowledgements:

We acknowledge the support of the Maryland NanoCenter, the Robert E. Fischell Institute for Biomedical Devices, the Functional Macromolecular Laboratory, and the Sheikh Zayed Institute for Pediatric Surgical Innovation. The authors would also like to thank Dr. John L. Daristotle for their insight and thoughtful discussions into this work. We thank Dr. Srinivasa Raghavan for allowing us the use of the rheometer in his lab and Dr. Nikhil Subraveti from this lab for assistance with the rheological measurements. Research reported in this publication was supported by the National Institute of General Medical Sciences of the National Institutes of Health under Award Number R01GM141132. M.E. was supported by the National Institute of Diabetes and Digestive and Kidney Diseases of the National Institutes of Health under Award Number F31DK129021. The content is solely the responsibility of the authors and does not necessarily represent the official views of the National Institutes of Health.

Table of Contents

List of Tables

List of Figures

Chapter 1: Introduction

Investigation of polymer biomaterials derived from clinical need, especially those targeting surgical applications, and their sequential translation the focus of this dissertation. Our lab has developed innovative approaches in this regard through direct in situ deposition of biodegradable polymer scaffolds via a technique known as solution blow spinning. To this end we have published numerous research articles that improve upon a widely employed surgical product, as well as address material phenomena with a high potential for future in vivo applications.

Currently, conformal bandages used exclusively in the clinic are coated with a synthetically derived adhesive, where the mechanism of adherence is facilitated by compressive pressure application. Though they effectively adhere to skin, pressure sensitive adhesives are not only non-degradable, but also often strip the wound of newly healed tissue. Hence, we explored use of molecular weight blends of a biodegradable polymer in poly(lactide-co-caprolactone) (PLCL) as to create a viscoelastic material sensitive to pressure in a bandage adhesive application. Results from this project showed that our synthesized material dramatically improved tissue adhesive properties on both dry and wet tissue surfaces.

The second focus of this dissertation focuses on controlling inflammatory behavior of fibrous adhesions generated post-surgery via therapeutic release. Efficacy concerns in widely available clinical materials are highlighted by poor mechanical properties and difficulty in precise application to an injured tissue surface in vivo. Due to its surface

eroding nature, a select PLCL blends prove to be an advantageous tool in physically preventing prolonged adherence of fibro- and angio- genic constituents implicated in adhesions formation, but also controlled release of an anti-inflammatory agent. Work in this dissertation successfully tune degradation kinetics to that of adhesions formation and quantify mechanical properties of PLCL blends as to create an effective adhesion barrier. In vitro studies demonstrate that inclusion a particular PLCL blend yields a polymer scaffold with steady degradation and improved wet tissue adhesive strength versus other blend and neat PLCL compositions. In high impact clinical models, select PLCL blend significantly reduces abdominal adhesions severity versus both no treatment and clinically treated controls.

Chapter 2: Polymer nanomaterials for use as adjuvant surgical tools

2.1 Introduction

Materials employed in the treatment of conditions encountered in surgical and clinical practice frequently face barriers in translation to application. Shortcomings can be generalized through their reduced mechanical stability, difficulty in handling, and inability to conform or adhere to complex tissue surfaces. To overcome an amalgam of challenges, research has sought utilization of polymer-derived nanomaterials deposited in various fashions and formulations to improve application and outcomes of surgical and clinical interventions. Applications of particular interest include topical wound dressings, tissue adhesives, surgical sealants, hemostats, and adhesion barriers, all of which have displayed potential to act as superior alternatives to current materials and clinical procedures. In this review, emphasis will be placed not only on applications, but also on various design strategies employed in fabrication. This review is designed to provide a broad and thought-provoking understanding of nanomaterials for use as effective surgical tools.

Conventional materials deployed in surgery for treatment of clinical pathologies suffer from a combination of inferior mechanical properties, difficult handling, and poor biocompatibility. These material shortcomings lead to decreased treatment efficacy and poor outcomes in wound dressings (**Figure 2.1A**), tissue adhesives (**Figure 2.1B**),

surgical sealants (**Figure 2.1C**), hemostats (**Figure 2.1D**), and post-operative mesothelial tissue injury (**Figure 2.1E**).

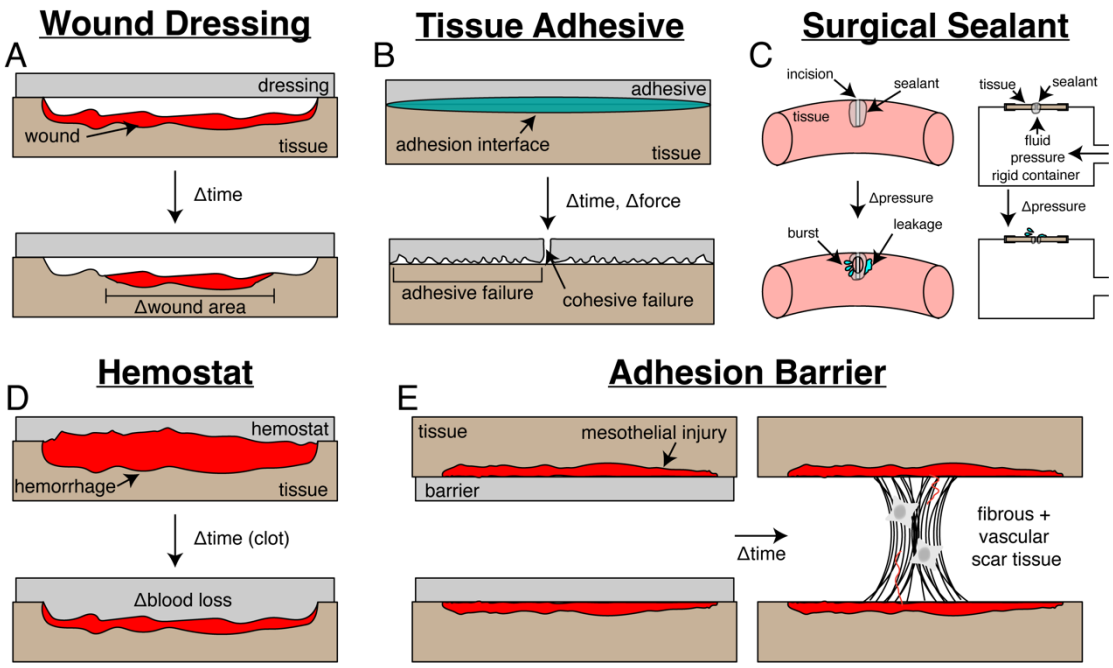

Figure 2.1. Schematic of intended function, metrics for clinical assessment, and failure modes for materials deployed in surgery.
(A) Wound dressings often encounter minimal shrinkage of damaged tissue as quantified via epidermal wound closure. (B) Tissue adhesives fail due to a combination of bulk and interfacial modes as assessed via adhesion strength. (C) Surgical sealants are ineffective if low burst pressure values are presented in sealing of a defect. (d) Hemostats have limited utility if long clotting times and significant blood loss is encountered. (E) Adhesion barrier failure leads to post-operative scar tissue formation that can be quantified via a scoring rubric.

Novel research nanomaterial approaches in the treatment of multiple clinical conditions are often polymer fibers or swellable polymer networks. Use of solution blow spinning as a means for deposition of fibers through pressure driven airbrush flow of a polymer solution has been developed in the Medeiros, Kofinas, and Sandler research groups.[3,4] This potentially allows for simple deposition of polymer fiber mats with nanoscale diameter (80 – 1000nm) and porosities (~1000nm) for a multitude of surgical applications (**Figure 2.2A**). Electrospinning is an additional method for deposition of

similar nanoscale fibers (90 – 1000nm diameter), which in contrast to a simple airbrush setup, necessitates an electrically conductive substrate, an electric field with polarizing current, 10 times slower deposition times, and dissolution of polymer in toxic solvent (**Figure 2.2B**).[4–7]. Hydrogels are polymer networks with nanometer scale pores (~100nm) that swell with water in aqueous environments within tissue, thereby preventing dehydration and accelerating the rate of fibrogenesis and angiogenesis (**Figure 2.2C**).[8] Sealing of a tissue site via a hydrogel also presents a diffusion limitation to external pathogen transport to site of injury, thereby reducing risk of infection as compared to dry materials.[9,10] However, hydrogel-based systems present subpar mechanical behavior. They are usually brittle and tend to swell rapidly when excess fluid is present. Fabrication complexities highlight further translational barriers of applying hydrogels in surgery, such as 1) requiring a dual barrel syringe injection approach in which pre-polymer solution is mixed at a tip with a crosslinking initiator or 2) benchtop solution casting and molding for a specific clinical application. This review will compile research on nanomaterials utilized in combating the shortcomings of clinical, tissue adhesive materials used in surgery, while also highlighting their respective modes of application.

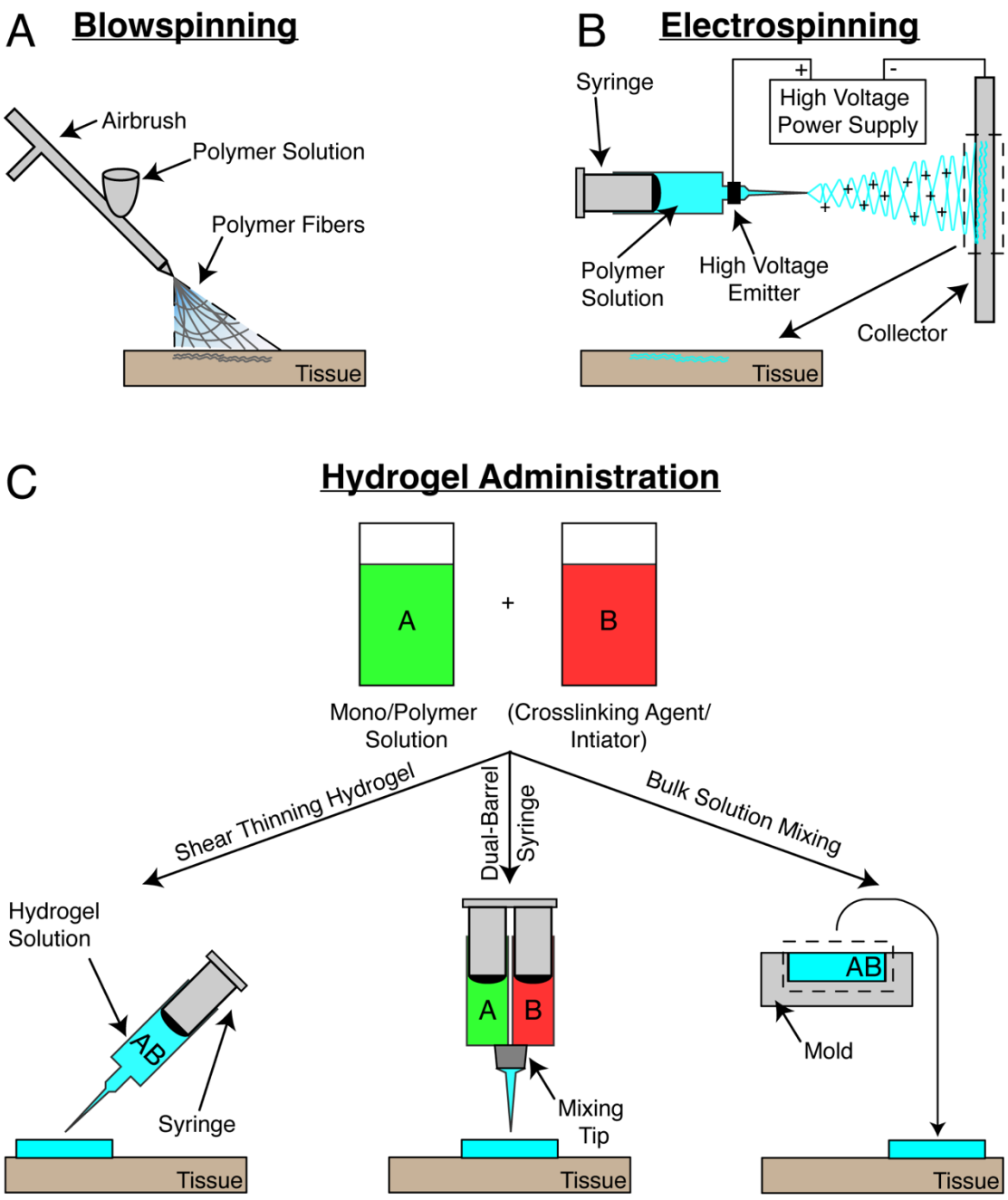

Figure 2.2. Schematic of application approaches for nanomaterials used in surgery.
(A) Solution blow spinning employs pressure driven flow through a nozzle to generate a collection of fibers with nanoscale diameter and porosity. (B) Electrospinning utilizes a high voltage current and conductive substrate to deposit a nanofiber mat onto a collector and harvested for application to tissue. (C) Hydrogels are synthesized through either combination of a monomer solution with crosslinking agents and initiators or a standalone, neat polymer solution. Injectable hydrogels are ones that display shear thinning behavior and can be injected through a syringe (left). Non-injectable solutions are either mixed in an attached tip of a dual-barrel syringe (middle) or are mixed as bulk solutions in a mold (right) that are then formed for specific application.

2.2 Wound Dressings

Wounds from burns or trauma account for approximately 1.2 million hospital admissions each year, with resultant infections presenting a 75% risk of mortality if left untreated.[11] The high mortality and infection rates underscore the inability of current materials to facilitate biocompatible and effective wound healing, as they fail to create the ideal environment sealed off from potential infectious agents and fluid loss. Examples of prefabricated poly(urethane) film (Tegaderm) and poly(urethane) foam (Mepilex) dressings frequently deployed in wound care are coated with an acrylic adhesive layer that is non-degradable, and thereby cannot remain indefinitely at the point of application. Both materials are non-conformal to nanoscale tissue topography, irregular in shape and depth, and frequently detach from their applied substrate. This necessitates either repeated dressing replacements that disrupt the continuous wound healing process or additional modes of fixation to tissue. Hence, a combination of non-degradability and subpar mechanical properties in current commercial dressings implores exploration of novel research materials. Clinically relevant materials will be ones with an optimized balance between biodegradation rate, epidermal tissue adherence, and mode of administration.

Translationally effective wound dressings should be inherently robust, yet flexible and adhesive, and contain materials with rapid deposition times to the site of injury *in situ*. This milieu of properties aids in the promotion of angio- and fibro- genesis in wound models of various depths. A common and relevant metric studied in wound healing is the measurement of epidermal wound closure assessed either through top-down images

of wounds or histological cross sections sampled over a clinical time course (**Figure 2.1A**).

Table 2.1. Select fibrous and hydrogel-based nanomaterials employed as wound dressings in surgery.

Composition	Architecture	Mode of Administration	Animal Model, Wound Type	Skin Wound Closure (control vs. test)	Refs.
Poly(lactic-co-glycolic acid) and poly(ethylene glycol)	*Fiber*	*Blowspinning*	*Pig, partial thickness*	*100% vs. 80% (t=7d)*	[12]
Poly(lactide-co-caprolactone)	*Fiber*	*Blowspinning*	*Pig, partial thickness*	*100% vs. 80% (t=7d)*	[1]
Chitosan-poly(vinyl alcohol)-zinc oxide	Fiber	Electrospinning	Rabbit, full thickness	38% vs. 100% (t=12d)	[13]
L-nitroarginine polyester amide with Pluronic F127 and Tegaderm	Hydrogel	Prefabricated	Rat, full thickness	40% vs. 80% (t=7d)	[14]
Chitosan loaded with rose bengal, poly(pyrrole), poly(vinyl alcohol)	Hydrogel	Prefabricated	Rat, partial thickness	15% vs. 40% (t=8d)	[15]
Gelatin/dopamine	Hydrogel	Injection	Mouse, full thickness	40% vs. 80% (t=7d)	[16]
Poly(dopamine)–poly(acrylamide)	Hydrogel	Prefabricated	Mouse, full thickness	10% vs. 50% (t=5d)	[17]

Research performed by Kofinas and Sandler groups have been italicized.

Blowspun burn wound dressings developed by Behrens et al. and Daristotle et al. deposited a blend of poly(lactic-co-glycolic acid) and poly(ethylene glycol), that upon warming up to body temperature at 37°C, induces adhesion to epidermal tissue due to melting of the poly(ethylene glycol) plasticizer within the poly(lactic-co-glycolic acid) matrix.[12,18] An additional application by Daristotle et al. employed the same technology in a viscoelastic blend of poly(lactide-co-caprolactone) as to create a biocompatible bandage adhesive with pressure dependent adhesive properties.[1] Prefabricated

electrospun fiber mats are a popular dressing medium due to the porous and rigid structure of the resultant nanomaterial. Ahmed et al. explored electrospun chitosan-poly(vinyl alcohol)-zinc oxide fibers in a rabbit model, displaying marked success in epidermal skin wound closure versus clinical control.[13] This is due in large part to the presence of chitosan, a naturally occurring biopolymer that harbors great biocompatibility, antimicrobial properties, and ability to facilitate fibroblast proliferation as a result of biodegradation products. While these technologies employ mechanisms of biocompatible, non-toxic adhesive curing and porous fiber mats allowing for oxygen permeation, both classes of nanofiber mats could benefit from an aqueous environment native to tissue.[19–24]

While the inability for rapid, in situ fabricated, hydrogel-derived, dressing material presents a practical disadvantage, such systems are a popular research material as wound healing mediums due to an aqueous environment adept to wound healing. He at al. explored use of an amino acid-derived inhibitor of nitric oxide to lower the inflammatory response and promote collagen regeneration.[14] Although this presents a promising biological pathway to improving wound healing efficacy, such a material is notably prefabricated and requires a secondary, clinical polyurethane control (Tegaderm) to secure it at the site of injury and facilitate a critical moist environment. Wang et al. also embodies a similar, therapeutic approach through loading of chitosan microspheres with poly(pyrrole) and rose bengal — a staining compound explored as a treatment for skin conditions — as to promote recruitment of angiogenic growth factors and antibacterial activity.[15] Translation concerns are highlighted not only

through their manufacturing technique, but also the necessity of an additional visible light and near infrared light curing step as to induce antibacterial activity of loaded compounds. With inspiration derived from underwater mussel foot protein adhesion, dopamine containing hydrogels present a novel bioinspired pathway to improving tissue adhesion and retention at the site of application for wound healing materials. While dopamine does encourage nanoscale, non-covalent interactions with substrates, its binding interaction is intrinsically rigid on its own and thereby necessitates blending of additional support structures such as those explored by Huang et al. , Han et al., and others.[16,17,23,25–31] Delineation of chemically-derived dopamine adhesion versus physically-derived hydrogel adhesion could be better highlighted to elucidate novelty, while in addition supporting structures with improved flexibility. Several other hydrogel incorporating strategies have been explored, but present lesser success in epidermal skin wound closure versus control than those mentioned.[32–50]

Table 2.2. Supplementary fibrous and hydrogel-based nanomaterials employed as wound dressings in surgery.

Composition	**Architecture**	**Mode of Administration**	**Animal Model, Wound Type**	**Skin Wound Closure (control vs. test)**	**Refs.**
Chitosan-poly(ethylene oxide)-teicoplanin	Fiber	Electrospinning	Rat, full-thickness	93% vs. 100% (t=14d)	[19]
ECM-related protein Olfactomedinlike	Fiber	Electrospinning	Mouse, full thickness	70% vs. 75% (t=6d)	[20]
Silk fibroin	Fiber	Electrospinning	Rat, full thickness	10% vs. 20%(t=7d)	[21]
Chitosan and poly(ethylene oxide) with vascular endothelial growth factor and platelet-derived growth factor	Fiber	Electrospinning	Rat, full thickness	0% vs. 30% (t=7d)	[22]

Gelatin methacryloyl with fatty acids/aspirin, encapsulated poly(dopamine)	Hydrogel	Electrospinning	Mouse, full thickness	45% vs. 80% (t=7d)	[23]
Gelatin methacryloyl	Fiber	Electrospinning	Mouse, full thickness	60% vs. 80% (t=14d)	[24]
Dopamine methacrylamide and sodium tetraborate decahydrate with silver nanoparticles	Hydrogel	Injection	Rat, full thickness	23% vs. 50% (t=10d)	[26]
Gelatin-grafted-dopamine and poly(dopamine)-coated carbon nanotubes	Hydrogel	Injection	Mouse, full thickness	60% vs. 80% (t=7d)	[27]
Catechol modified methacryloyl chitosan	Hydrogel	Injection	Mouse, full thickness	60% vs. 85% (t=7d)	[28]
Cross-linked poly(glycerol sebacate)-co-poly(ethylene glycol)-g-catechol and ureido-pyrimidinone modified gelatin	Hydrogel	Injection	Rat, full thickness	95% vs. 100% (t=10d)	[29]
Dopamine-grafted oxidized sodium alginate and poly(acrylamide)	Hydrogel	Prefabricated	Rat, full-thickness	10% vs. 20% (t=5d)	[30]
Poly(dopamine) nanoparticles with poly (N-isopropylacrylamide) and loaded endothelial growth factor	Hydrogel	Prefabricated	Rat, full thickness	50% vs. 65% (t=9d)	[31]
Poly(N-isopropyl acrylamide) and alginate with silver nanoparticles	Hydrogel	Prefabricated	Mouse, full-thickness	40% vs. 60% (t=7d)	[32]
Benzaldehyde-terminated poly(ethylene glycol) and dodecyl-modified chitosan with vascular endothelial growth factor	Hydrogel	Injection	Mouse, full-thickness	60% vs. 80% (t=7d)	[33]
Methacrylamide dopamine and 2-(dimethylamino)ethyl methacrylate with chitosan	Hydrogel	Injection	Rabbit, full thickness	20% vs. 50% (t=7d)	[34]
Multi-armed poly(ethylene glycol)-	Hydrogel	Injection	Mouse, full thickness	20% vs. 40% (t=7d)	[35]

vinyl sulfone with RGD peptide and FXIIIa coagulant					
N-carboxyethyl chitosan and benzaldehyde-terminated Pluronic F127/carbon nanotubes	Hydrogel	Injection	Injection	70% vs. 85%(t=7d)	[36]
Quaternized chitosan-tannic acid-ferric iron	Hydrogel	Injection	Mouse, full thickness	40% vs. 70% (t=7d)	[37]
Functionalized quaternized chitosan-gelatin methacrylate-graphene oxide	Hydrogel	Injection	Mouse, full thickness	60% vs. 75% (t=7d)	[38]
j-carrageenan polysaccharide loaded with nanosilicates	Hydrogel	Injection	In vitro scratch assay	30% vs. 90% (t=36h)	[39]
Sodium alginate/graphene oxide/poly(vinyl alcohol)	Hydrogel	Prefabricated	Mice, full-thickness	65% vs. 70% (t=10d)	[40]
Quaternized chitosan and benzaldehyde-terminated Pluronic®F127	Hydrogel	Injection	Mouse, full thickness	80% vs. 90% (t=10d)	[41]
Sodium alginate-chitosan-poly(acrylamide)	Hydrogel	Injection	Mouse, full thickness	60% vs. 60% (t=7d)	[42]
Collagen-hyaluronic acid	Hydrogel	Injection	Mouse, full thickness	70% vs. 85% (t=7d)	[43]
Quaternized chitosan-g-polyaniline and benzaldehyde functionalized poly(ethylene glycol)-co-poly(glycerol sebacate)	Hydrogel	Injection	Mouse, full thickness	80% vs. 85% (t=10d)	[44]
Dual-crosslinked chitosan via trans-cyclooctene/tetrazine and four arm poly(ethylene glycol)	Hydrogel	Injection	Mouse, full thickness	62% vs. 85% (t=7d)	[45]
Aminoethyl methacrylate hyaluronic acid and methacrylated methoxy poly(ethylene glycol), chlorhexidine diacetate-loaded nanogels	Hydrogel	Injection	Mouse, full thickness	35% vs. 70% (t=7d)	[46]
Carboxymethyl chitosan and	Hydrogel	Injection	Mouse, partial thickness	30% vs. 80% (t=7d)	[47]

dialdehyde-modified cellulose nanocrystal					
Hyaluronic acid-graft-dopamine and reduced graphene oxide	Hydrogel	Injection	Mouse, full thickness	40% vs. 80% (t=7d)	[48]
Silver/zinc oxide loaded chitosan	Hydrogel	Prefabricated	Mouse, partial thickness	40% vs. 100% (t=7d)	[49]
Poly(ε-caprolactone-co-lactide)-b-poly(ethylene glycol)-b-poly(ε-caprolactone-co-lactide) with gelatin	Hydrogel	Injection	Mouse, full thickness	40% vs. 90% (t=7d)	[50]

2.3 Tissue Adhesives

Polymeric tissue adhesives currently deployed in surgery include acrylate and poly(ethylene glycol) (PEG) based materials. n-Butyl cyanoacrylate (ex. Histoacryl) and 2-Octyl cyanoacrylate (ex. Dermabond) are commonly employed chemistries of topical adhesives.[51] These materials are presented as a liquid that polymerize in the presence of water to form a "glue" and adhere to applied tissue substrates.[52] Non-degradability of acrylate-based adhesives present toxicity concerns, largely restricting them to topical application on skin, where even then cases of allergic contact dermatitis and stripping of healthy skin during healing are presented.[53–55] An additional class of synthetic tissue adhesives constructed with PEG presents a non-toxic and biocompatible alternative to acrylate-based materials.[56] However, a high degree of swelling and utilization of ultraviolet light-initiated polymerization to interface with tissue highlight drawbacks of PEG-based tissue adhesives. Coupled with poor cohesive strength, researched tissue adhesives need to explore an approach that optimize a synergy of administration in surgical settings, and mechanical properties of both cohesion and adhesion (**Figure 2.1B**).

Table 2.3. Select fibrous and hydrogel-based nanomaterials employed as tissue adhesives in surgery.

Composition	Architecture	Mode of Administration	Ex Vivo Tissue Type Used	Adhesion Strength (kPa)	Refs.
Poly(lactide-co-caprolactone)	*Fiber*	*Blowspinning*	*Pig skin*	*10*	[1]
Poly(lactide-co-caprolactone)	*Fiber*	*Blowspinning*	*Pig skin / pig intestine*	*10 / 10*	[2]
Poly(lactide-co-caprolactone)	*Fiber*	*Blowspinning*	*Pig aorta*	*30*	[57]
Poly(dopamine) nanoparticles with poly (N-isopropylacrylamide) and loaded endothelial growth factor	Hydrogel	Prefabricated	Pig skin	85	[31]
Mussel adhesive protein-hyaluronic acid shell with silk fibroin core	Needle patch	Prefabricated	Pig skin / pig intestine	125 / 105	[58]
Four armed poly(ethylene glycol)-N-Hydroxysuccinimide ester	Hydrogel (glue)	Injection	Pig skin	175	[59]
Multi armed poly(caprolactone)-N-Hydroxysuccinimide ester	Hydrogel (glue)	Prefabricated	Rat skin	100	[60]
Gelatin/chitosan and crosslinked poly(acrylic acid) grafted with N-hydrosuccinimide ester	Hydrogel	Prefabricated	Pig skin / pig intestine / pig aorta	120 / 100 / 100	[61]

Research performed by Kofinas and Sandler groups have been italicized.

A candidate tissue adhesive for surgery needs be easily applied, present minimal toxicity concerns, and exhibit a combination of high adhesive strength and cohesive strength as to reduce risk of failure. Deposition of tissue adhesive nanofiber mats has been explored by Kofinas and Sandler through solution blow spinning. Behrens et al. and Daristotle et al. devised an inventive method of adhesive curing through simple melting of PEG at body temperature within a PLGA matrix, while Daristotle et al. and

Erdi et al. employed polymer viscoelasticity as to create a pressure sensitive tissue adhesive. [1,2,18,57] Both are non-toxic adhesive curing approaches employing fundamental material phenomena and present appreciable adhesion to various *ex vivo* tissue surfaces in the range of 10 - 30 kPa. Adhesion to tissue through solely physical interactions — namely short-range, nanoscale Van der Waals and hydrogen bonding — limits the adhesion strength.[62–64] Specific nanoscale chemical interactions rather than macroscopic, physical polymer entanglements with tissue could prove to be an optimal method for generating adhesion.

Hydrogel systems with added chemical moieties designed to interact with functional groups expressed on tissue present an intriguing route to biocompatible tissue adhesion. Bioinspired approaches are highlighted through physical and chemical binding of mussel adhesive proteins to terminal amine and oxygen-containing residues expressed on both internal, mesothelial tissue and external, epidermal tissue.[65,66] Han et al. introduced poly(dopamine) nanoparticles into a thermally-reversible, self-healing poly (N-isopropylacrylamide) hydrogel matrix and provided for excellent adhesion to pig skin (~85 kPa).[31] A multi-step synthesis that includes an additional soaking of their hydrogel in a poly(dopamine) nanoparticle suspension and thereby diminishes the practical value of their material in surgical settings. A patch application studied by Jeon et al. uses a mussel adhesive protein hydrogel coating on silk-based microneedles.[58] While significant adhesion strength is presented on both dry pig skin (~125 kPa) and pig intestine (~105 kPa), similar concerns are expressed. However, reduced cohesive

strength (i.e. brittleness) and specificity of chemical interactions contributing to adhesion is of note in mussel inspired materials.[17,27–30,48,67–74]

N-hydrosuccinimide (NHS) ester chemistry is a widely employed technique for hydrogel synthesis.[75] This is due to simple carbodiimide activation of carboxylate molecules that then readily react with primary amine groups and form stable amide bonds. However, prevalence of amine groups expressed on various tissue also presents an opportunity to couple covalently with an NHS ester functionalized material. Kelmansky et al. (~175 kPa on pig skin) and Zhang et al. (~100 kPa on rat skin) each deploy a singular approach to generating tissue adhesion through use of NHS ester functionalized polymers as injectable glues.[59,60] Yuk et al. employs a two-factor approach in generating tissue adhesion through grafting of NHS onto poly(acrylic acid) (PAA) in a biopolymer composite hydrogel of gelatin and chitosan supported by a poly(ethylene) backing as to create a "tape-like" material.[61] The studied hydrogel system facilitates rapid hydration and swelling — effectively drying wet tissue surfaces — while also providing for a baseline level of cohesive strength. Reactivity of NHS ester with primary amine groups contained in protein structures on the dried tissue provides for improved adhesive strength. A combination of unique cohesive and adhesive strength inducing mechanisms thereby yields high levels of tissue adhesion (120 kPa / 100 kPa / 100 kPa) on a multitude of ex vivo pig tissue substrates (skin / intestine / aorta). Both glue and complex hydrogel systems generate significantly improved levels of tissue adhesion as compared to previously described neat fiber and hydrogel systems. However, such approaches are not inherently biocompatible or

inherently translatable for clinical application. It is known that unreacted carbodiimide used in NHS activation presents concentration-dependent toxicity to collagen scaffolds containing fibroblasts and keratinocytes.[76,77] Glue systems by Kelmansky et al. and Zhang et al. present diminished levels of cohesive strength critical for extensive, internal in vivo implantation. In the tape system by Yuk et al., an extensive fabrication and application process involving ultraviolet curing of their composite hydrogel, deposition onto a backing layer, storage under desiccation, and sequential peeling of backing layer upon application reduces its clinical translatability. Similar concerns are expressed in other materials approaches deriving tissue adhesion via NHS ester chemistry.[78–80]

Other neat and combinatorial hydrogel systems that employ neither bioinspired mussel adhesion nor NHS ester chemistry have been explored, but only present moderate increase in adhesion strength, as some were not necessarily designed to act as an effective tissue adhesive in surgery.[81–95] The collection of these nanomaterials similarly present translational barriers of prefabrication, brittle mechanical properties, or toxicity of unreacted hydrogel synthesis components.

Table 2.4. Supplementary fibrous and hydrogel-based nanomaterials employed as tissue adhesives in surgery.

Composition	Architecture	Mode of Administration	Ex Vivo Tissue Type Used	Adhesion Strength (kPa)	Refs.
Poly(dopamine)–poly(acrylamide)	Hydrogel	Prefabricated	Human skin (self, in vivo)	17	[17]

Gelatin-grafted-dopamine and poly(dopamine)-coated carbon nanotubes	Hydrogel	Injection	Pig skin	6	[27]
Catechol modified methacryloyl chitosan	Hydrogel	Injection	Pig skin	18	[28]
Cross-linked poly(glycerol sebacate)-co-poly(ethylene glycol)-g-catechol and ureido-pyrimidinone modified gelatin	Hydrogel	Injection	Pig skin	5	[29]
Dopamine-grafted oxidized sodium alginate and poly(acrylamide)	Hydrogel	Prefabricated	Pig skin	6	[30]
N-carboxyethyl chitosan and benzaldehyde-terminated Pluronic F127/carbon nanotubes	Hydrogel	Injection	Pig skin	8	[36]
Quaternized chitosan-tannic acid-ferric iron	Hydrogel	Injection	Pig skin	70	[37]
Quaternized chitosan and benzaldehyde-terminated Pluronic®F127	Hydrogel	Injection	Pig skin	6	[41]
Sodium alginate-chitosan-poly(acrylamide)	Hydrogel	Injection	Pig skin	15	[42]
Quaternized chitosan-g-polyaniline and benzaldehyde functionalized poly(ethylene glycol)-co-poly(glycerol sebacate)	Hydrogel	Injection	Pig skin	5	[44]
Dual-crosslinked chitosan via trans-cyclooctene/tetrazine and four armed poly(ethylene glycol)	Hydrogel	Injection	Pig skin	16	[45]
Hyaluronic acid-graft-dopamine and reduced graphene oxide	Hydrogel	Injection	Pig skin	5	[48]
Poly(ε-caprolactone-co-lactide)-b-poly(ethylene glycol)-b-poly(ε-caprolactone-co-lactide) with gelatin	Hydrogel	Injection	Rat skin	100	[50]
Poly(γ-glutamic acid) and dopamine	Hydrogel	Injection	Pig skin	50	[67]
Dopamine conjugated gelatin macromer	Hydrogel	Prefabricated	Pig skin	25	[68]
Poly(dopamine)−chondroitin sulfate−poly(acrylamide)	Hydrogel	Prefabricated	Pig skin	20	[69]
Poly(acrylic acid)−poly(acrylamide)−poly(dopamine) with poly(N-isopropylacrylamide)	Hydrogel	Prefabricated	Hog skin	12	[70]
Dopamine-modified four-armed poly(ethylene glycol) with Laponite nanosilicate	Hydrogel	Injection	Pig aorta	8	[71]
Poly(ethylene glycol) diacrylate with dopamine and silica nanoparticles	Hydrogel	Prefabricated	Cow aorta	4.5	[72]
Quaternized chitosan-poly(dopamine)	Hydrogel	Prefabricated	Mice liver	24	[73]
Poly(dopamine)−sodium alginate−polyacrylamide	Hydrogel	Prefabricated	Pig skin	25	[74]
Hyperbranched poly(ethylene glycol)-poly(ester)	Hydrogel	Prefabricated	Pig skin /	40 / 60	[78]

			pig aorta		
Eight arm poly(ethylene glycol)-N-hydrosuccinimide ester and tannic acid	Hydrogel	Injection	Pig skin	50	[79]
Four arm poly(ethylene glycol)-N-hydrosuccinimide ester	Hydrogel	Injection	Pig skin	20	[80]
Poly(glycerol sebacate)-acrylate and alginate nanoparticles	Hydrogel (glue)	Injection	Pig aorta	15	[81]
Poly(allylamine)−hydrocaffeic acid with catechol and Laponite	Hydrogel	Injection	Pig skin	17	[82]
Poly(glycerol sebacate acrylate)	Hydrogel	Prefabricated	Cow aorta / pig intestine	12.5 / 10	[83]
Corticosteroid-modified gelatin particles	Particle suspension	Dropwise	Pig intestine	8	[84]
Hydroxyapatite with poly(dimethylacrylamide)	Hydrogel	Prefabricated	Mouse skin	42	[85]
Antimicrobial peptide in gelatin methacryloyl	Hydrogel	Injection	Pig gingiva	55	[86]
Gelatin	Hydrogel	Prefabricated	Pig skin	90	[86]
Poly(diolcitrate) with poly(methyl methacrylate)	Hydrogel	Prefabricated	Pig skin	70	[87]
Gelatin and chondroitin sulfate	Hydrogel	Injection	Pig skin	30	[88]
Methacryloyl-substituted tropoelastin	Hydrogel	Prefabricated	Pig skin / rat artery	75 / 60	[89]
Poly(acrylamide-methyl acrylate-acrylic acid)	Hydrogel	Prefabricated	Pig intestine	8	[90]
Gelatin methacryloyl	Hydrogel	Injection	Pig skin	45	[91]
Hydrocaffeic acid-modified chitosan with chitosan lactate	Hydrogel	Injection	Pig skin	8	[92]
Gelatin methacryloyl with N-(2-aminoethyl)−4-(4-(hydroxymethyl)−2-methoxy-5-nitrosophenoxy) butanamide with hyaluronic acid	Hydrogel	Injection	Pig intestine	40	[93]
3,4-dihydroxy-L-phenylalanine and hyaluronic acid	Hydrogel	Injection	Pig skin / rat bladder	120 / 140	[94]
Silk fibroin with tannic acid	Hydrogel	Prefabricated	Pig skin / pig aorta	125 / 85	[95]

2.4 Surgical Sealants

Clinically adopted surgical sealants include fibrin (ex. TISSEEL) and PEG based (ex. CoSeal) materials. However, neither formulation is effective in preventing leakage due to a combination of their method of application or weak adhesion to tissue. Fibrin glues are a cocktail of quickly clotting blood proteins (fibrinogen, thrombin, etc.), but are expensive — as components need to be isolated from autologous or donor sources — and are complex to deploy.[96–98] PEG based sealants that employ reactive NHS ester chemistry as to interface with tissue are prevalent in the clinic, but require extensive preparation and present high degrees of swelling leading to injury of surrounding structures. Extraneous sutures and staples are common non-biomaterial approaches in preventing leakage but can be intensive processes that rely upon natural fibrosis to seal off affected segments of tissue. Such shortcomings have led to research into biocompatible, resourceful, and effective surgical sealant approaches (**Figure 2.1C**).

Table 2.5. Select fibrous and hydrogel-based nanomaterials employed as surgical sealants.

Composition	**Architecture**	**Mode of Administration**	**Ex Vivo Tissue Type Used**	**Burst Pressure (kPa)**	**Refs.**
Poly(lactide-co-caprolactone)	*Fiber*	*Blowspinning*	*Pig intestine*	*40*	*57*
Poly(lactic-co-glycolic acid)/poly(ethylene glycol)	*Fiber*	*Blowspinning*	*Mouse intestine*	*9*	18,99
Poly(lactic-co-glycolic acid)/poly(ethylene glycol)/silica	*Fiber*	*Blowspinning*	*Pig intestine*	*19*	*100*
Chitosan film with transglutaminase enzyme	Film	Prefabricated	Collagen membrane / pig intestine	7 / 125	101
Gelatin	Hydrogel	Prefabricated	Pig intestine	60	86

Gelatin and chondroitin sulfate	Hydrogel	Injection	Pig skin	35	[88]
Four arm poly(ethylene glycol)-N-hydrosuccinimide ester	Hydrogel (glue)	Injection	Pig vein	40	[80]
Gelatin methacryloyl with N-(2-aminoethyl)−4-(4-(hydroxymethyl)−2-methoxy-5-nitrosophenoxy) butanamide with hyaluronic acid	Hydrogel	Injection	Pig intestine	40	[93]

Research performed by Kofinas and Sandler groups have been italicized.

Polymer nanofiber mats deposited via solution blow spinning (SBS) are a facile method for generating a surgical sealant that overcomes translational barriers of conventional materials. In investigations by the Kofinas and Sandler research groups, Behrens et al. and Kern et al. utilize this technology in creation of a PLGA and PEG composite fiber mat with body temperature mediated adhesion.[18,99] Such an approach provides for a combination of adhesive strength via melting of PEG within a cohesive rigid PLGA matrix and thus yields an appreciable burst pressure (~ 9kPa). Further improvements in burst pressure strength via SBS via incorporation of aggregating, hemostatic silica nanoparticles by Daristotle et al. was investigated.[100] Mechanically rigid nanoparticles improve properties of cohesion, leading to a markedly higher burst pressure (~19 kPa). In a separate investigation, Daristotle et al. studied ratio blends of low and high molecular weight poly(lactide-co-caprolactone) (PLCL).[57] Adhesive strength and tissue spreadability is induced via liquid-like low molecular weight chains able to form interfacial physical bonds with tissue at the nanoscale, while cohesion strength is provided by solid-like, high molecular weight constituents. Despite being designed to act as a biodegradable tissue adhesive, burst pressure values were the highest here as

compared to the group's previous investigations (~40 kPa). Variable ratios and molecular weights could be further explored to increase burst pressure and tune to *in vivo* sealant applications.

Novel hydrogel architectures present a promising pathway for development of surgical sealant nanomaterials. Blending of biocompatible chitosan with a microbial enzyme by Fernandez et al. aims to overcome poor tissue adhesiveness in neat chitosan materials.[101] While a high burst pressure (~125 kPa) is achieved on a clinically relevant pig intestine, spray deposition of enzyme catalyzed chitosan via a double cannister spray device necessitated a 5-minute adhesive curing period that would not lend itself well to fast-paced operating conditions. Other chitosan-based sealant systems present a combination of moderate burst pressure due to inherent brittleness of chitosan in addition to clinical translation difficulties.[92,102] Shirzaei Sani et al. and Zhou et al. both synthesize hydrogels derived from gelatin — a naturally occurring biopolymer in connective tissue — and present moderately high pressures in pig intestine (~60 kPa) and pig skin (~35 kPa), respectively.[86,88] The initial system proposed necessities a visible-light adhesive curing of a prepolymer solution containing methacrylic anhydride that if left unreacted reacts exothermally with water. Burst pressure as tested by the authors employs a modified setup with stainless steel plates and air driven flow, similar to that proposed in Figure 1C, and thereby fails to directly mirror aqueous conditions and water driven flow in intestinal systems. The former scheme necessitates a 20-minute self-crosslinking step following injection of prepolymer solution, thereby diminishing clinical applicability. Hong et al. investigates a gelatin-hyaluronic acid

derived system that necessitates a toxic, ultraviolet light source for *in situ* gelation at incision site on pig intestine (~40 kPa), while Bu et al. employs use of PEG-NHS ester chemistry that requires a 5-minute gelation period prior to testing and aforementioned concerns of concentration-dependent toxicity and dual-syringe injection.[80,93] Other gelatin [91,103], NHS ester [59,79,104], and blended hydrogel [58,89,90,105] systems have been studied as surgical sealant materials, yet they present moderate burst pressure values and encounter great concerns stemming from their prefabricated form.

Table 2.6. Supplementary fibrous and hydrogel-based nanomaterials employed as surgical sealants.

Composition	Architecture	Mode of Administration	Ex Vivo Tissue Type Used	Burst Pressure (kPa)	Refs.
Hydrocaffeic acid-modified chitosan with chitosan lactate	Hydrogel	Injection	Pig intestine	10	[92]
Chitosan-catechol	Film	Prefabricated	Rat intestine	27	[102]
Gelatin methacryloyl	Hydrogel	Injection	Collagen membrane / rat lung	15 / 6	[91]
Hyaluronic acid/gelatin	Hydrogel	Injection	Dog intestine	20	[103]
Four arm poly(ethylene glycol)-N-hydrosuccinimide ester	Hydrogel	Injection	Collagen membrane	9	[59]
Eight arm poly(ethylene glycol)-N-hydrosuccinimide ester and tannic acid	Hydrogel	Injection	Pig artery	24	[79]
Four armed poly(ethylene glycol)-poly(lactic-co-glycolic acid)-N-Hydroxysuccinimide ester	Hydrogel (glue)	Injection	Collagen membrane	13	[104]
Mussel adhesive protein-hyaluronic acid shell with silk fibroin core	Needle patch	Prefabricated	Pig intestine	13	[58]
Methacryloyl-substituted tropoelastin	Hydrogel	Prefabricated	Collagen membrane / rat lung / pig lung	12 / 6 / 3	[89]

Poly(acrylamide-methyl acrylate-acrylic acid)	Hydrogel	Prefabricated	Pig intestine	13	[90]
Agarose−ethylenediamine conjugate and dialdehyde-functionalized poly(ethylene glycol)	Hydrogel	Prefabricated	Pig skin	16	[105]

2.5 Hemostats

Effective hemostatic materials are those that present an ability to absorb blood and prevent blood loss at sites of epithelial tissue injury (laceration, amputation, puncture, etc.) (**Figure 2.1D**). Failure of current materials to treat hemorrhage accounts for 33% of all traumatic deaths in controlled clinical settings, whilst also accounting for nearly 90% of deaths in the military sector.[106,107] Fibrin based glues (ex. TISSEEL) currently deployed in the clinic are expensive and are often dependent on patient blood composition to induce coagulation, hence their approval namely as adjuncts in surgery.[96] Biologically derived hemostats approved for use in the clinic are frequently biopolymer (ex. Angio-Seal) or protein (ex. ProGel) based hydrogel materials restricted to use in select clinical pathologies.[108,109] Though effective in certain instances, there exists a need to further improve range of applicability and time-dependent coagulation of hemostatic materials.

Table 2.7. Select fibrous and hydrogel-based nanomaterials deployed as hemostats in surgery.

Composition	Architecture	Mode of Administration	Animal Model - Blood Loss	Blood Loss (control vs. test)	Clotting Time - Model	Clotting Time (control vs. test)	Refs.
N-(3-aminopropyl)methacrylamide	*Hydrogel particles*	*Prefabricated*	*Rat liver puncture / rat tail amputation*	*500 mg vs. 200 mg / 3 g vs. 500 mg*	*Rat liver puncture / rat tail amputation*	*1.5 min vs. 0.25 min / 18 min vs. 5 min*	*110*
Zeolite-loaded alginate-chitosan	*Hydrogel particles*	*Prefabricated*	*N/A*	*N/A*	*In vitro whole blood*	*9 min vs. 15 s*	*111*
Poly(lactic-co-glycolic acid)/poly(ethylene glycol)/silica	*Fiber*	*Blowspinning*	*N/A*	*N/A*	*Pig liver laceration*	*4 min vs. 3 min*	*100*
Quaternized chitosan-poly(dopamine)	Hydrogel	Prefabricated	Mouse tail amputation / mouse liver prick / rat liver incision / rabbit liver resection / pig skin laceration	125 mg vs. 10 mg / 500 mg vs. 20 mg / 960 mg vs. 30 mg / 10 g vs. 1 g / 400 mg vs. 30 mg	Mouse tail amputation / mouse liver prick / rat liver incision / rabbit liver resection / pig skin laceration	545 s vs. 80 s / 316 s vs. 20 s / 204 s vs. 60 s / 425 s vs. 200 s / 200 s vs. 50 s	73
Dopamine and antimicrobial peptide modified gelatin methacryloyl with poly(caprolactone) layer	Film	Prefabricated	Mouse skin biopsy / rat liver incision	275 mg vs. 10 mg / 440 mg vs. 50 mg	Mouse skin biopsy / rat liver incision	450 s vs. 200 s / 330 s vs. 60 s	112
Silk fibroin with tannic acid	Hydrogel	Prefabricated	Rat liver puncture	425 mg vs. 40 mg	In vitro whole blood	5.5 min vs. 1 min	95

Agarose−ethylenediamine conjugate and dialdehyde-functionalized poly(ethylene glycol)	Hydrogel	Prefabricated	Rabbit liver incision	700 mg vs. 200 mg	Rabbit liver incision	75 s vs. 10 s	[105]
Chitosan/gelatin composite sponge	Foam	Prefabricated	Rabbit liver puncture / rabbit ear artery puncture	17 g vs. 4 g / 3 g vs. 1 g	Rabbit liver puncture / rabbit ear artery puncture	100 s vs. 40 s / 100 s vs. 50 s	[113]
Poly(dextran aldehyde)	Foam	Prefabricated	Rabbit liver incision / rabbit ear artery incision / rabbit femoral artery incision	1.1 g vs. 0.3g / 7.5 g vs. 0.1 g / 8 g vs. 0.1 g	Rabbit liver incision / rabbit ear artery incision / rabbit femoral artery incision	420 s vs. 240 s / 250 s vs. 50 s / 180 s vs. 120 s	[114]

Research performed by Kofinas and Sandler groups have been italicized.

Early investigations in the Kofinas and Sandler research groups by Behrens et al. and Fathi et al. studied hydrogel particle suspensions of N-(3-aminopropyl)methacrylamide (APM) and zeolite-loaded alginate-chitosan, respectively.[110,111] Both APM and chitosan are charged, cationic materials that aid in the process of hemostasis through activation of the coagulation cascade.[115] Hydrogel swellability in both formulations further augments hemostatic properties through formation of a physical, plug-like barrier. While each displays marked success in reducing clotting time in vitro and in vivo, both are prefabricated via inverse suspension polymerization technique, followed by repeated washing and drying steps, and a 5-minute application process *in vivo*. Deposition of hemostatic material by Daristotle et al. via solution blow spinning counteracts the extensive synthesis process and slow deposition times in both hydrogel particle approaches.[100] A polymer blend of poly(lactic-co-glycolic acid)/poly(ethylene

glycol) with negatively charged silica nanoparticles induces coagulation through a glass effect, whilst also providing for far improved cohesive and adhesive strength via enhanced interfacial interactions with tissue at the nanolevel.[116] However, only a moderate change in coagulation time is achieved in vivo (~3 min) versus clinical control (~4 min). Additional synthetic hydrogels and liquid suspensions have been explored due to their natural swelling ability and sequential formation of a physical barrier to hemostasis, albeit to lesser success versus clinical control in both low and high impact animal models.[87,92,93,103,117–119]

Bioinspired marine mussel adhesion via binding of catechol-containing proteins to amine and oxygen-containing residues on tissue is a prevalent route for generating hemostasis. Formed nanostructures yield strong adhesion in the presence of water and other aqueous media due to the formation of both chemical and physical bonds with substrates.[120] Hence, materials containing catecholic structures (ex: dopamine) provide a pathway to reducing failure of materials in which excess blood is present. Li et al. incorporates poly(dopamine) into naturally hemostatic chitosan as to form a cryogel (i.e. lyophilized hydrogel).[73] Though the material presents ubiquitous applicability to act as a hemostat through testing in various animal models, the extensive prefabrication process and need to use a toxic, strong oxidizing agent ($NaIO_4$) as to generate a poly(dopamine) structure hinders its value in fast-paced surgical settings. Xuan et al. similarly employs use of dopamine-based chemistry in a bilayer nanosheet containing gelatin and poly(caprolactone) (PCL).[112] Gelatin containing dopamine induces hemostatic activity through its combinatorial swelling and wet tissue adhesive

properties, while the PCL layer provides for mechanical robustness. A complex spin coating of the gelatin/dopamine layer containing an oxidizing agent ($CaCl_2$), coupled with both plasma and ultraviolet curing steps, lessens excitement for use in the clinic. Bai et al. adopts a more biocompatible approach through combination of a dopamine analogue in tannic acid within a silk protein.[95] The authors evidence the ability of natural silk fibers to self-assemble into nanostructures through physical interactions and thus contribute to formation of a physical, plug-like bulk structure critical to hemostasis. Though effectively reduced clotting time (~1 min) is presented in a rat liver puncture model versus control (~5.5 min), reliance upon expensive natural silk production and solely tannic acid-tissue interactions for generating adhesion inhibit clinical scalability. Other catechol containing bioinspired hemostats have been explored but are either less effective in reducing blood flow or present translatability concerns.[121]

Porous nanostructures within materials present a physical mechanism to hemostasis through rapid uptake of blood. Zhang et al. implements such an approach through an agarose-poly(ethylene glycol) hydrogel with self-healing properties.[105] However, the use of remnant benzaldehyde in the system to generate adhesion with tissue surface proteins presents toxicity concerns, in addition to its involved synthesis and prefabrication. Synthetic foam sponges such as those made by Lan et al. and Liu et al. accomplish that through chitosan and dextran-based chemistries, respectively.[113,114] The non-biodegradable nature necessitates removal following application at the site of injury, deterring from its use in surgery. Both approaches, in addition to other porous

nanomaterials, could also benefit from testing in larger and more intensive animal models as to qualify hemostatic efficacy.[122–126]

Table 2.8. Supplementary fibrous and hydrogel-based nanomaterials deployed as hemostats in surgery.

Composition	Architecture	Mode of Administration	Animal Model - Blood Loss	Blood Loss (control vs. test)	Clotting Time - Model	Clotting Time (control vs. test)	Refs.
Poly(diolcitrate) with poly(methyl methacrylate)	Hydrogel	Prefabricated	Rat liver puncture	500 mg vs. 200 mg	N/A	N/A	[87]
Hydrocaffeic acid-modified chitosan with chitosan lactate	Hydrogel	Injection	Rat liver incision	375 mg vs. 20 mg	Rat liver incision	120 s vs. 30 s	[92]
Gelatin methacryloyl with N-(2-aminoethyl)−4-(4-(hydroxymethyl)−2-methoxy-5-nitrosophenoxy) butanamide with hyaluronic acid	Hydrogel	Injection	Rabbit liver resection	220 mg vs. 90 mg	N/A	N/A	[93]
Hyaluronic acid/gelatin	Hydrogel	Injection	Rat liver incision	240 mg vs. 100 mg	N/A	N/A	[103]
Poly(2-hydroxyethyl methacrylate)-methacrylic acid N-hydroxysuccinimide ester-fluorescein methacrylate with transglutaminase factor XIIIa	Suspension	Dropwise	N/A	N/A	Rat artery catheter	1 min vs. 0.75 min	[117]
RADA16-I peptide with hyaluronic acid coated gauze	Film	Prefabricated	N/A	N/A	Pig skin 8 mm biopsy	5 min vs. 2 min	[118]
N-(2-hydroxypropyl)-3-trimethylammonium chitosan	Hydrogel	Injection	Rat liver puncture	170 mg vs. 45 mg	N/A	N/A	[119]

chloride and poly(dextran aldehyde)							
Silica nanoparticle coated with poly(dopamine)	Particle suspension	Dropwise	Rat femoral artery incision / rat liver incision	4.5 g vs. 1.25 g / 1 g vs. 0.2 g	Rat femoral artery incision / rat liver incision	250 s vs. 170 s / 120 s vs. 100 s / 140 s vs. 80 s	[121]
Hydrophobically modified chitosan	Foam	Aerosol spray	Rat liver resection	28 mL vs. 9 mL	N/A	N/A	[122]
Collagen sponge with chitosan/calcium pyrophosphate	Foam	Prefabricated	Rabbit artery incision / rat liver resection	1.6 g vs. 1 g / 1.5 g vs. 1 g	Rabbit artery incision / rat liver resection	164 s vs. 135 s / 184 s vs. 106 s	[123]
Poly(caprolactone) foam coated with gelatin	Foam	Electrospinning	N/A	N/A	In vitro human whole blood	100 s vs. 20 s	[124]
Cellulose and chitosan with collagen	Foam	Prefabricated	Rat liver resection	140 mg vs. 60 mg	Rat liver resection	180 s vs. 90 s	[125]
Zeolite chabazite on the cotton fiber surface	Fiber	Prefabricated	Rabbit femoral artery incision	10 g vs. 7 g	Rabbit femoral artery incision	400 s vs. 150 s	[126]

2.6 Adhesion Barriers

Adhesions are rigid, fibrous bands that adjoin tissue surfaces as a result of inflammatory or ischemic conditions following postoperative mesothelial injury (abrasion, ligation, anastomosis, etc.) (**Figure 2.1E**). Studies have shown a 93% occurrence rate following abdominal surgery and complications of small bowel obstruction, chronic pelvic pain and female infertility occur, and accounts for over $2 billion in healthcare costs.[127–130] A dried biopolymer, sheet-like film (Seprafilm) currently deployed in surgery is often described by operators as “brittle” and “sticky”,

thus rendering it difficult to apply and inconsistent in treatment efficacy. Additional conventional strategies include gel-based materials designed to sustain shear forces imparted by the perpetual shifting of organs *in vivo*, as well as dropwise administration (Icodextrin) of anti-inflammatory and hemostatic therapeutics targeting non-physical pathways.[131] Clinical translation of barriers is largely impeded by either their mechanical properties or means of application, while delivery of anti-inflammatory drugs presents issues of controlled release and systemic effects even when topically administered.

Table 2.9. Select fibrous and hydrogel-based nanomaterials deployed as adhesion barriers in surgery.

Composition	**Architecture**	**Mode of Administration**	**Animal Model (Evaluation Time Point)**	**Adhesion Score (control vs. test) (Scale)**	**Refs.**
Poly(lactide-co-caprolactone)	*Fiber*	*Blowspinning*	*Mouse cecal ligation (t=7d)*	*3.5 vs. 2.5 (0 to 5)*	[2]
Poly(ethylene glycol)/poly(caprolactone)	Fiber	Electrospinning	Rabbit tendon anastomosis (t=14d)	3.5 vs. 1 (0 to 5)	[132]
Dodecyl-modified hydroxypropyl methylcellulose with poly(ethylene glycol)-b-poly(lactic acid)	Hydrogel	Injection	Rat cardiac infarct (t=28d) / Rat abdominal wall ligation (t=28d)	4.2 vs. 0.6 (0 to 5) / 3.2 vs. 1.35 (0 to 5)	[133,134]
N,Ocarboxymethyl chitosan and aldehyde hyaluronic acid	Hydrogel	Injection	Rat abdominal wall abrasion (t=7d)	5 vs. 0.3 (0 to 5)	[135]
Poly(ethylene glycol)-block-poly(L-lactide-co-glycolide) with 10-hydroxycamptothecin and diclofenac sodium drugs	Fiber	Electrospinning	Mouse cecal abrasion (t=14d)	2.9 vs. 0.3 (0 to 4)	[136]

Celecoxib-loaded poly(L-lactic acid)-poly(ethylene glycol) and hyaluronic acid	Fiber	Electrospinning	Rabbit tendon anastomosis (t=21d)	4 vs. 1.75 (0 to 5)	[137]

Research performed by Kofinas and Sandler groups have been italicized.

Deposition of polymer fibers presents a unique method of generating tissue adherent scaffolds for use as solid adhesion barriers. In a recently published collaborative investigation by the Kofinas and Sandler research groups, Erdi et al. spray deposited viscoelastic molecular weight blends of poly(lactide-co-caprolactone) (PLCL) via solution blow spinning.[2] Prevention of high grade, rigid scar tissue formation in a mouse cecal ligation model is achieved through a tuned, surface degradation mechanism preventing prolonged adherences of molecules capable of generating adhesions. An alternative method for fiber generation via electrospinning of poly(ethylene glycol)/poly(caprolactone) by Chen et al. generates nanofibrous membranes to prevent adhesion deposition.[132] Here, a porous structure allows for nutrient diffusion whilst inhibiting fibroblast penetration and proliferation yields significantly reduced adhesion severity in a rabbit tendon anastomosis model. Utility of fibrous and electrospun materials in surgical settings, such as long deposition times and a complex setup requiring a conductive substrate in vitro, diminishes their value in operational conditions.[138,139]

Hydrogel based materials aim to prevent adhesion via hydrophilic and lubricious surface properties at the material-tissue interface that inhibit the prolonged adherence of fibro- and angio- genic molecules. Stapleton et al. synthesizes a physical hydrogel through incorporation of poly(ethylene glycol)-b-poly(lactic acid) nanoparticles within

a hydrophobically modified cellulose matrix.[133,134] Traditional hydrogel systems achieve gelation through formation of chemical, static crosslinks via use of a toxic initiator. Here, the authors employ non-covalent entropic and hydrogen bonding nanoscale interactions between particle and hydrogel as to form dynamic crosslinks in a biocompatible manner. Though reduction of scored scar tissue severity is achieved in two separate rat animal models, it is important to consider the brittle and swellable nature of hydrogels once formed. Song et al. alternatively introduces hemostatic chitosan within a hyaluronic acid hydrogel matrix as to induce significant reduction of severe adhesions in a rat abdominal wall abrasion model.[135] The authors here employ a strong oxidizer ($NaIO_4$) and strong acid ($ClCH_2COOH$) in synthesis of each individual component, whilst also taking 66 seconds to fully gelate following subcutaneous injection. In hydrogel focused work by Stapleton et al., Song et al, and others, there exists a potential to fail if injured tissue at the site of application flexes too greatly or is in a confined space with other organs in its proximity that may experience undue pressure. Other neat hydrogel approaches have been studied but are frequented with either toxic initiators for gelation or do not study high impact models for adhesion formation.[140–151]

Ischemic conditions and a disrupted inflammatory response highlight the biological foundation of adhesions and thereby present an additional pathway to an augmented treatment approach. Localized anti-inflammatory release from an adherent fibrous polymer or hydrogel could inhibit the rapid fibroblast proliferation within a fibrin matrix presented in adhesions pathology. However, the process that contributes to

adhesion formation cannot be completely prevented utilizing anti-inflammatory medications as it would also inhibit wound healing and immune response to infection. Hence, controlled release platforms are a necessity when designing a therapeutically focused adhesion barrier material. Jiang et al. introduces celecoxib — a non-steroidal anti-inflammatory drug (NSAID) — into a multi-layer, electrospun hyaluronic acid and poly(L-lactic acid)-polyethylene glycol structure as to inhibit fibroblast proliferation and collagen generation.[137] Whether loaded drug directly elicits a reduction in fibrotic scar tissue deposition is unclear since rigorous in vitro release data is not provided, and there exists minimal basis for clinical assessment at 21 days in rabbit tendon anastomosis model. Li et al. instead studies utility of 10-hydroxycamptothecin and diclofenac sodium drugs in electrospun poly(ethylene glycol)-block-poly(L-lactide-co-glycolide) nanofibers.[136] Minimal difference in percent release in tested formulations leads one to believe that a majority of drug diffuses out from polymer fibers in a burst fashion within the first few hours. Release of therapeutics in a controllable fashion is crucial in counteracting a 14-day fibrotic process, as cellular uptake rate and dose dependent toxicity are of great concern.[152] Fibrous and hydrogel materials with drug release tuned exactly to fibrotic response following mesothelial tissue injury harness great potential as adhesion barriers.

Table 2.10. Supplementary fibrous and hydrogel-based nanomaterials deployed as adhesion barriers in surgery.

Composition	Architecture	Mode of Administration	Animal Model (Evaluation Time Point)	Adhesion Score (control vs. test) (Scale)	Refs.
Squid ring teeth protein coated poly(propylene)	Mesh	Prefabricated	Rat abdominal wall resection (t=7d)	3.1 (0 to 5)	[138]
Poly(lactide-co-glycolide)/poly(lactide)-b-poly(ethylene glycol) fibers with layers of carboxymethyl chitosan sponge	Electrospinning and foam	Electrospinning and prefabricated	Rat abdominal wall abrasion (t=10d)	2.4 vs. 0.23 (0 to 3)	[139]
Pullulan hydrogel	Hydrogel	Injection	Mouse cecal abrasion (t=14d)	2.67 vs. 0.5 (0 to 4)	[140]
Carboxymethyl chitosan/carboxymethyl cellulose/collagen	Hydrogel	Prefabricated	Rat cecal abrasion (t=7d)	3 vs. 0.5 (0 to 4)	[141]
Poly(N-isopropylacrylamide)grafted to chitosan and conjugated with hyaluronic acid	Hydrogel	Injection	Rat cecal abrasion (t=14d)	3 vs. 0 (0 to 3)	[142]
Pluronic F127 and oxidized hyaluronic acid	Hydrogel	Injection	Rat cecal abrasion (t=7d)	4.5 vs. 0.33 (0 to 5)	[143]
Alginate and hyaluronic acid	Hydrogel	Prefabricated	Rat cecal and abdominal wall abrasion (t=14d)	2.5 vs. 0.1 (0 to 3)	[144]
Silicate nanoplatelets and poly(ethylene oxide)	Hydrogel	Injection	Rat abdominal wall ligation (t=14d)	1.25 vs. 0 (0 to 3)	[145]
Hyaluronic acid with phenolic hydroxyl moieties	Hydrogel	Injection	Mouse abdominal wall abrasion (t=7d)	2.8 vs. 0.6 (0 to 3)	[146]
Hyaluronic acid with tempo-oxidized nanocellulose/methyl cellulose/poly(ethylene glycol)	Hydrogel	Injection	Rat cecal abrasion (t=7d)	3.5 vs. 0 (0 to 4)	[147]

Hyaluronic acid with tempo-oxidized nanocellulose/methyl cellulose/poly(ethylene glycol)	Hydrogel	Injection	Rat cecal abrasion (t=7d)	3.875 vs. 0 (0 to 4)	[148]
Carboxymethyl cellulose and glycol chitosan	Hydrogel	Injection	Rat cecal abrasion (t=14d)	4.9 vs. 1.7 (0 to 5)	[149]
Poly(N-acryloyl alaninamide)	Hydrogel	Injection	Rat cecal abrasion (t=14d)	4.8 vs. 0.2 (0 to 5)	[150]
Galactose modified xyloglucan	Hydrogel	Injection	Rat cecal abrasion (t=7d)	4.25 vs. 0.125 (0 to 5)	[151]

2.7 Conclusion

Biomaterials developed in research laboratories frequently present reduced clinical translatability when applied in surgery, due to a combination of a non-optimized cohesion and adhesion, extensive prefabrication methods, or prolonged application times to tissue substrates in vivo. Material selection plays a large role in respective metrics of efficacy such as wound area, adhesion strength, burst pressure, blood loss, and scar tissue severity. In wound dressing, hemostat, and adhesion barrier applications, one could contend cohesive strength is more favored, so the applied material does not fracture and still retains functionality. Whereas in tissue adhesive and surgical sealant applications, there is an argument for the greater importance of adhesiveness to tissue, so material is retained at the site of application. Application methods further play a major role in dictating whether the material can be easily and rapidly applied in the fast-paced setting of an operating room. Such a wide variety of approaches to improving upon commercial materials is evidence that there is no singular solution for the variable clinical scenarios described.

Future investigations into synthesizing polymeric materials for use in surgery could focus on methods for creating rapid, non-toxic curing approaches in situ. Biocompatible approaches highlighted in this review include 1) thermally mediated adhesion occurring at body temperature, 2) simple pressure application for use to applied substrate, and 3) use of non-toxic initiators for increasing adhesion at material-tissue interface whilst also fostering polymer network formation. Such methods would shift away from prevalent approaches of caustic initiators and ultraviolet light curing methods for generating nanolevel adhesion critical to enact relevant function.

Chapter 3: Biodegradable, Tissue Adhesive Polyester Blends for Safe, Complete Wound Healing

3.1 Introduction

Conformal bandages available both over-the-counter and exclusively in the clinic are coated with a pressure sensitive adhesive (PSA). PSAs, which allow fixation to a surface simply by applying pressure to the interface without any curing event, are typically composed of acrylic, polyisobutylene (PIB), or poly(styrene-butadiene-styrene) (PSBS) block copolymers blended with a phenolic tackifying resin of relatively low molecular weight.[53–55] While these synthetic rubber PSAs can adhere effectively to skin—which is dry and hydrophobic unlike the wet, hydrophillic tissue surfaces of internal organs—they are non-degradable, have been shown to cause allergic dermatitis, and may strip the healing wound of newly deposited tissue.[153–155] Despite these challenges, synthetic rubber PSAs are widely used as adhesives for various medical devices, especially bandages and wound dressings.[156,157]

Advances in medical PSAs have focused on reducing damage to the healing wound during removal, developing switchable chemistries, improving water permeability, and using biologically-derived materials. Silicone adhesives have been developed to prevent the adherence of healing skin tissue to the adhesive during bandage removal.[158–162] Responsive chemistries also allow for adhesion to be reduced on-demand, aiding in bandage removal. Various formulation changes have been made to improve water absorption, exudate control, and water transport.[163–165] Some

biologically-derived sugar-incorporating adhesives were developed for enhanced biocompatibility by accelerating biodegradation, although with limited effect due to having incorporated non-degradable acrylic.[166,167] However, few of these developments have yielded demonstrable improvements to effectiveness in controlled preclinical trials, and useful applications of advanced wound dressings are dependent on specific characteristics of the wound.[168]

Biodegradable polyesters, such as poly(lactic-co-glycolic acid) (PLGA) or poly(caprolactone) (PCL) have been used to create surgical sealants and other adhesive devices. [100,169–172] Most have the advantage of degrading completely into metabolites with low toxicity, making them superior to acrylic, PIB, or PSBS PSAs, which either do not degrade, release toxic byproducts, or have the potential to cause a harmful immune response. PSAs developed from a biodegradable polyester could be incorporated as the adhesive layer in conventional bandages—as a cost-effective replacement for typical PSAs—or could be used as a standalone spray to secure non-adhesive devices such as gauze. Polyester-derived PSAs intergrate within wound bed—forming a polymer-scab hybrid scaffold during healing— and are later cleared hepatically upon complete biodegradation. We have previously used solution blow spinning (SBS) to deposit tissue adhesive polymers from an organic solvent. In SBS, the volatile solvent evaporates during spraying, yielding a dry, conformal fiber mat, and cytotoxicity studies show that fibroblast cell viability is unaffected by the spraying solvent and process.[12,173] Herein, we used *in vivo* experiments with a porcine partial thickness wound model and adhesive tests with *ex vivo* skin sections to demonstrate

that blends of low and high molecular weight poly(lactide-co-caprolactone) (PLCL) deposited via SBS could be used to create a sprayable and biodegradable PSA for various wound healing applications.

3.2 Materials and Methods

Polymer Solutions for Producing Pressure-Sensitive Tissue Adhesives

Polymer solutions were prepared at a 20% w/v concentration in acetone. Three polymer solutions were investigated: (1) a low molecular weight solution (LMW) consisting of poly(D,L-lactide-co-caprolactone) (70:30 L:CL, acid endcap, Mn 15,000-25,000 Da, Akina), (2) a high molecular weight (HMW) solution consisting of poly(D,L-lactide-co-caprolactone) (70:30 L:CL, acid endcap, Mn 35,000-45,000 Da, Akina), (3) a polymer blend solution (denoted 50:50 L:H) containing a 50:50 mass ratio of LMW and HMW. An airbrush (Master Airbrush, G22-SET, 0.2 mm nozzle diameter) was used to deposit the tissue adhesives as dry, conformal polymer fibers. The airbrush was connected to a compressed CO_2 tank equipped with a pressure regulator set to 20 psig.

Mass Loss and Degradation Testing

Unless stated otherwise, polymer samples were produced by solution blow spinning (SBS) onto a 22 mm by 22 mm glass coverslip, with the distance between airbrush nozzle and cover slip at approximately 10 cm. Polymer samples for mass loss studies were produced by spraying 2 mL of polymer solution onto a coverslip. A microbalance (Sartorius ME-5) was used to determine the net increase in mass after the spinning process was complete, which is the initial sample mass, m_i. Samples submerged in 4 mL of 1X PBS in wells of a 6-well plate and stored in a shaker incubator at 37°C and

100 rpm. Samples were removed at time points of 1, 3, 7, and 14 days. At these points, the PBS was removed, and the samples were stored in a vacuum desiccator for three days. The samples were weighed again to determine the final mass, m_f, and mass loss (m_i - m_f) was calculated as a percentage of m_i. Samples that swell with water may produce a negative mass loss because of incomplete water removal and salt that remains in the polymer matrix. Five samples were used for each time point and polymer composition (n = 5).

Gel Permeation Chromatography

Polymer samples from time points of degradation (1, 3, 7, 14 days) and non-degraded samples (i.e. 0 days) were dissolved at 3 mg ml^{-1} in tetrahydrofuran (THF). Samples were run on the Waters e2695 Separations Module with Waters 2414 Refractive Index Detector, and Waters HSPgel columns in series (HR MB-Land HR 3.0 columns, 6.0 mm I.D. x 15 cm). Molecular weight is reported as polystyrene relative molecular weight, as calculated from a 10-point calibration curve generated using Agilent EasiCal polystyrene standards dissolved at 2 mg ml^{-1} in THF. GPC analysis was performed using Waters Empower 3 Chromatography Data software. The weight-average molecular weight, number-average molecular weight, and polydispersity of each sample were then obtained from the sample curves and recorded. Each sample type was replicated 3 times (n = 3).

Differential Scanning Calorimetry

Polymer samples were sealed in aluminum hermetic pans (TA Instruments) using a sample encapsulation press. DSC measurements were made on a TA Instruments DSC Q100. Samples were held isothermal at -50°C for 5 min and then heated and cooled from -50 to 80 to -50°C, at a rate of 3°C min^{-1}, ±0.20°C amplitude, with a modulation period of 60 s for two continuous cycles. Glass transition temperature (T_g) was calculated using the tangent intersection method.

Porcine Partial-Thickness Wound Healing Model

Animal studies were performed in the research animal facility at Children's National Health System. Experiments were approved by the Institutional Animal Care and Use Committee (protocol #30454) and were performed in accordance with the "Guide for the Care and Use of Laboratory Animals" published by the National Institutes of Health. Two 20–25 kg Yorkshire swine were used in this pilot study. Six partial thickness (0.6 mm depth) skin wounds were made on each side of the paravertebral skin with a dermatome (Humeca), making a total of twelve wounds per animal. The wounds were made 1.5 cm long in cranial-caudal direction and 4 cm wide. Each wound was separated by 1.5 cm of normal skin. The wounds were randomized to treatment with either Tegaderm (3M) (a polyurethane-based clinical control), HMW PLCL, or 50:50 L:H, resulting in a total of five wounds per dressing group (n = 5) over two animals. Wounds were uniformly sprayed with 2 mL of polymer solution, which produced complete wound coverage as determined by a surgeon. Wounds were assessed daily for healing and signs of infection by visual inspection. Dressing

replacement was performed as needed until PWD 14. The experimental endpoint was chosen to be thirty-five days after initial wound creation. Wound healing was followed by wound size and scar tissue measurements by caliper on PWD 3, 7 and 35. 5 mm full thickness punch biopsies of the wounds were also taken on PWD 3, 7 and 35. Each biopsy was taken from different areas of the same wound.

Histological Analysis

Biopsied tissues were kept in 10% neutral buffered formalin until histological processing (Histoserv Inc.). Punch biopsy samples were bisected along the longitudinal axis then embedded in paraffin wax. 5μm sections were prepared and fixed onto glass slides and then stained with Masson's trichrome. Digital images of the histology slides were taken with TissueScope LE (Huron Digital Pathology) at 40x magnification then exported for analysis with ImageJ (National Institutes of Health). Images were scaled to 1μm/pixel. Epidermal and dermal thicknesses were measured after cropping images to 3000μm by 3000μm. Epidermis thickness was measured at areas that show at least a basal layer of epidermal cells, stained red in Masson's trichrome. Total dermis thickness was measured from the base of the epidermis to the level of subdermal fat. Also measured was the thickness of the evolving dermal matrix, seen as disorganized collagen bundles (in light blue) above the layer of organized collagen bundles (dark blue). Thickness measurements were taken at the left, middle, and right third of the images, and then averaged. The vascular density (vessels per mm^2 of dermis) of each biopsy was measured by counting the number of unique vessel structures in the dermis,

including arterioles and venules, but not capillaries. Dermis area was measured using ImageJ. Density measurements were made by two researchers and averaged.

Wound Healing Gene Expression

Gene expression of α-SMA (α-smooth muscle actin), VEGF (vascular endothelial growth factor), TGF-β1 (transforming growth factor-β1), collagen I and collagen III in the healed wounds were quantified using real-time reverse transcription-PCR (RT-PCR). Full thickness biopsies were taken from the center of the healed wounds at PWD 35. Normal uninjured skin biopsies were also taken from both sides of the paraspinal back skin with samples from the upper and lower back. Gene expressions in the wounds were measured relative to those expressed in normal skin tissue. Biopsied tissues were snap-frozen in liquid nitrogen, and then stored at -80^{o}C until analysis.

RNA extraction from frozen tissue was performed by tissue homogenization in Trizol reagent (Life Technologies) and PureLink RNA Mini Kit (Thermo Fisher Scientific). For all experiments, 3μg RNA was used to synthesize first strand cDNA using High-Capacity cDNA Reverse Transcription kit (Life Technologies). Real-time PCR was performed using TaqMan® Gene Expression Master Mix (Life Technologies) in a QuantStudio 7 Flex Real-Time PCR System (Thermo Fisher Scientific), according to the manufacturer's instructions. Reactions were performed in triplicate, including no template controls and amplification of a housekeeping gene, GAPDH. Gene-specific assays were Ss03373340_m1 for COL1A1, Ss04245588_m1 for α-SMA, Ss04323768_g1 for COL3A1, Ss03382325_u1 for TGF-β1, and Ss03375629_u1 for

GAPDH (Life Technologies). Changes in relative gene expression normalized to GAPDH levels were determined using the ΔΔCt method. The difference between the Ct values (ΔCt) of the gene of interest and the housekeeping gene is calculated for each experimental sample. Then, the difference in the ΔCt values between the experimental and unwounded skin samples ΔΔCt is calculated. The fold-change in expression of the gene of interest between the two samples is then equal to $2^{(-\Delta\Delta Ct)}$

Adhesive Bandage Pull-Apart Adhesion Testing

Pull-apart testing was performed on the TA Instruments DMA Q800. CVS Health Plastic One-Size Bandages were placed in baths of ethanol to remove the adhesive. The bandages were then cut into 8 mm square segments, and the polymer bandage samples were produced by spraying 2 mL of polymer solution directly onto the smooth surface of the bandage that was previously coated in the adhesive layer. BioGlue-based lung sealant (Progel™, Beckton Dickinson) constituted of a crosslinked human serum albumin (HSA) – poly(ethylene glycol) (PEG) network, or a topical skin adhesive (SwiftSet™, Covidien) derived from cyanoacrylate (CA), were used as clinical controls and deposited onto the bandage in an analogous fashion. The polymer coated bandage was allowed to set for 15 minutes in 37°C ambient air. Square sections of 8 mm frozen porcine skin were cut and warmed to room temperature by coating the tissue in water and letting the tissue warm for 10 minutes in 37°C ambient air. Prior to testing, porcine skin samples with clinical control as adhesive were coated until total surface coverage (approximately 250 µL of solution). Warmed polymer coated bandages or uncoated bandages in the case of clinical controls were brought into contact with porcine skin

and superglued to the clamps of the dynamic mechanical analyzer in compression mode—the porcine skin to the fixed clamp and the polymer coated or uncoated bandage to the movable clamp. The samples were compressed at 1 N for 5 minutes and after this compression period a controlled force ramp was used to increase pull-apart force at a rate of 1 N min^{-1} until failure. The adhesion strength of each sample was recorded. Each sample type was replicated five times (n = 5).

Wound Closure Strength Testing

Wound closure strength testing was performed on the TA Instruments DMA Q800. 1 cm by 1 cm sections of porcine skin were attached to rectangular clamps using cyanoacrylate glue. The rectangular clamps were brought together end to end, and 1 mL of adhesive polymer solution was deposited via SBS on this joint, closing the gap between the two skin-coated clamps (see ASTM F2458–05).[174] The adhesive was carefully applied and trimmed to avoid coating the interface between the ends and edges of the clamps. It was then allowed to set at 37 °C for 10 minutes before testing. A controlled force ramp was used to increase force at a rate of 1 N min^{-1} until failure. Failure type was recorded as either adhesive or cohesive. Force values were normalized to the surface area of skin coated by the adhesive, which was measured using calipers, giving adhesive strength. Each sample type was replicated five times (n = 5).

Statistical Analysis

Statistical analysis was performed on Origin (OriginLab, Northampton, MA). Typically, one-way ANOVA was used to compare group variation, followed by post-

hoc pairwise Tukey or Holm-Sidak (for pull-apart adhesion testing) comparisons to determine significant differences between the groups. For adhesion testing, positive and negative controls were excluded from statistical analysis because of differences in variability. Statistical significance is considered for $P < 0.05$. Typically, averages were plotted with error bars representing standard error.

3.3 Results

An airbrush was used to deposit polymer fibers directly onto porcine partial thickness wounds, allowing us to assess the effects of a biodegradable PSA composed of PLCL on wound healing compared to a bandage with a conventional non-biodegradable adhesive (**Figure 3.1A**). Three different pressure sensitive blends of PLCL were studied (**Figure 3.2**), one containing pure high molecular weight (HMW) PLCL (Mn 35,000-45,000 Da), one containing a 50:50 blend (50:50 L:H) of HMW PLCL and low molecular weight (LMW) PLCL (Mn 15,000-25,000 Da), which acts as a tackifier to enhance adhesion while degrading, and one containing pure LMW PLCL (**Figure 3.1B** and **S3**). Pure adhesive (with no backing) was used in these experiments to isolate the effects of polymer choice. PLCL blends transition from a fibrous covering to a thin, conformal, and transparent film (**Figure 3.4A**). We tracked wound dressing changes over the first 14 days of healing to determine how the adhesive affected the frequency at which the dressing had to be replaced (**Figure 3.4B**). Both HMW and 50:50 L:H PLCL-based adhesives required fewer dressing changes than the control dressing, Tegaderm, which is a conventional PSA backed with a thin polyurethane film.[175]

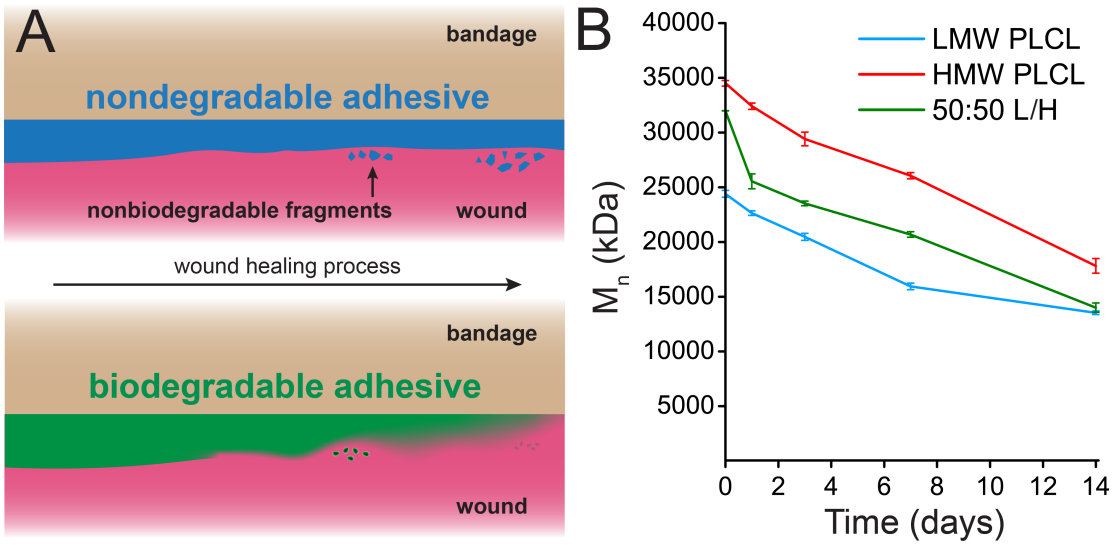

Figure 3.1. Schematic of nondegradable and biodegradable adhesives and GPC of neat and blend PLCL.
(A) While the adhesive on a conventional bandage may produce non-biodegradable fragments that irritate the skin, a biodegradable adhesive can degrade into absorbable monomers. (B) Gel permeation chromatography of low molecular weight (LMW) poly(lactide-co-caprolactone) (PLCL), high molecular weight PLCL, and a 50:50 blend of those two polymers (50:50 L:H), which has pressure-sensitive adhesive properties, during *in vitro* degradation. Schematic A made by John L. Daristotle. Figure B data and plotting by Metecan Erdi. Adapted with permission.[1] Copyright 2021, American Chemical Society.

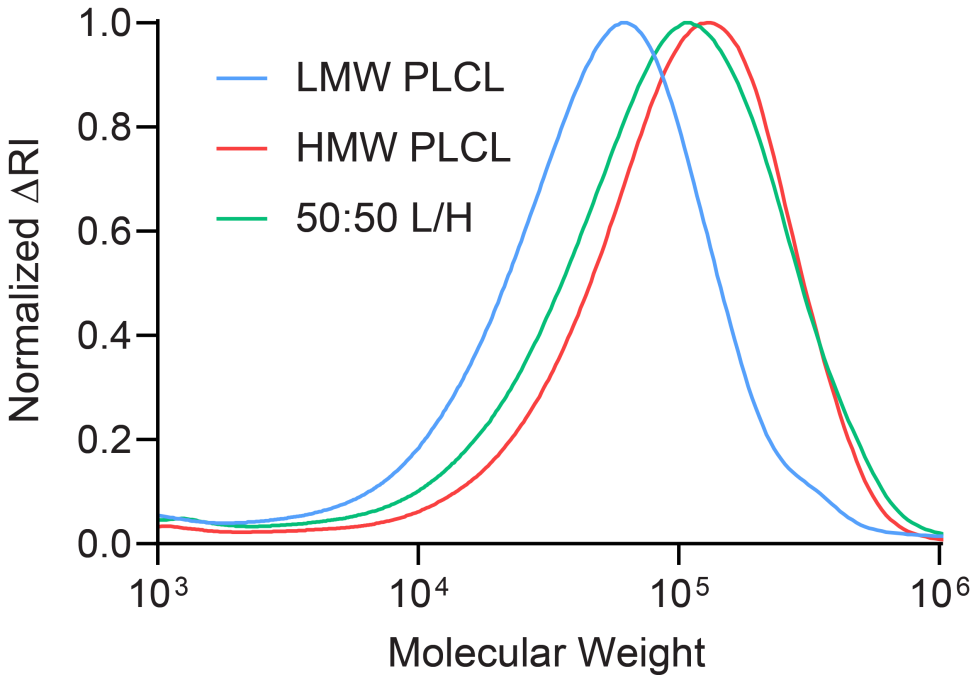

Figure 3.2. Gel permeation chromatography of low molecular weight (LMW) poly(lactide-co-caprolactone) (PLCL), high molecular weight PLCL, and a 50:50 blend of those two polymers (50:50 L/H), which has pressure-sensitive adhesive properties.

Figure data and plotting by Metecan Erdi. Adapted with permission.[1] Copyright 2021, American Chemical Society.

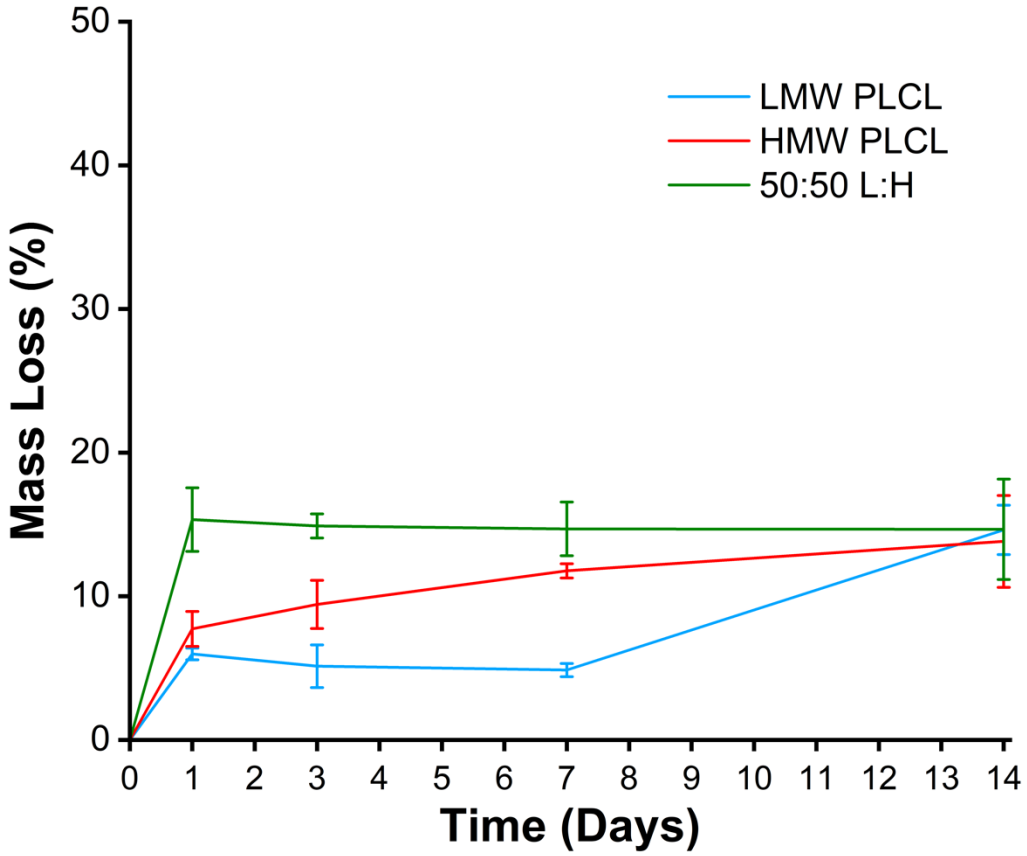

Figure 3.3. Mass loss data for low molecular weight (LMW) poly(lactide-co-caprolactone) (PLCL), high molecular weight PLCL, and a 50:50 blend of those two polymers (50:50 L/H), which has pressure-sensitive adhesive properties, during *in vitro* degradation.
Figure data and plotting by Metecan Erdi. Adapted with permission.[1] Copyright 2021, American Chemical Society.

Visual assessment of the wounds was regularly performed by the surgeon as they were healing, with pictures presented at post-wound day (PWD) 3, PWD 7, and PWD 21 (**Figure 3.4C–E**). Some exudate buildup was apparent underneath the Tegaderm dressing at PWD 3 (**Figure 3.4Ciii**). At PWD 21, most wounds appeared to show similar amounts of scarring. While few wounds displayed any healed epidermis at

PWD 3, nearly all wounds showed complete epidermis coverage by PWD 7, which was confirmed with histology (**Figure 3.5A**).

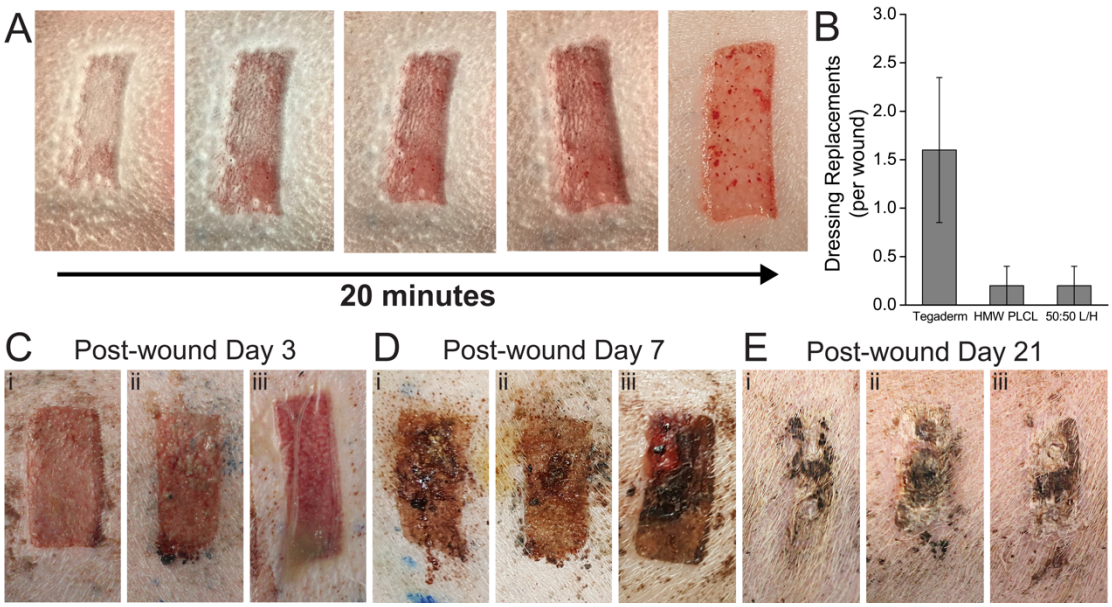

Figure 3.4. Clinical comparison of clinical Tegaderm control to neat and blend PLCL in porcine partial-thickness wound healing.
(A) Partial thickness wound sprayed with PLCL blend pressure sensitive adhesive, transitioning from solution blow spun fibers to a transparent film. (B) Number of required dressing replacements per wound due to dressing deadherence. Sample images of healing wounds at (C) 3 days, (D) 7 days, and (E) 21 days after wound creation, using either (i) HMW PLCL, (ii) 50:50 L:H PLCL, or (iii) Tegaderm. Figure A-E data and plotting by John L. Daristotle. Adapted with permission.[1] Copyright 2021, American Chemical Society.

Increased epidermis thickness was noted in the 50:50 L:H blend at PWD 7 but returned to levels comparable to the other wound dressings at PWD 35 (**Figure 3.5B**). Neodermis ratio was significantly lower for HMW PLCL dressings at PWD 7 and PWD 35 (**Figure 3.5C**). Revascularization is an indication of wound healing, as angiogenesis plays a critical role during the proliferative stage of wound repair.[176,177] Blood vessel regeneration was decreased for Tegaderm at PWD 3, while 50:50 L:H displayed increased blood vessel density relative to the no wound control at PWD 7 (**Figure**

3.5D). All returned to normal levels at PWD 35. Representative histological images from which these data are compiled are shown in from PWD 3 to PWD 35 in **Figure 3.6,** and unwounded skin is shown in **Figure 3.7**.

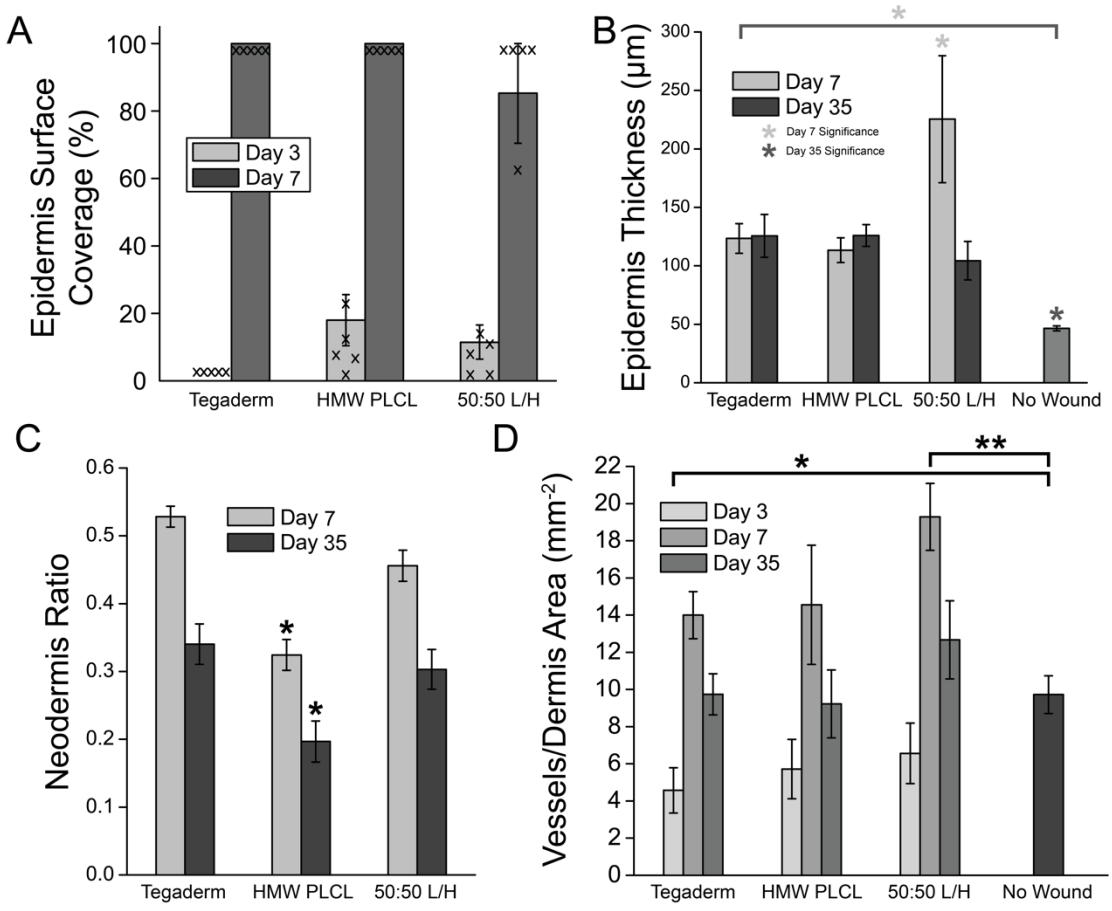

Figure 3.5. Histological characteristics of porcine partial-thickness wound healing for PLCL-based pressure sensitive adhesives.
(A) Epidermis surface coverage on the healing wound at Day 3 and Day 7. Individual data points are overlaid. (B) Epidermis thickness of the healing wounds. (C) Ratio of neodermis thickness to total dermis thickness. (D) Blood vessel density in the dermis of the healing wound. Asterisks indicate statistical significance: * = $P < 0.05$, ** = $P < 0.01$. Figure A-D data and plotting by John L. Daristotle. Adapted with permission.[1] Copyright 2021, American Chemical Society.

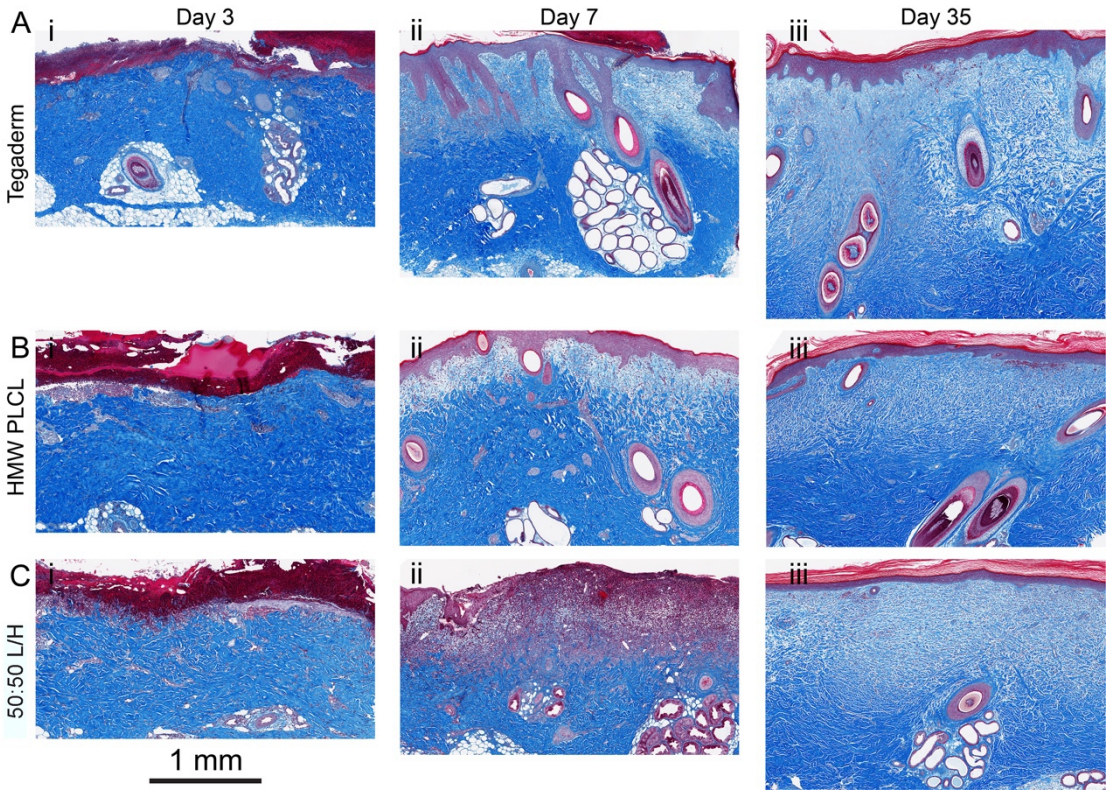

Figure 3.6. Histological image comparison of clinical Tegaderm control to neat and blend PLCL in porcine partial-thickness wound healing.
Representative histological images at post-wound day 3, day 7, and day 35 from porcine partial thickness wounds sealed with (A) Tegaderm, (B) HMW PLCL, and (C) 50:50 L:H. Each time series of images is from one wound. Images collected by John L. Daristotle. Adapted with permission.[1] Copyright 2021, American Chemical Society.

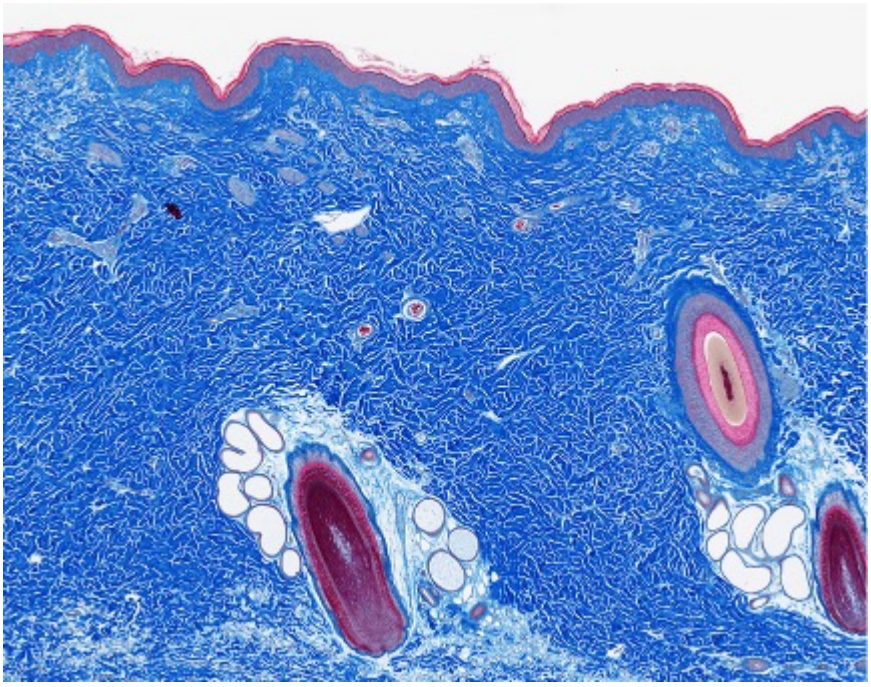

Figure 3.7. Histological image of unwounded porcine skin tissue.
Image collected by John L. Daristotle. Adapted with permission.[1] Copyright 2021, American Chemical Society.

Samples were collected from the center of wound at PWD 3, PWD 7, and PWD 35. Sections were stained with Masson's trichrome to identify collagen (blue), keratin in the epidermis (dark red), and blood vessels (red). The overall trajectory of collagen type I and collagen type III mRNA expression over 35 days was similar for all groups (**Figure 3.8A–B**), while alpha smooth muscle actin (α-SMA), transforming growth factor beta (TGF-β), and vascular endothelial growth factor (VEGF) were expressed similarly between the three groups (**Figure 3.8C–E**). High relative amounts of collagen III, which is disorganized compared to collagen I, indicates potential scarring. At Day 35, all wound dressing types produce similar Type I to Type III ratios, although only Tegaderm's is significantly lower than unwounded skin (**Figure 3.8F**).

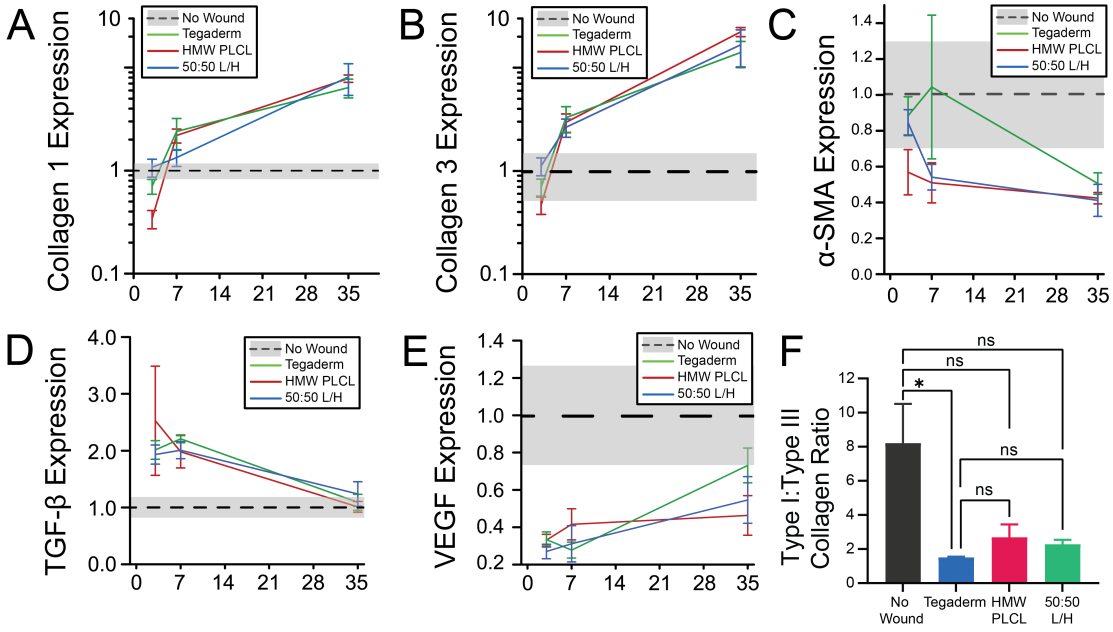

Figure 3.8. Wound healing gene expression comparison of clinical Tegaderm control to neat and blend PLCL in porcine partial-thickness wound healing.
RT-PCR measurements of (A) Collagen I, (B) Collagen III, (C) α-SMA, (D) TGF-β, and (E) VEGF. Gene expression measured relative to those of normal uninjured (no wound) skin, which is plotted with a black dotted line and a gray band indicating standard error. (F) Collagen Type I to Collagen Type III ratio at day 35. * = $P < 0.05$. Figure A-F data and plotting by John L. Daristotle. Adapted with permission.[1] Copyright 2021, American Chemical Society.

After validating the safety and efficacy of using PLCL for use in wound healing applications, we further characterized its adhesive properties and processability, towards its eventual use as the adhesive layer on a bandage. PLCL adhesives are sprayable with tunable fiber morphology, consistently forming a mesh with long fibers at a 50:50 L:H ratio (**Figure 3.9A**). The fibers can be sprayed onto various targets and form a thin adhesive film after transitioning (**Figure 3.9B**), allowing for simple fabrication. During pull-apart adhesion testing and wound closure strength testing, the film is soft and sticky enough to form tendrils during cohesive failure, indicating the formation of a strong bond (**Figure 3.9C–D**).

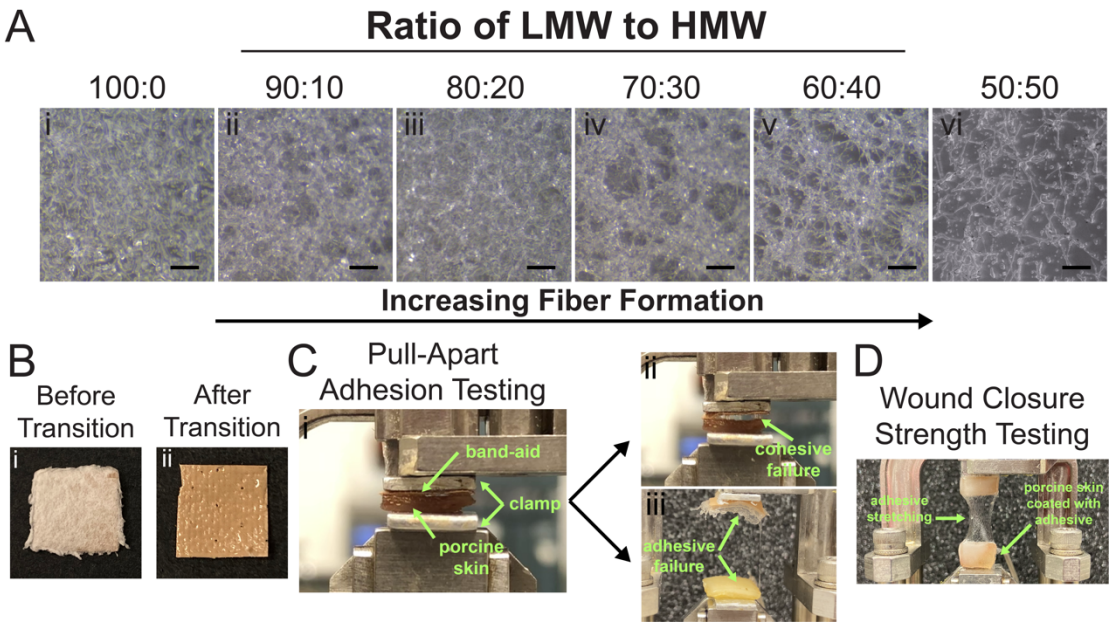

Figure 3.9. Fiber morphology images and pull-apart adhesion and wound closure strength testing of neat and blend PLCL.
(A) When more HMW PLCL is incorporated, fiber mats are produced by solution blow spinning from an airbrush. (B) PLCL blends transition from fibers to a thin, adhesive film after 30 minutes. (C) During pull-apart adhesion testing, the adhesive stretches and breaks via cohesive or adhesive failure (green arrows). (D) Wound closure strength test with shear force applied to the joint. Figure A-B data and plotting by John L. Daristotle. Figure C-D data and plotting by Metecan Erdi. Adapted with permission.[1] Copyright 2021, American Chemical Society.

We sprayed PLCL adhesives onto the backing of a typical plastic bandage (**Figure 3.10A**) and compared pull-apart adhesion strength to the same plastic bandage as manufactured—coated with a conventional PSA. After spraying and transitioning, both PLCL adhesives formed a thin film with similar morphology to the conventional adhesive (**Figure 3.10B–C**). PLCL has a glass transition temperature of approximately –11°C (**Figure 3.10D**), which allows it to soften significantly as it warms to body temperature. Pull-apart adhesion strength to porcine skin was significantly greater for both the 50:50 L:H blend of PLCL and Progel control than either pure LMW PLCL or pure HMW PLCL, while the acylate-based SwiftSet skin adhesive was much greater than all other groups other than conventional bandage PSA (**Figure 3.10E**). In wound

closure strength testing, the 50:50 L:H blend of PLCL displayed a significant increase compared to pure LMW PLCL (**Figure 3.10F**). This provides strong evidence in favor of using a combination of tackifying (LMW PLCL) and reinforcing (HMW PLCL) polymers to promote both adhesive and cohesive strength, mimicking the properties of a PSA. 50:50 L:H produces comparable adhesion strength (12 ± 2 kPa) to Progel control (12 ± 3 kPa) and conventional bandage (11 ± 2 kPa), whose PSA coating has a much lower T_g than PLCL (**Figure 3.10D**).

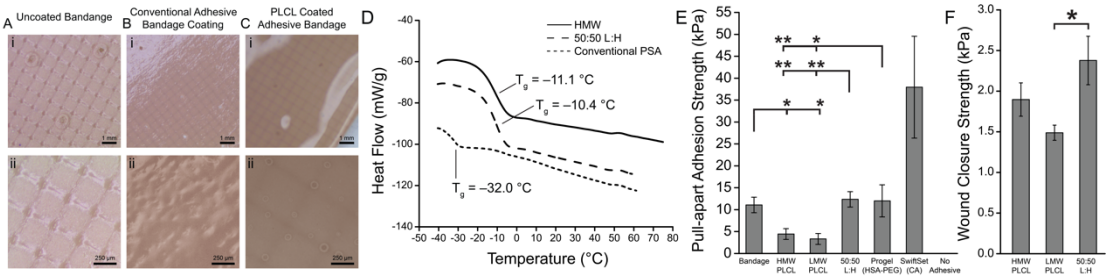

Figure 3.10. Biodegradable PLCL pressure sensitive adhesives were sprayed onto plastic bandages, producing comparable adhesive strength to a conventional polybutylene pressure sensitive adhesive.
Optical microscopy of (A) an uncoated plastic bandage, (B) a plastic bandage coated with conventional pressure sensitive adhesive (PSA), and (C) a plastic bandage and coated with PLCL blend adhesive. (D) Differential scanning calorimetry of HMW PLCL, PLCL blend adhesive, and conventional PSA utilized with bandage. (E) Pull-apart adhesion strength between bandage and porcine skin for neat and blended PLCL, conventional bandage PSA, Progel lung sealant (HSA-PEG), and SwiftSet topical skin adhesive (CA). (F) Wound closure strength of PLCL 50:50 L:H blend compared to pure LMW and HMW polymers. Asterisks indicate statistical significance: * = $P < 0.05$, ** = $P < 0.01$. Figure A-D data and plotting by John L. Daristotle. Figure E-F data and plotting by Metecan Erdi. Adapted with permission.[1] Copyright 2021, American Chemical Society.

3.4 Discussion

Biodegradable and tissue adhesive polymers have been investigated as alternatives to sutures,[18,99] stand-alone wound dressing materials,[12,173,178] and replacements for biomedical devices.[83,179] However, biodegradable polymers have not been investigated as a replacement for conventional pressure sensitive adhesives in a conventional

bandage—one that consists of a flexible backing coated with a thin layer of strong, tacky adhesive. Yet due to their low cost, ease of use, and availability to consumers, there is a larger market for these simple tapes and bandages than "advanced" wound dressings.[180,181] They are desirable targets for innovation because of the growing body of evidence indicating that the ubiquitous non-degradable PSAs commonly used in them may cause allergic dermatitis. Acrylates, methacrylates, and phenolic resins that are common in bandage adhesives[182] are implicated in controlled studies of allergic and irritant contact dermatitis.[153,183,184]

We first rigorously characterized the biocompatibility of polyester blends in a partial thickness wound model, establishing that treated wounds have effective barrier properties (**Figure 3.4**), complete dermal and epidermal healing (**Figure 3.5** and **Figure 3.6**), and normal biochemical composition (**Figure 3.8**). However. for effective translation, a bandage adhesive must also be easily applied as a thin layer on a textile backing during manufacture, stick readily to both the backing and skin, and remain stable at room temperature. The PLCL blends investigated are easily sprayed onto a target (**Figure 3.9A**), transition into a thin layer (**Figure 3.9B**), and have a desirable balance of cohesive and adhesive strength in pull-apart tests (**Figure 3.9C–D**). Furthermore, the layer has a similar morphology to the conventional adhesive layer on a bandage (**Figure 3.10A**), with similar thermal properties that allow PLCL blends to soften at room temperature (**Figure 3.10B**), and comparable adhesion strength in *ex vivo* wound closure and pull-apart models (**Figure 3.10E–F**). These observations align with previous studies from our group on the pressure sensitive tissue adhesion of

viscoelastic polyester blends.[57] Future studies could validate this approach by employing biodegradable polyesters as adhesives in new wounds models and further assessing the biocompatibility with contact dermatitis patch and bandage testing.

3.5 Conclusions

Based on robust preclinical safety data, we have isolated two safe and effective biodegradable polyesters spanning the molecular weight range of interest for developing a strong bonding tissue adhesive that minimizes the need for dressing replacements. We then demonstrated that a 50:50 blend of low and high molecular weight PLCL maximizes adhesion strength. It can also be processed using conventional methods and applied using a typical plastic backing. These polymers could potentially be used safely as a replacement for conventional bandage adhesives with better biocompatibility and comparable adhesion.

Chapter 4: Sprayable Tissue Adhesive with Biodegradation Tuned for Prevention of Post-Operative Abdominal Adhesions

4.1 Introduction

Abdominal adhesions are deposits of dense, connective scar tissue that form between organ surfaces as a result of uncontrolled fibrogenesis following surgery, trauma, inflammation, infection, or tissue ischemia.[185,186] Such uncleaved fibrous bridges are frequently reported in the human peritoneum following surgical interventions resulting in broad serous tissue injury (ex. abrasion, suturing), and are particularly common following abdominal surgeries such as laparotomy and appendicectomy.[152,187] Pathologic adhesion formation occurs due to an imbalance between the early fibrin deposition and degradation that occurs as part of healing after trauma, as well as the proximity of an injured surface to other structures.[188–190] In normal abdominal tissue healing, the entire injured surface heals uniformly, and affected cells secrete numerous pro-inflammatory cytokines, growth factors, and coagulants such as fibrin. Fibrous matrix deposition begins within 3 hours of tissue injury and increases until post-injury day 4 or 5, where it is then enzymatically degraded through fibrinolysis over the course of 1 week. In post-surgical adhesion formation, fibrin deposition outpaces fibrinolysis during the healing process and permanent connective adhesions are created between organs, with up to 93% of patients developing adhesions following operation in the abdomen or pelvis.[127–129] Such unsuppressed proliferation of fibrous tissue frequently causes small bowel obstruction, female infertility, or chronic abdominal or pelvic pain and is implicated in up to 60%, 40%, and 80% of cases, respectively.[130,191–193]

Removal of post-surgical adhesions through adhesiolysis can be attempted laparoscopically as to reduce frequency and severity in the abdominal cavity, but ultimately these procedures only have a ~70% success rate while also increasing the risk of new adhesion formation.[194] Treatment of small bowel obstruction accounts for up to 1% of all general surgical admissions, 3% of all laparotomies, over $2 billion in hospitalization and surgical expenditures annually, as well an approximated 900,000 days of inpatient care.[129,195–197] Because these surgical interventions to treat adhesions prove to be largely ineffective and costly, prophylactic barrier materials are needed that can prevent adhesions between organs before they form. Hydrogel-based adhesion barriers are the most widely adopted tool in surgical settings, but are difficult to apply, poorly adhesive to the target organ, and degrade too quickly to effectively prevent adhesions.[192]

Currently available clinical products to prevent adhesion formation include Seprafilm (Genzyme)—a pre-dried hydrogel film made of carboxymethylcellulose-hyaluronic acid that swells once in contact with aqueous abdominal fluid—and Interceed (Johnson & Johnson), a woven cellulose mat. Both products act as solid barriers and physically prevent adhesions by separating injured mesothelial surfaces through interfacial lubrication imparted ay their hydrophilic surface properties. Because they are pre-fabricated, such clinical products are brittle and difficult to apply, with limited flexibility when conforming to geometrically complex tissue surfaces. They also degrade rapidly in moist environments in the critical 5-day maturation period for

adhesions, exhibit impeded wound healing, and inability to seal sites of injury, the combination of which limits their use in clinical practice.[198–203] Further, Seprafilm undergoes a 90% loss in tensile strength within 30 minutes due to swelling of its carboxymethylcellulose-derived network, which renders it largely ineffective in the abdominal cavity where organs are in perpetual motion and tissue surfaces are routinely extending.[198,199] Recent biomaterials research efforts have recently focused on use of physically crosslinked hydrogels comprised of nanoparticles dispersed in a cellulose matrix.[133,134] However, they exhibit reduced flexibility and adherence to wet tissue, and also require an intricate syringe-based deposition technique. Other investigated hydrogel systems include ones forming chemical crosslinks to tissue in-situ via reactive end group chemistries, as the resultant material mimics biological tissue stiffness and thereby promotes biocompatible interfacing upon implantation.[204–206] However such materials frequently swell, causing undue pressure on surrounding tissue, and utilize crosslinking approaches that employ either toxic initiators or adhesive curing processes such as ultraviolet light and high temperature.[56,207] An implanted material for use as an adhesion barrier must not only be retained at the sight of application, but also maintain mechanical integrity during critical stages of fibrosis and wound healing.

To develop an adhesion barrier that is sprayable, tissue adhesive to only the target organ, degradable at the same rate as the abdominal tissue wound healing process, and does not impede wound healing, we investigated solution blow spinning (SBS) of dry, conformal polymer fibers with controllable surface erosion. Through blending of fast degrading low molecular weight and slow degrading high molecular weight surface

eroding polymers at defined ratios, we can design sprayable fiber mats with linear biodegradation profiles tuned to a clinically relevant rate. Previous research investigations from our group have reported the biocompatibility and efficacy of SBS-deposited polymer materials for in-vivo surgical applications including antimicrobial burn wound dressings[12], sealants for intestinal anastomosis[18,99,173], and hemostats for traumatic bleeding[100]. While stretchy, durable materials are desirable for high tissue adhesion, viscoelasticity and tunable biodegradation are necessary to provide a matrix that facilitates complete wound healing in a moist environment. For example, cohesively strong poly(lactic-co-glycolic acid) (PLGA) not only displays a lack of wet tissue adherence unless blended with an additional adhesive component, but also induces abdominal adhesions in a clinical mouse model over a 10 day time course.[57] Such shortcomings are a result of a near 0% loss in polymer mass and remaining polymer providing a template for fibrous tissue growth. In contrast, separate biodegradable viscoelastic polymer blends were investigated as the primary dressing in a porcine partial thickness wound model, exhibiting high wet tissue adherence (>1 N/cm^2) and complete wound healing in a pressure sensitive tissue adhesive (PSTA) application.[1,57]

In this report, we studied the effect of various molecular weight blends of PLCL on biodegradation profile, cohesive strength, and tissue adhesion, followed by implementation into a preclinical mouse model of abdominal adhesions. Multiple low and high molecular weight combinations of PLCL were studied to modulate surface erosion rate and determine its subsequent effect on adhesion prevention. Since

degraded fragments of PLCL continually erode from the surface, PLCL has the potential to act as a favorable adhesion barrier material if its degradation profile is tuned to coincide with adhesions formation (**Figure 4.1**). A constantly eroding surface will mitigate cell adhesion and fibrin deposition, which are necessary steps for the formation of adhesions.[208,209] The barrier itself—tuned to retain the necessary mechanical properties at the application site—is critical to occlude atypical deposition of fibrous, vascular scar tissue until the target wound itself has healed. We aimed to strike a balance between the presence of critical wound healing components through kinetic control of degradation, as well as necessary cohesive and adhesive strength through facile tuning of high and low molecular weight ratios. PLGA was referenced as a bulk degrading control that undergoes minimal erosion during the adhesions-forming period. First, in-vitro biodegradation and mechanical testing techniques were used to determine the optimal composition of PLCL molecular weight blends for adherence to wet tissue and biocompatibility. Then, PLCL blend adhesion barriers were studied in an in-vivo mouse cecal ligation model via assessment of adhesions severity and subsequent immunological analysis to demonstrate the potential benefits of a spray deposited, wet tissue conforming, adhesion barrier material.

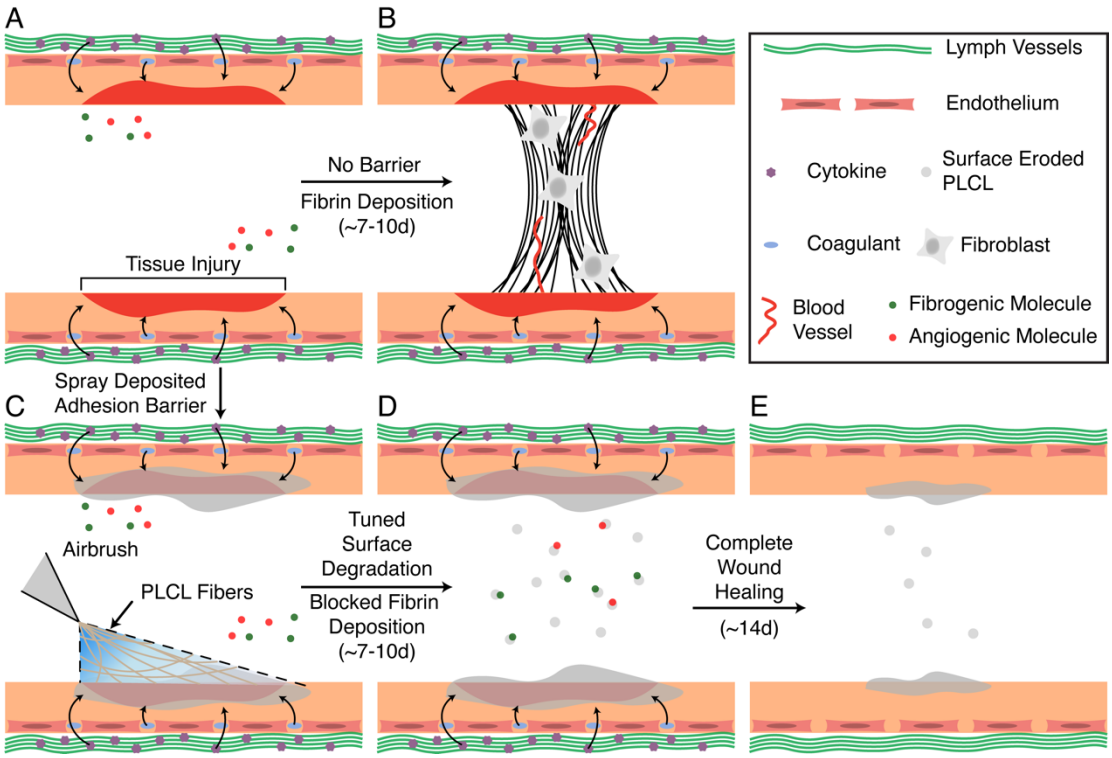

Figure 4.1. Illustration of adhesion formation in the presence of no barrier and treatment via surface eroding polymer adhesion barrier.
(A) Formation of adhesions is a consequence of reduced fibrinolytic activity following ischemic mesothelial tissue injury, (B) leading to deposition of connective wound healing tissue. (C) Our poly(L-lactide-co-caprolactone) (PLCL) molecular weight blends yield a viscoelastic, wet tissue adhesive rapidly deposited via solution blowspinning (SBS) for application and retention in the abdominal cavity, while also presenting a surface erosion degradation mechanism apt to (D) prevention of adhesion formation and (E) wound healing. Adapted with permission.[2] Copyright 2022, Wiley.

4.2 Materials and Methods

Polymer Solution Preparation

Polymer solutions were prepared at a 20% (w/v) concentration in ethyl acetate for polymers characterized in-vitro and in-vivo. Previous research investigations have demonstrated appreciable biocompatibility and fibrous morphology of SBS fibers deposited from ethyl acetate and other solvents, as all liquid evaporates during the process and does not accumulate on the target substrate.[12,18] When used in its pure

liquid form, ethyl acetate is regarded as a Class 3 solvent with low toxic potential by the U.S. Food and Drug Administration and the International Council for Harmonisation of Technical Requirements for Pharmaceuticals for Human Use, hence the selection of ethyl acetate in all datasets.[12,210] Both neat polymer solutions and blends comprised of neat poly(D,L-lactide-co-caprolactone) were investigated for "low" molecular weight (LMW) compositions terminologically defined as 5k PLCL (70:30 L:CL, acid endcap, Mn 1,000-5,000 Da, Akina) or 20k PLCL (70:30 L:CL, acid endcap, Mn 15,000-25,000 Da, Akina), and "high" molecular weight (HMW) compositions defined as 40k PLCL (70:30 L:CL, acid endcap, Mn 35,000-45,000 Da, Akina) or 80k PLCL (70:30 L:CL, acid endcap, Mn 75,000-85,000 Da, Akina). Polymer blends were mixed in a 70:30 mass ratio for a total of four blends of 1) 80k/20k, 2) 80k/5k, 3) 40k/20k, and 4) 40k/5k, where the leading component in the abbreviation is the majority (i.e., 70%) component of the blend and the secondary component is in minority (i.e., 30%). This ratio was selected as to remain in a similar material regime of published work using PLCL molecular weight blends for pressure sensitive tissue adhesive (PSTA) applications where multiple ratios were studied.[1,57] An airbrush (Master Airbrush, G222-SET, 0.2 mm nozzle diameter) was used to deposit the solutions as dry, conformal polymer fibers. The airbrush was connected to a compressed CO_2 tank equipped with a pressure regulator set to 20 psig.

Mass Loss and Degradation Testing

Polymer samples were produced by solution blow spinning (SBS) onto a 22 mm by 22 mm glass coverslip, with the distance between airbrush nozzle and cover slip at

approximately 10 cm. Polymer samples for mass loss studies were produced by spraying 2 mL of polymer solution onto a coverslip. A microbalance (Sartorius ME-5) was used to determine the net increase in mass after the spinning process was complete, which is defined as the initial sample mass, m_i. Samples submerged in 4 mL of 1x PBS in wells of a 6-well plate and stored in a shaker incubator at 37°C and 100 rpm. Samples were removed at time points of 1, 3, 7, and 14 days. At these points, the PBS was removed, and the samples were stored in a vacuum desiccator for three days. The samples were weighed again to determine the final mass, m_f, and mass loss (m_i - m_f) was calculated as a percentage of m_i. Five samples were used for each time point and polymer composition (n = 5).

Gel Permeation Chromatography

Polymer samples from time points of degradation (1, 3, 7, 14 days) and non-degraded samples (i.e., 0 days) were dissolved at 3 mg ml^{-1} in tetrahydrofuran (THF). Samples were run on the Waters e2695 Separations Module with Waters 2414 Refractive Index Detector, and Waters HSPgel columns in series (HR MB-L and HR 3.0 columns, 6.0 mm I.D. x 15 cm). Molecular weight is reported as polystyrene relative molecular weight, as calculated from a 10-point calibration curve generated using Agilent EasiCal polystyrene standards dissolved at 2 mg mL^{-1} in THF. GPC analysis was performed using Waters Empower 3 Chromatography Data software. The weight-average molecular weight, number-average molecular weight, and polydispersity of each sample were then obtained from the sample curves and recorded. Each sample type was replicated 3 times (n = 3).

Tensile Strength Testing

Tensile strength testing was performed to determine the mechanical properties of the polymer samples over time. For the 0-day (i.e., non-degraded) experiment, samples were produced by spraying 2 mL of polymer solution onto a glass coverslip. For 1, 3, 7, and 14-day timepoints, polymer samples were degraded according to the procedure described in the degradation testing section, removed from the coverslips, and trimmed to a rectangular shape approximately 10 mm by 5 mm in size. Sufficient stiffness data was not collected for 80k/5k and 40k/5k PLCL blend compositions past 1-day of biodegradation in vitro, as samples were inherently "sticky" and difficult to mount to DMA clamp. Exact sample dimensions were measured immediately prior to testing. Tensile testing was performed on a TA Instruments DMA Q800 equipped with a film tensile clamp. Samples were stretched under a controlled force ramp from 0 N to 5 N at a rate of 0.01 N min^{-1} and measurements made at room temperature. Elastic modulus was calculated from the linear region of the resulting stress versus strain curve, with a 0.2% offset used to calculate sample yield stress and strain. Each sample type was replicated 5 times (n = 5).

Pull-Apart Adhesion Testing

Pull-apart testing was performed on the TA Instruments DMA Q800. For testing on porcine skin, CVS Health Plastic One-Size Bandages were placed in baths of ethanol to remove the adhesive. For testing on porcine intestine, Gore-Tex Cardiovascular Patch (polytetrafluoroethylene, Gore Medical) were used as is. Both types of substrate material were cut into 8 mm square segments with 1mL of polymer solution sprayed

onto each, and 1mL sprayed onto section of either porcine skin or intestine. Polymer coated bandages and cardiac patch sections were allowed to set for 15 minutes in 37°C ambient air. Square sections of 8 mm frozen porcine skin or intestine were cut and warmed to room temperature by coating the tissue in water and letting the tissue warm for 10 minutes in 37°C ambient air. Warmed polymer coated substrates were brought into contact with porcine skin or intestine and superglued to the clamps of the dynamic mechanical analyzer in compression mode—the porcine skin to the fixed clamp and the polymer coated or uncoated bandages to the movable clamp. The samples were compressed at 1 N for 5 min and after this compression period a controlled force ramp was used to increase pull-apart force at a rate of 1 N min^{-1} until failure. The adhesion strength of each sample was recorded. Each sample type was replicated five times (n = 5).

Cell Viability

Cytotoxicity of polymer compositions was tested against L929 mouse fibroblasts by an elution method as described by ISO-10993-5.[211] 40k/5k PLCL blend and neat 40k PLCL and 5k PLCL compositions were sprayed onto sterile 22 mm by 22 mm glass coverslips. The polymer mats were then removed from the coverslips and eluted at mass concentration of 10 mg/mL in culture media of Dulbecco's modified Eagle medium supplemented with 10% fetal bovine serum (Gemini Bio-Products Inc.), L-glutamine and 1% penicillin and streptomycin at standard conditions (37ºC, 5% CO_2) for 24 hours. The elutions were diluted to 1x, 10x, and 100x dilutions, and cell viability was tested against the different dilutions.

L929 fibroblasts (10^5 cells/mL) were plated into 96-well plates at 100uL per well and incubated for 24 hours under standard conditions. The culture media was removed by pipette. Finally, wells were then treated to control (standard media), 25 ug/mL puromycin, or diluted elutions of 40k/5k PLCL blend, neat 40k PLCL, and neat 5k PLCL compositions. This measurement was repeated five times for each diluted elution (n = 5).

Mouse Cecal Ligation Adhesions Model

All animal procedures were approved by the Children's National Hospital Institutional Animal Care and Use Committee (IACUC protocol #000030703), and the animals were treated in accordance with PHS Policy on Humane Care and Use of laboratory Animals, the National Institute of Health Guide for the Care and Use of Laboratory Animals, and the Animal Welfare Act. Forty, 7–15-week-old C57BL/6 female mice were used (Jackson Laboratory). Mice were randomized into groups based on treatment group. Normal saline injection was used as a negative control, while Seprafilm® (Genzyme) was used as an anti-adhesion, clinical control. Experimental endpoint was 7 days after surgery with a total of five mice (n =5) allocated per group. Polymer solutions of 40k/5k PLCL blend and neat 40k PLCL were made under sterile conditions in a biosafety cabinet, and later sterilized by UV irradiation in their respective vials. Prior to surgery, a dedicated airbrush was sterilized with ethanol and placed under UV radiation along with polymer solutions.

All mice were anesthetized with a 100 mg kg^{-1} ketamine and 10 mg kg^{-1} xylazine solution (0.1 mL / 10 g mouse mass). After anesthesia, the mice were positioned supine, and skin prepped with betadine solution. In sterile fashion, a 1 cm laparotomy incision was made at the midline. After dissection into the abdominal cavity, the cecum was exposed and ligated with 4-0 Vicryl® Suture (Ethicon) approximately 1cm from distal end. In the case of normal saline injection, cecum was placed back into the abdominal cavity and 0.1 mL sterile saline was dripped onto ligated cecum. For the Seprafilm control group, the cecum was placed back into the abdominal cavity and a 1cm square section gently placed on top of ligated cecum. For polymer treatment groups, 0.5 mL of solution was sprayed onto ligated cecum prior to replacement in abdominal cavity. Upon reinsertion of cecum, skin was closed using 4-0 Vicryl® Suture (Ethicon) in a running fashion, and approximately 0.1 mL buprenorphine was given as an analgesic at the end of the surgery.

Each animal was weighed both pre-operatively and at 7 days after initial surgery prior to euthanasia. Midline laparotomy was performed post-euthanasia, and images of the abdominal cavity were taken with a camera. The abdominal space was then examined by a surgeon who was blinded to treatment groups and assessed for adhesions formation with scores on a Mazuji-derived scale assigned to each attached organ pair, as well as signs of inflammation and degradation of the polymer sample.[212]

Histological Analysis

Ligated cecum tissues were harvested on postoperative day 7 and kept in 10% neutral buffered formalin until histological processing (Histoserv Inc.), then embedded in paraffin wax. Five µm sections were prepared, fixed onto glass slides, and stained with hematoxylin and eosin (H&E). Digital images of the histology slides were taken with TissueScope LE (Huron Digital Pathology) at 5x and 40× magnification then the 40x images were exported for analysis intestinal wall cellularity. One section per mouse, with 5 separate low-powered and high-powered fields of view were imaged per section. Using ImageJ (National Institutes of Health), images were scaled to 1 µm/pixel and converted to an RGB stack. A threshold of 100 was set, and the percent area of the image stained purple was obtained for each image. These percentages were then averaged for each mouse.

Wound Healing Gene Expression

RNA was extracted from frozen cecal tissue using Trizol reagent (Life Technologies, Frederick, MD). In all experiments, 6 µg RNA was used to synthesize first strand cDNA using High-Capacity cDNA Reverse Transcription Kit (Life Technologies). Real-time PCR was performed using TaqMan® Gene Expression Master Mix (Life Technologies) in a QuantStudio7 Flex RT-PCR system (Thermo Fisher Scientific, Waltham, MA), according to the manufacturer's instructions. Reactions were performed in triplicate, including no template and endogenous control using GAPDH. Gene-specific assays were Mm00434228_m1 for Il1b, Mm0046190_m1 for Il6, Mm00443258_m1 for Tnfa, Mm00437306_m1 for Vegfa, Mm01178820_m1 for

Tgfb1, Mm00433287_m1 for Fgf2, Mm00801666_g1 for Col1a1, Mm00802305_g1 for Col3a1, and Mm99999915_g1 for Gapdh (Life Technologies, Thermo Fisher). Changes in relative gene expression normalized to GAPDH levels were determined using the ΔΔCt method. First, the difference between the Ct values (ΔCt) of the gene of interest and the housekeeping gene was calculated for each sample. Then the ΔCt values for the control samples were averaged. The difference in the ΔCt values between each experimental sample and the control sample (ΔΔCt) was calculated. The fold-change in expression of the gene of interest compared to the housekeeping gene for each sample was calculated as $2^{-\Delta\Delta Ct}$, and the results were averaged for graphical representation.

Contact Angle

Surface wettability was characterized by water contact angle measurements at room temperature, with images captured on a Sony a7R IV D3400 (Sony) and subsequent analysis performed in ImageJ (National Institutes of Health). Non-degraded (Day 0) and degraded polymer samples (Day 14) were prepared as described above. Advancing contact angle of 10 μL droplets of deionized (DI) water was measured using the sessile drop technique. Five samples were used for each polymer composition and time point (n = 5).

Statistical Analysis

Statistical analysis was performed on Origin (OriginLab). Typically, one-way ANOVA was used to compare group variation, followed by post-hoc pairwise Tukey comparison

to determine significant differences between the groups. Typically, averages were plotted with error bars representing standard error. Asterisks are used to indicate statistically significant differences: * = $P < 0.05$, ** = $P < 0.01$, *** = $P < 0.001$. If no asterisks are shown, there are no significant differences amongst the groups. Real-time PCR results were analyzed using t-tests comparing the $\Delta\Delta Ct$ values.

4.3 Results

Degradation of surface eroding PLCL blends was studied by immersing samples in 37°C water. Samples were then removed at select time intervals, and following a vacuum dry step, measured for mass loss, and then prepared for both molecular weight distribution analysis via gel permeation chromatography (GPC) and tensile stiffness measurements via dynamic mechanical analysis (DMA).

Molecular weight blends of surface eroding polymers present an opportunity to finely tune composite degradation profile due to the faster erosion rate of low molecular weight (LMW) chains. LMW chains in the initially fabricated fiber mat accumulate at the material surface and decrease the contact angle of blends over time (**Figure 4.2A-B**). Contact angle measurements for neat HMW PLCL are unchanged over 14 days, but they decrease significantly when blended with 5k PLCL, indicating the presentation and erosion of LMW chains with hydrophilic endgroups at the fiber mat surface.

Adhesions form within 5-7 days and then mature over two weeks. Any potential barrier material needs to prevent contact between surfaces during the initial stages of fibrin deposition and persist until the injured mesothelium is healed. Blending HMW 40k or 80k PLCL with LMW 5k PLCL at a 70:30 ratio results in a linear degradation profile for up to 14 days (~50% mass loss) (**Figure 4.2B**) while also displaying distinct bimodal molecular weight distributions in GPC not presented in other blends and neat compositions (**Figure 4.2C-D, 4.3**). As these particular blends begin to degrade and decrease in molecular weight, there is a shift to a unimodal distribution with a high PDI

(~3) due to the presence of 5k PLCL as synthesized, along with degraded portions of 40k or 80k PLCL. Since all other blend compositions yield only 5-20% mass loss and plateau in later stages, 40k/5k and 80k/5k PLCL blends have the potential to equivalently release short chain fragments from the polymer surface over a 14d treatment period for adhesions. The fast, linear erosion rate will decrease accumulation of fibro- and angio- genic molecules, such as fibrinogen and vascular endothelial growth factor (VEGF), reducing scar tissue formation on healing mesothelium.

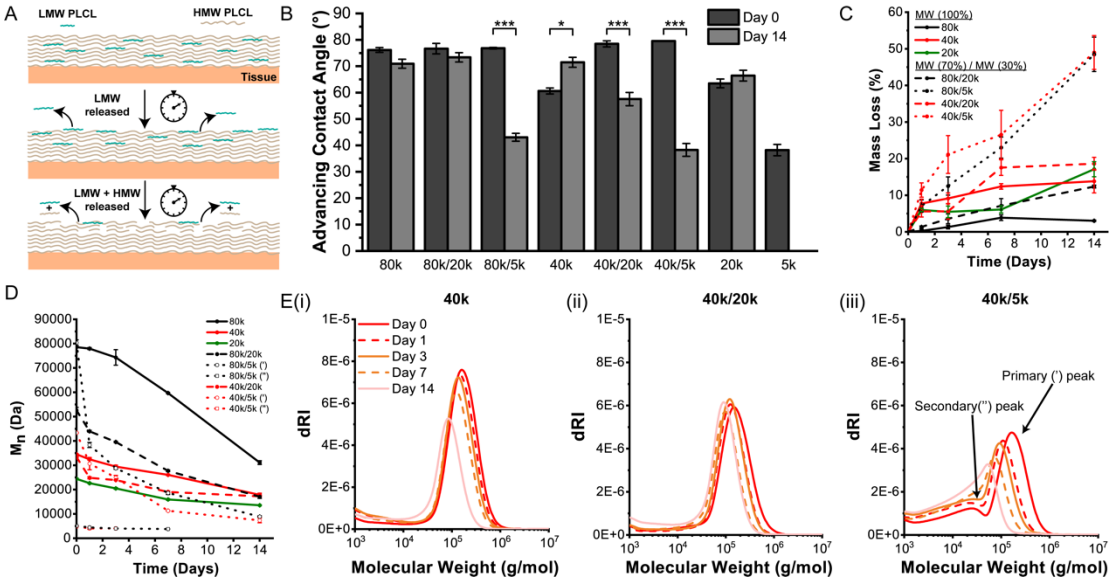

Figure 4.2. Biodegradation characterization of neat and blend PLCL measured via mass loss and GPC.
(A) Schematic of degradation mechanism for poly(L-lactide-co-caprolactone) (PLCL) via polymer surface erosion. (B) Advancing water droplet contact angle of neat and blend PLCL at start and end of in-vitro degradation. (C) Mass loss for neat and blend PLCL. (D) Number average molecular weight and (E) overall distributions for PLCL blends during in-vitro degradation. HMW = "high" molecular weight. Blending of different molecular weights allows for tunable degradation with rapid linear degradation in the first several days for 80k/5k and 40k/5k blends. LMW = "low" molecular weight. (') = HMW peak of blend. ('') = LMW peak of blend. Data is plotted as mean ± s.e. * $p < 0.05$; ** $p < 0.01$; *** $p < 0.001$. Adapted with permission.[2] Copyright 2022, Wiley.

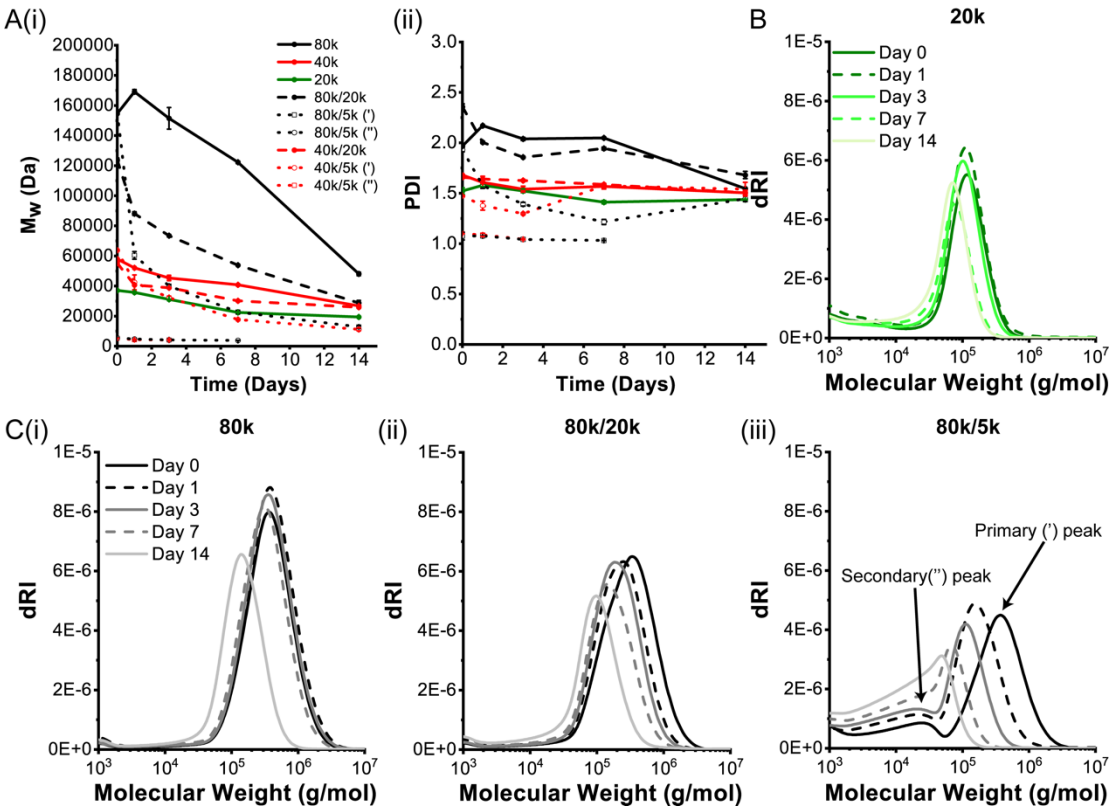

Figure 4.3. Supplementary biodegradation characterization of neat and blend PLCL measured via mass loss and GPC.
(A) (i) Weight average molecular weight and (ii) polydispersity index (PDI) for neat and blend poly(L-lactide-co-caprolactone) (PLCL) during *in vitro* degradation. (B-C) Overall distributions for PLCL blends during *in vitro* degradation. (') = HMW peak of blend. ('') = LMW peak of blend. Data is plotted as mean ± s.e. Adapted with permission.[2] Copyright 2022, Wiley.

Blending either LMW 5k or 20k PLCL in a HMW 40k or 80k PLCL matrix greatly promotes tensile elasticity as both are near (20k) or below (5k) entanglement molecular weight, whilst presenting viscous behavior that permits flow upon application of an external force. 40k/5k and 80k/5k PLCL blends in particular display improved adhesive strength to tissue versus their neat 40k or 80k PLCL compositions, as the 5k component allows the sealant to spread across a given surface under application of pressure. Adhesion to a surface under these conditions is facilitated through physical mechanisms of polymer chain entanglement with complex tissue topography and short-

range interactions (ex. Van der Waals) with surface molecules as facilitated through the viscoelastic nature of our adhesive.[62–64]

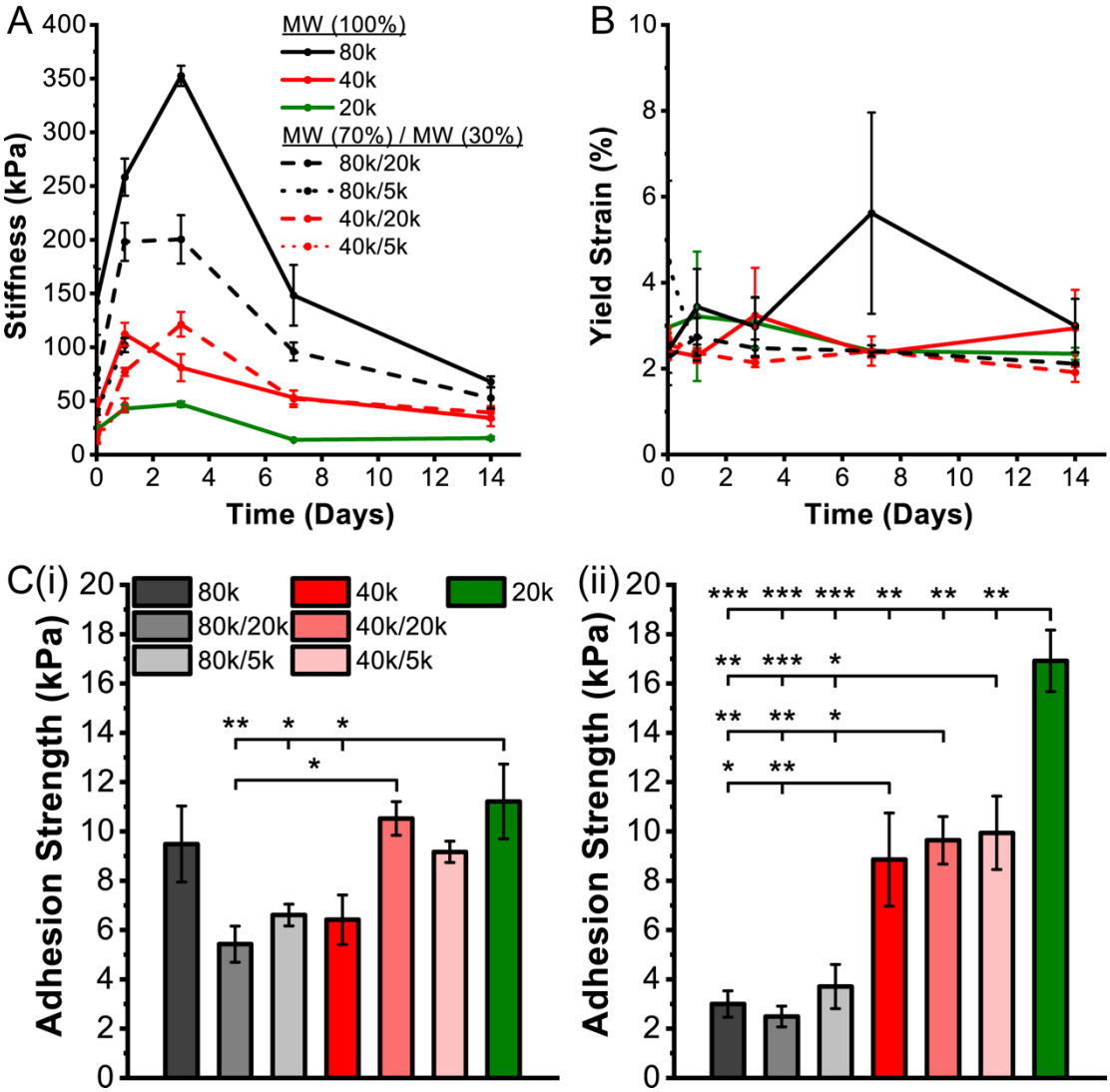

Figure 4.4. Mechanical characterization of tensile modulus, yield strain, and pull-apart adhesion strength of degraded neat and blend PLCL measured via DMA.
(A) Tensile stiffness, (B) yield strain, and (C) day 0 pull-apart adhesion strength for (i) bandage-to-skin-tissue and (ii) cardiac-patch-to-intestine-tissue of neat and blend poly(L-lactide-co-caprolactone) (PLCL) during in-vitro degradation. MW = molecular weight. Both pull-apart adhesion tests were done with 1 min of applied pressure, as to show the positive effect on tissue adherence with blending 20k or 5k PLCL. Data is plotted as mean ± s.e. Asterisks indicate statistical significance: * $p < 0.05$; ** $p < 0.01$; *** $p < 0.001$. Adapted with permission.[2] Copyright 2022, Wiley.

As expected, blending 5k or 20k PLCL produces materials with decreased stiffness (**Figure 4.4A**) and values of yield stress (**Figure 4.5**) versus neat HMW compositions during in-vitro degradation. Interestingly, yield strain values remain in the same order of magnitude no matter the compositions, indicating similarity in elastic range across all compositions and time points (**Figure 4.4B**). Blends of PLCL with 5k or 20k components exhibit augmented pull-apart adhesion strength versus respective neat HMW compositions on not only dry porcine skin, but also internal wet porcine intestine (**Figure 4.4C**). Such an improvement is due to an adjusted balance between cohesive strength and adhesive strength. While neat 20k PLCL displays significantly increased adhesive strength versus other compositions in wet tissue on porcine intestine, the lack of cohesive strength elucidated by tensile stiffness measurements, as well as an unfavorable non-linear degradation profile (**Figure 4.2C**), make it a poor adhesion barrier material candidate. The equivalent biodegradation rate over 14d (**Figure 4.2C**) for 40k/5k PLCL, coupled with superior dry and wet tissue adhesion strength (**Figure 4.4C**), makes this blend particularly promising as a favorable adhesion barrier.

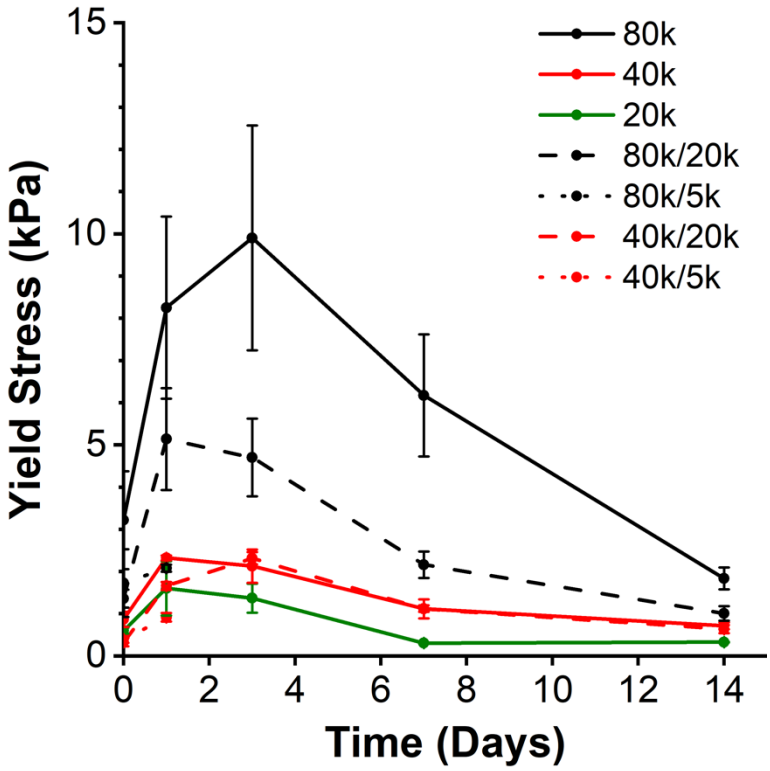

Figure 4.5. Yield stress values of degraded neat and blend PLCL measured via DMA.
Data is plotted as mean ± s.e. Adapted with permission.[2] Copyright 2022, Wiley.

Below entanglement molecular weight polymers (~1 kDa) formed in-vivo can exhibit toxic effects due to an ability to disrupt cell membrane integrity.[213] We therefore assessed toxicity prior to in-vivo implantation of 5k PLCL in either neat or blend compositions. L929 mouse fibroblasts were treated with supernatant of degraded polymer. Neat 5k PLCL significantly reduced cell viability (~50%) of L929 mouse fibroblasts at 1x concentration, while neat 40k and blended 40k/5k PLCL compositions had no effect on cell viability at all dilutions (**Figure 4.6A**). This indicates that 40k/5k PLCL blends have low toxicity and could be safely used as an implanted adhesion barrier material.

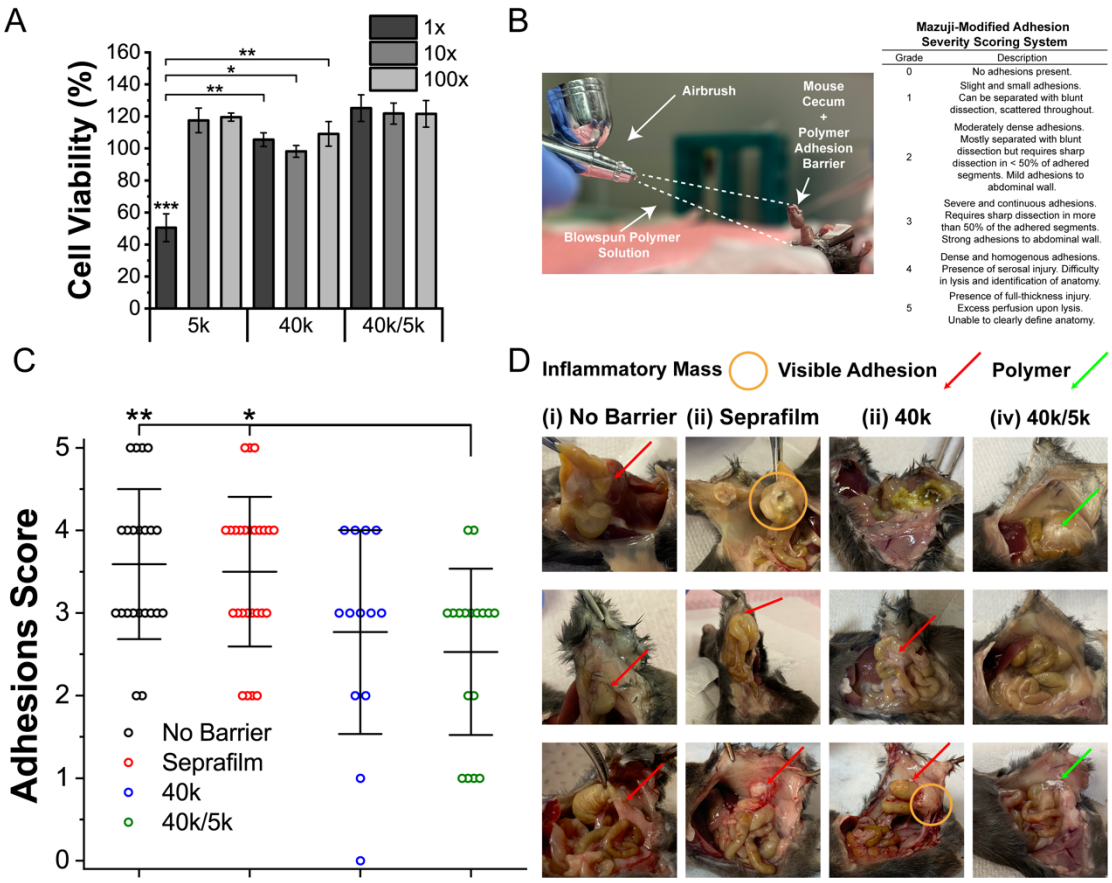

Figure 4.6. Severity scoring comparison of clinical Seprafilm control to neat and blend PLCL in mouse cecal ligation model of abdominal adhesions.
(A) L929 mouse fibroblast cell viability (versus media only control) of neat and blended poly(L-lactide-co-caprolactone) (PLCL) for 1x, 10x, and 100x dilutions of treatment media. (B) Application of polymer adhesion barrier during mouse cecal ligation and Mazuji-derived adhesion scoring rubric used in clinical assessment. (C) Clinical scores and (d) gross pathology for (i) no barrier, (ii) Seprafilm, and (iii and iv) PLCL treated groups post-cecal ligation at t = 7 days. PLCL treatment groups showed increased significance versus empty and clinical controls in reducing adhesions severity. Data is plotted as mean ± s.e. Asterisks indicate statistical significance: * $p < 0.05$; ** $p < 0.01$; *** $p < 0.001$ (5k PLCL versus unmarked groups in cell viability). Adapted with permission.[2] Copyright 2022, Wiley.

An accurate in-vivo animal model for adhesion formation should produce consistent and reproducible mesothelial injury and ischemia. Forceful abrasion of serosal tissue lining the abdominal cavity and cecal ligation have been previously used to induce adhesions.[214] Though more directly related to operative conditions, abrasion models are largely subjective as the amount of force applied by the operator can vary. Therefore, a cecal ligation mouse model was adopted as the procedure greatly reduces

variability in creation of local tissue ischemia via mesenteric and mesothelial disruption. After cecal ligation, mice were randomized and treated with either saline (negative control), Seprafilm (clinical control), or SBS 40k/5k or 40k PLCL polymer (treatment groups). Adhesion formation and wound healing response were assessed after 7 days. Mice that did not undergo laparotomy and cecal ligation were also assessed as a no wound control.

A surgeon, blinded to the treatment group, assessed efficacy of SBS deposited fiber mats as adhesion barriers using a Mazuji-derived scoring rubric of clinical severity (**Figure 4.6B**). 40k/5k PLCL blends significantly reduced adhesion severity versus No Barrier and Seprafilm treated controls (**Figure 4.6C-D**), while neat 40k PLCL did not exhibit the same affect. Additionally, adhesions in 40k/5k PLCL treated groups were more frequently described as localized and sealed off from the surrounding space in blinded assessment, with fewer involved organ systems and amassed pockets of inflammatory exudate versus the 40k PLCL treatment group (**Figure 4.7**). Such a contrast in adhesions prevention efficacy between the two polymer groups versus control groups is likely attributable to differences in biodegradation profiles (**Figure 4.2C**) and tensile strength (**Figure 4.4A**). PLCL 40k/5k balances cohesive strength and strong tissue adhesion at the site of injury with rapid erosion, which mitigates the adherence of cells and fibrin that lead to formation of adhesions.

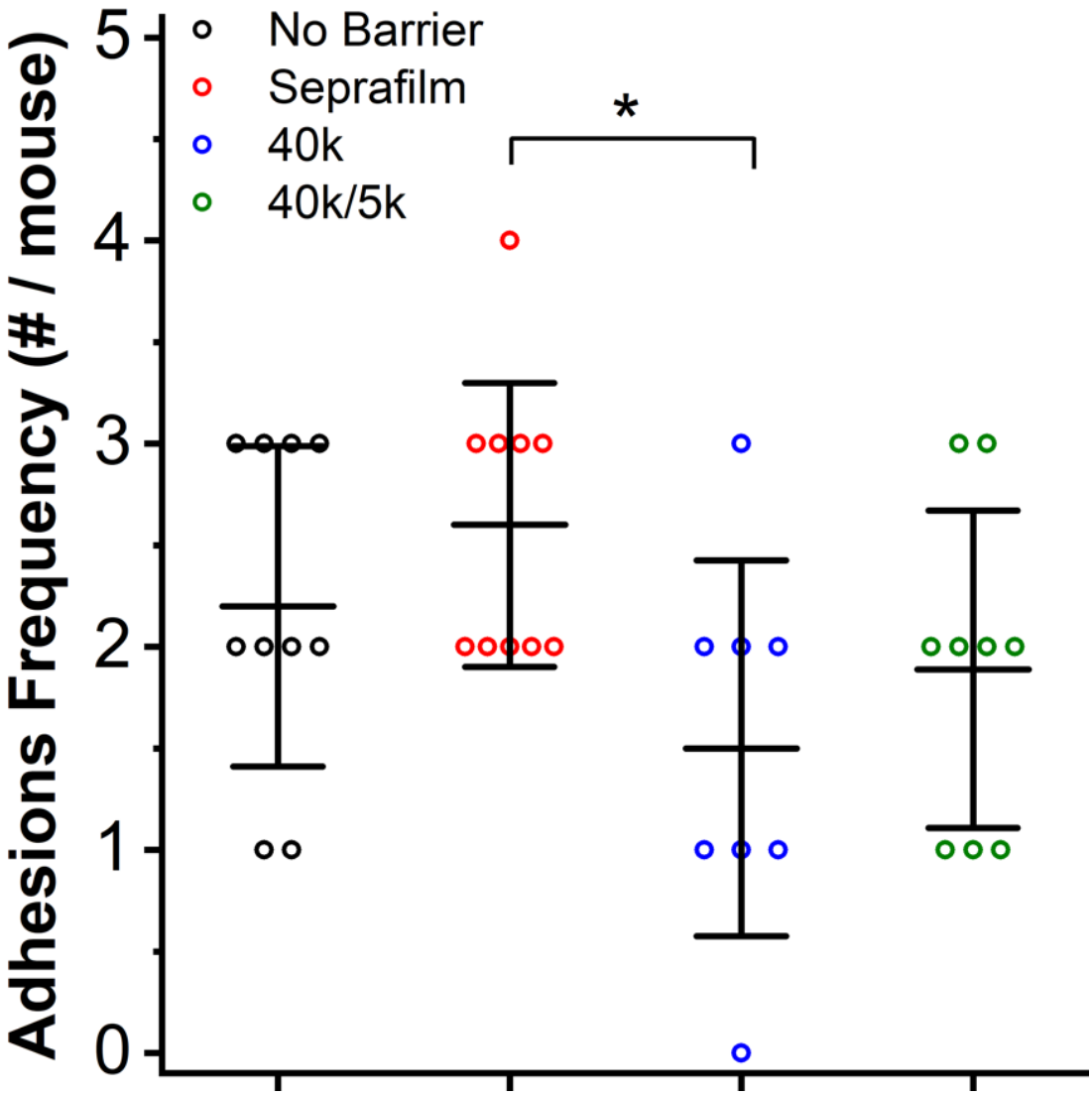

Figure 4.7. Frequency comparison of clinical Seprafilm control to neat and blend PLCL in mouse cecal ligation model of abdominal adhesions.
Total number of adhesions per mouse for (i) no barrier, (ii) Seprafilm, and (iii) and iv) poly(L-lactide-co-caprolactone) (PLCL) treated groups post-cecal ligation at t = 7 days. Data is plotted as mean ± s.e. Asterisks indicate statistical significance: * $p < 0.05$. Adapted with permission.[2] Copyright 2022, Wiley.

Since fibrin deposition and remodeling is a process regulated by pro-inflammatory signaling molecules,[215,216] cecal tissue was extracted from the mice at Day 7 for analysis of gene expression and histology. Histologic evidence of inflammation, which coincides with adhesions formation, or healing can be used to corroborate assessments of adhesion score severity. Hematoxylin and eosin (H&E) stained cecum displayed

infiltration of neutrophils and eosinophils throughout the entire intestinal wall in all cecal ligation groups (**Figure 4.8A-B, 4.9**). Quantitative measurements of gross inflammation further assessed via cellularity analysis did not demonstrate significant differences between saline, Seprafilm, and polymer groups, though all cecal ligation groups displayed increased cellularity compared with the "no surgery" group, as expected.

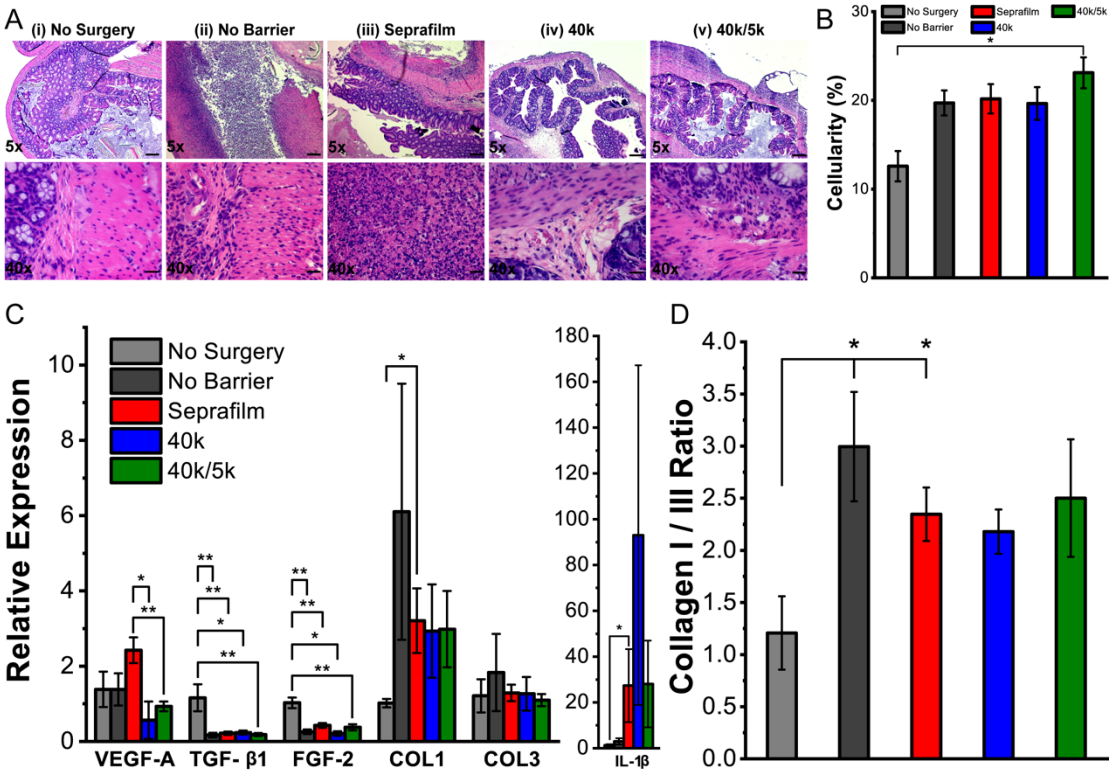

Figure 4.8. Histological image and wound healing gene expression comparison of clinical Seprafilm control to neat and blend PLCL in mouse cecal ligation model of abdominal adhesions.
(A) Histological cross sections and (B) cellularity of mouse cecum, and (C) mRNA expression levels measured via RT-PCR of vascular endothelial growth factor (VEGF-A), transforming growth factor-β1 (TGF-β1), fibroblast growth factor-2 (FGF-2), collagen I (COL1), collagen III (COL3), and interleukin-1β (IL-1β) wound healing gene markers and (D) ratio of collagen I to collagen III expression for (i) no surgery, (ii) no barrier, (iii) Seprafilm, and (iv and v) poly(L-lactide-co-caprolactone) (PLCL) treated groups post-cecal ligation at t = 7 days (n = 4-5). Scale bars = 200μm (top row) and 20μm (bottom row). Data is plotted as mean ± s.e. Asterisks indicate statistical significance: * $p < 0.05$; **$p < 0.01$; ***$p < 0.001$. Adapted with permission.[2] Copyright 2022, Wiley.

Expression of critical wound healing genes in IL-6, TNF-α, VEGF-A, TGF-β1, FGF-2, collagen I, collagen III, and IL-1β were measured for ligated cecum samples after 7 days via real-time PCR and compared to tissue from normal ("no surgery") mice (**Figure 4.8C, 4.10**). Levels of angiogenic growth factors (VEGF-A) were significantly reduced in the polymer groups versus Seprafilm. Fibrogenic (TGF-β1 and FGF-2) growth factors exhibited reduced expression in all cecal ligation groups versus the normal "no surgery" group. Levels of collagen I and III expression were decreased in the Seprafilm and polymer groups versus the no barrier saline group. Collagen I to Collagen III ratio is an indicator of scar-forming collagen prevalent in cases of severe adhesions and was significantly elevated in no barrier saline and Seprafilm treated groups versus normal controls (**Figure 4.8D**).

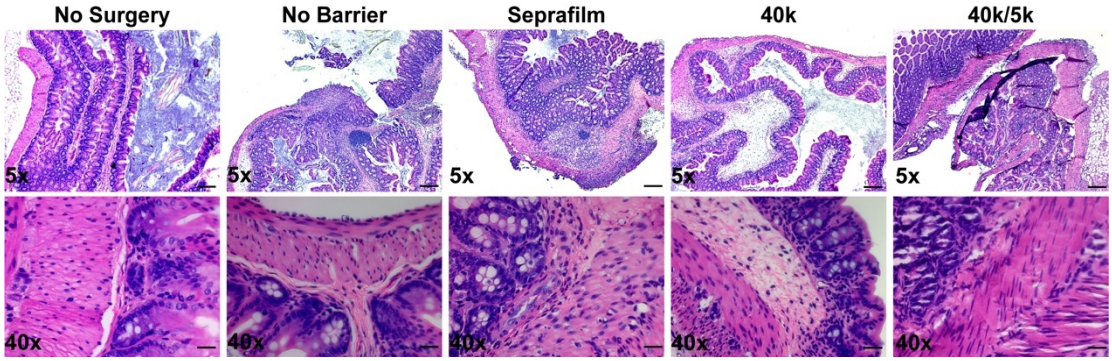

Figure 4.9. Supplementary histological image comparison of clinical Seprafilm control to neat and blend PLCL in mouse cecal ligation model of abdominal adhesions.
Additional histological cross sections of mouse cecum for (i) no surgery, (ii) no barrier, (iii) Seprafilm, and (iv and v) poly(L-lactide-co-caprolactone) (PLCL) treated groups post-cecal ligation at t = 7 days. Scale bars = 200μm (top row) and 20μm (bottom row). Adapted with permission.[2] Copyright 2022, Wiley.

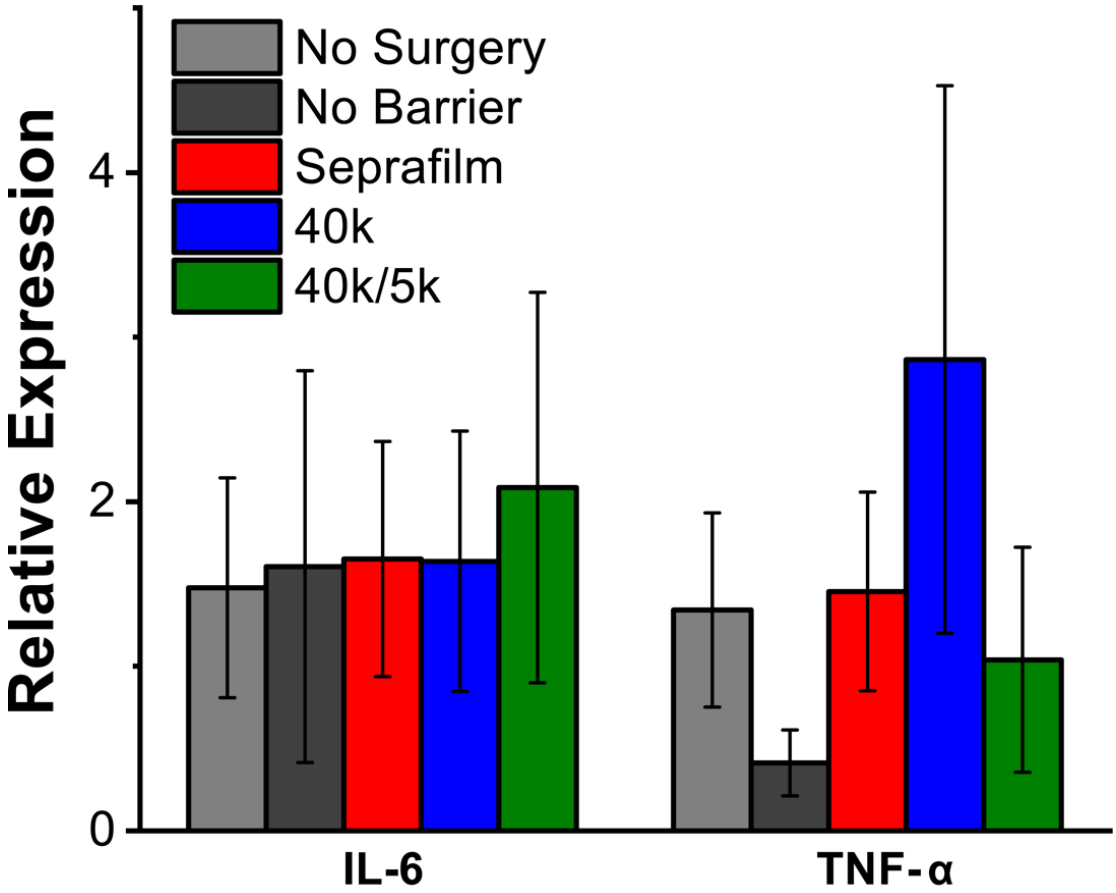

Figure 4.10. Supplementary wound healing gene expression comparison of clinical Seprafilm control to neat and blend PLCL in mouse cecal ligation model of abdominal adhesions.
mRNA expression levels measured via RT-PCR of interleukin-6 (IL-6) and tumor necrosis factor-α (TNF-α) for no surgery, no barrier, Seprafilm, and poly(L-lactide-co-caprolactone) (PLCL) treated groups post-cecal ligation at t = 7 days (n = 4-5). Data is plotted as mean ± s.e. Asterisks indicate statistical significance: * $p < 0.05$; ** $p < 0.01$; *** $p < 0.001$. Adapted with permission.[2] Copyright 2022, Wiley.

4.4 Discussion

An ideal adhesion barrier is one that is easily applied, biodegradable, facilitates complete wound healing, and prevents contact between injured surfaces while allowing for normal healing to occur. Here, we demonstrate that molecular weight blends of PLCL, a surface eroding polymer, permit facile in-situ spray deposition of a flexible adhesion barrier while adequately adhering to wet tissue in a dynamic abdominal space. Sprayable "no touch" fiber deposition with SBS addresses practical concerns about

imprecise application that surgeons encounter with currently available clinical adhesion barriers. Flexible and viscoelastic PLCL blends address further concerns about brittleness and durability. A biocompatible (**Figure 4.6A**) 40k/5k PLCL molecular weight blend yields a barrier that is not only a surface eroding material with an equivalent degradation rate over 14d tuned exactly to fibrotic scar tissue deposition (**Figure 4.2C**), but also improved wet tissue adherence and tensile elasticity when compared with neat high molecular weight components (**Figure 4.4**).

Advantages of solid adhesion barriers include an ability to withstand dynamic shear forces frequently present in-vivo due to intestinal peristalsis or shifting of organs. Hydrogel based clinical barriers such as Seprafilm are hydrophilic and present surface properties capable of delaying a fibrotic response via reduction of tissue-tissue contact time. Seprafilm was chosen as the clinical control for in-vivo studies. However, these cellulose-derived dressings are inherently brittle prior to swelling due to their crystallinity, and lose significant adhesive and cohesive strength after swelling.[198,199] Additionally, Seprafilm and other synthetic hydrogel-based materials may impede wound healing and are especially difficult to use in abdominal surgery, resulting in limited usability in clinical settings.[200–203]

Both neat 40k and 40k/5k blend compositions of PLCL exhibited an ability to reduce abdominal adhesions severity in a cecal ligation mouse model versus no barrier saline and Seprafilm controls, with 40k/5k in particular demonstrating statistical significance (**Figure 4.6C-D**). In addition to having less-severe adhesive disease as denoted by our

clinical scoring rubric (**Figure 4.6B**), mice treated with polymer had a decreased overall level of inflammation, as qualified through visible accumulation of inflammatory exudate by a blinded surgeon during clinical assessment. Though polymer groups were scored as having less-severe disease when compared with the current FDA-approved adhesion barrier Seprafilm, analysis of the gene expression of collagens I and III demonstrated equivalence between the Seprafilm and polymer groups with respect to wound healing extent, as all three groups displaying decreased levels versus no barrier saline controls (**Figure 4.8**).

Extent of fibrosis was assessed via histology and quantification of wound healing gene expression, where expression levels across controls and treatment groups were similar, with the exception of a significant decrease in angiogenic growth factor VEGF-A for 40k/5k blend PLCL versus no barrier and Seprafilm controls (**Figure 4.8**). The significance of these findings, and implications for adhesion formation and healing, is not entirely clear. Perhaps assessment at t=7d, when the majority of initial fibrin remodeling had concluded, accounts for the absence of major differences. VEGF-A could potentially be involved in angiogenic processes during both adhesion formation and normal tissue healing.

4.5 Conclusions

The most common adhesion barriers currently utilized in surgery are hydrogels like Seprafilm, due to their fast biodegradation and ability to interface with tissue in a biocompatible fashion. These dressings are often brittle and fracture during application,

resulting in placement of irregular fragments that are difficult to apply and frequently fail to adhere to the intended tissue site. This work demonstrates that PLCL molecular weight blends are an effective and tissue adhesive adhesion barrier material, preventing fibrosis through controlled polymer surface erosion. Spray deposition of such solid barriers via SBS allows for simple and rapid application of a conformal biomaterial with substantial cohesive and adhesive strength. The use of PLCL blends as an adhesion prevention tool is effective in reducing adhesion severity and facilitating complete wound healing as evidenced in a cecal ligation mouse model. Future studies should explore the effects of surface eroding polymer formulations on tissue healing, as these polymers have the potential to both prevent leakage by sealing tissues while also inhibiting adhesion formation.

Chapter 5: Biodegradation Driven Release of a Therapeutic Peptide in Sprayable Surgical Sealant for Prevention of Postoperative Abdominal Adhesions

5.1 Introduction

Adhesion formation is defined by the adjoining of traumatized and ischemic tissue surfaces exhibiting uncontrolled fibrogenesis, thereby leading to the deposition of dense, connective scar tissue. Such uncleaved fibrous "bridges" are frequently reported in the human peritoneum following surgical interventions as a result of injury to broad serous tissue with a surface area equivalent to that of skin.[152,187] Within the abdominal cavity, such tight connections are frequently presented through clinical pathologies such as small bowel obstruction and female infertility. When abdominal adhesions are symptomatic, surgical interventions of laparotomy are performed to separate adhesions for the acute symptoms, but are largely ineffective due to their increased tendency to reform, thereby necessitating exploration of novel barrier materials to prevent these occurrences.[192]

Prevalent commercial materials approved by the FDA include Seprafilm (Genzyme), a cellulose-derived hydrogel that begins as a dry "brittle" and "sticky" sheet-like film, thereby reducing its translational efficacy and ability to be applied to complex tissue surfaces in small organ spaces.[198,199] Upon swelling with aqueous peritoneal fluid, Seprafilm experiences a severe reduction in mechanical properties (90% loss in tensile strength) and rapidly degrades (~ 5 days) thereafter. [198] Pharmaceutical approaches to

counteracting adhesion formation have been investigated in the form of broadband anti-inflammatory agents such as nonsteroidal anti-inflammatory drugs[217,218] corticosteroids[219], and peritoneal dialysate[220]. These approaches utilize intravenous administration of the drug or an intraperitoneal (IP) dropwise application from a liquid suspension. Such non-specific therapeutic delivery mechanisms suffer from rapid clearance in the IP space whilst interfering with healing of injured mesothelium, thereby limiting translation of these liquid drug suspensions as effective adhesion barriers.[221–223]

Cargo release from implanted biomaterials is tuned through a combination of diffusion and degradation driven mechanisms as dictated by host matrix material properties.[224–226] Diffusive regulated release of drug is a physical process controlled through water-filled domains in various polymer structures (ex: hydrogels), with effective release rate controlled via network mesh size, thickness, or permeability. Degradation regulated release of drug is controlled through erosion of either the polymer surface or bulk. Surface eroding polymers present a unique opportunity for controlled drug delivery applications, as biodegradation kinetics are controllable since erosion rate exceeds the rate at which water penetrates the polymer. In contrast, bulk eroding materials yield less predictable release patterns, as water penetrates polymer faster than the rate at which hydrolytic biodegradation occurs homogenously throughout the system.

To develop a tissue adhesive adhesion barrier that is easily applied and undergoes continual degradation coinciding with adhesion formation, we investigate deposition

of molecular weight blends of surface eroding polymers via solution blow spinning (SBS). Previous research from our group has investigated use of SBS for deposition of an abdominal adhesion barrier[2], intestinal anastomosis sealants[18,99,173], antimicrobial burn wound dressings[12], hemostats for traumatic bleeding[100], and wet tissue adhesives[1,57]. In research recently published from our group, we successfully tuned biodegradation rate of a surface eroding polymer in poly(lactide-co-caprolactone) (PLCL) through combination of cohesively strong, slowly degrading high molecular weight (HMW) and adhesively strong, rapidly degrading low molecular weight (LMW) constituents.[2] Over a 14-day period in a pre-clinical mouse model of abdominal adhesions, we successfully reduced the severity of fibrotic scar tissue deposition in a mouse model due to continual, linear biodegradation (~50% at t=14d) occurring at the surface with a select PLCL blend, thereby preventing adsorption of fibro- and angio-genic molecules (i.e. fibrin) over the time course for adhesion formation (~14 days). We additionally presented mechanical characterization of our material, exhibiting both cohesive, tensile strength and wet tissue, pull-apart adhesive strength necessary for *in vivo* implantation and retention at the site of application.

Herein, we explore the use of kinetically tuned polymer surface erosion for controlled release of an apolipoprotein-derived therapeutic in treatment of abdominal adhesions. Apolipoproteins are amphipathic small molecules that bind lipids together in a lipoprotein structure allowing for transport of cholesterol and fatty proteins. A specific isoform in apolipoprotein E (ApoE) has presented immunomodulatory ability via lowering of inflammatory infiltrates in neurodegenerative diseases and intestinal

pathology models.[227–229] Through inhibited T-cell activation and a type I inflammatory response, mimetic peptides of ApoE have been pursued in efforts to enhance receptor binding affinity and immunosuppression.[230–232] An ApoE mimetic oligopeptide, COG133, is selected due to its an anti-inflammatory behavior fostered by an ability to downregulate pro-inflammatory cytokines such as NF-κB[233] and IFNγ[234] via binding to low density lipoprotein (LDL) receptors. First, mechanical testing and in vitro drug release studies of PLCL molecular weight blends containing COG133 were used to determine if adhesion barrier material would not only function as an effective defect sealant in a proposed animal model, but also if the therapeutic peptide is controllably released in an effective and biocompatible window. COG133-loaded PLCL blend adhesion barriers were then studied in an *in vivo* mouse cecal anastomosis model of assessment adhesion severity to determine its effect as an adhesion barrier material.

5.2 Materials and Methods

Polymer and Polymer-Drug Solution Preparation

Neat polymer solutions were prepared by dissolving 20% (w/v) concentration in ethyl acetate. Drug loaded polymer solutions were prepared by initially dissolving COG133 in dimethyl sulfoxide (DMSO) (1mg COG133 / 120μL DMSO), diluted with ethyl acetate to either .2% or .4% (w/v), then an appropriate amount of polymer added as to reach a 20% (w/v) of polymer in total solvent. This amount of COG133 loading was selected on the basis of in vitro data characterizing the drug's concentration dependent immunological behavior.[234] Amount of COG133 loaded into SBS solutions was determined based on where differences in cytokine expression in vitro were presented

in a concentration range of 3–30 μM. Mol amounts of COG133 (~10^{-7} mol) were extrapolated and fit to maximum amount of COG133 available per SBS spray deposited adhesions barrier (500 μL) in mouse cecal ligation and anastomosis experiments, an amount both immunomodulatory and sufficient to seal sites of anastomosis and ligation. Previous research investigations have presented appreciable biocompatibility of SBS fibers deposited from this solvent.[12,18] Both neat polymer solutions and drug loaded polymer blends comprised of neat poly(D,L-lactide-co-caprolactone) (PLCL) were investigated for pure "high" molecular weight (HMW) compositions defined as 40k PLCL (70:30 L:CL, acid endcap, Mn 35,000-45,000 Da, Akina) or 80k PLCL (70:30 L:CL, acid endcap, Mn 75,000-85,000 Da, Akina) and blends including "low" molecular weight (LMW) 5k PLCL (70:30 L:CL, acid endcap, Mn 1,000-5,000 Da, Akina) or 20k PLCL (70:30 L:CL, acid endcap, Mn 15,000-25,000 Da, Akina). Polymer blends were mixed in 70:30 mass ratio for a total of four blends of 1) 80k/20k, 2) 80k/5k, 3) 40k/20k, and 4) 40k/5k, where the leading component in the abbreviation is the majority (i.e. 70%) component of the blend and the secondary is in minority (i.e. 30%). This ratio was selected as to remain in the material regime of published work using PLCL molecular weight blends for pressure sensitive tissue adhesive (PSTA) applications where multiple ratios were studied.[1,57] An airbrush (Master Airbrush, G222-SET, 0.2 mm nozzle diameter) was used to deposit the solutions as dry, conformal polymer fibers. The airbrush was connected to a compressed CO_2 tank equipped with a pressure regulator set to 20 psig. Deposited polymer neat polymer and drug-loaded polymer mats were imaged as-is using a stereo optical microscope (AmScope).

Cell Viability

Cytotoxicity of drug-loaded polymer compositions was tested against L929 mouse fibroblasts by elution method as described by ISO-10993-5.[211] 40k/5k PLCL blend and neat 40k PLCL compositions loaded with either .2% or .4% COG133 were sprayed onto sterile 22 mm by 22 mm glass coverslips. The polymer mats were then removed from the coverslips and eluted at mass concentration of 10 mg/mL in culture media of Dulbecco's modified Eagle medium supplemented with 10% fetal bovine serum (Gemini Bio-Products Inc.), L-glutamine and 1% penicillin and streptomycin at standard conditions (37ºC, 5% CO2) for 24 hours. The elutions were then diluted to 1x, 10x, and 100x dilutions, and cell viability was tested against the different dilutions.

L929 fibroblasts (10^5 cells/mL) were then plated into 96-well plates at 100uL per well and incubated for 24 hours under standard conditions. The culture media was then removed by pipette. Wells were then treated to control (standard media), 25 ug/mL puromycin, or diluted elutions of 40k/5k PLCL blend and neat 40k PLCL loaded with COG133. This measurement was repeated five times for each diluted elution (n = 5).

COG133 Standard Curve and Release Testing

In vitro release of COG133 was quantified through the use of a ninhydrin stain of terminal lysine residues in the drug's peptide sequence (Leu-Arg-Val-Arg-Leu-Ala-Ser-His-Leu-Arg-Lys-Leu-Arg-Lys-Arg-Leu-Leu), thereby producing a concentration dependent colorimetric response. Initial solutions were made via dissolution of 1mg of COG133 in 1mL phosphate buffered saline (PBS) as to make a 461µM stock (A),

followed by creation of a 25µM stock (B) through mixing of 10.845µL of 461µM stock with 189.155461µL of PBS, and a 2% (w/v) ninhydrin solution in excess (C). PBS (D) was used in dilutions and creation of a standard curve in a 96 well plate and a 200µL working volume for each concentration, as described in the **Table 5.1**.

Table 5.1. Recipe for COG133 standard curve as created in a 96 well plate. (A) 461µM COG133, (B) 25µM COG133, (C) 2% ninhydrin, and (D) phosphate buffered saline (PBS).

Standard Curve Concentration (µM)	A (µL)	B (µL)	C (µL)	D (µL)
250	108.46	0	75	16.54
150	65.076	0	75	43.384
100	43.384	0	75	81.616
75	32.54	0	75	92.46
50	21.692	0	75	103.31
25	10.85	0	75	114.15
10	0	80	75	45
5	0	40	75	85
1	0	8	75	117
0.5	0	4	75	121

The plate was then sealed and placed in a 60°C for 20 minutes as to facilitate amine-ninhydrin binding yielding a purple-hue color change. Absorbance of each sample was read at 570nm on a SpectraMax M2e Microplate Reader (Molecular Devices) and analyzed through SoftMax® Pro 7 (Molecular Devices) and a standard curve was extrapolated.

As described in a previous section, COG133 loaded PLCL solutions were synthesized and sprayed onto sterile glass coverslips and sectioned into ~10mg pieces as to fit within wells of a separate 96 well plate, with masses recorded for each section. The

plate was then placed in a 37°C oven for 15 minutes to help facilitate the material's glass transition (**Figure 5.4**). The plate was then removed and 200µL of PBS pipetted into each well, followed by sealing of the plate with parafilm and electrical tape, and placed back in the 37°C oven for 2 hours. After this time, the plate was removed from the oven and 125µL of supernatant - containing degraded PLCL and eluted COG133 - transferred to a separate 96 well plate and remaining supernatant in sample wells was discarded. 200µL of PBS was then replenished in each sample well, the plate sealed in the same fashion, and placed back in a 37°C oven for testing release at later time points. 75µL of excess 2% ninhydrin solution was pipetted into each supernatant containing well, and the plate sealed once again with parafilm and electrical tape. The plate was then placed in a 60°C for 20 minutes and absorbance read at 570nm for each well. These steps were then repeated as above for additional time points of 8 hours, 18 hours, 24 hours, 3 days, 7 days, and 14 days. Background signal in absorbance spectra was calculated through samples of PLCL without COG133 and then subtracted from analyte signal.

To calculate release of COG133 from PLCL samples, each absorbance value obtained from supernatant was first normalized to mass (g) of polymer, and then multiplied by 1.6x to account for the difference in elution (200µL) and sampling (125µL) volume in procedure. Absorbance values for polymer only elutions were then subtracted from COG133 containing elutions as to obtain a background-subtracted absorbance value. This extrapolated absorbance value was then referenced against the created standard curve and multiplied by the sample volume (200µL) as to obtain nmol of COG133

eluted from each PLCL sample that were then averaged (n=>10). Cumulative release and percent release were then plotted as averages and plotted with pooled standard deviations as an error metric.

Burst Pressure Testing

Porcine small intestine purchased from a local butcher was cleaned with water and cut into 20 cm segments prior to use. For testing, the small intestine segments were rehydrated and heated to 37°C by soaking in 37°C phosphate buffered saline (PBS) for two minutes, followed by exposure to 37°C ambient air for four minutes, repeating this process twice, and finally drying with gauze (Fisherbrand). Once rehydrated, a half diameter incision was made to simulate a leaky anastomosis and the ends of the tissue were closed with zip ties. Approximately 1 mL of polymer solution was deposited directly onto the intestinal tissue at the site of the anastomosis using the SBS process. For cyanoacrylate, 500 µL of adhesive was applied. For Seprafilm, a 1cm x 1cm section was gently placed on the incision. After applying the adhesive, the sealed intestine was allowed to set for 15 minutes at 37°C in ambient air.

Once the adhesive was set, the intestine was connected to the burst pressure testing set up. A syringe was used to inject 1x PBS dyed with 0.05% (w/v) methylene blue into the intestine at a constant rate using an 18-gauge needle. A digital pressure gauge was attached to the injection line using a three-way stopcock to measure the injection pressure. The maximum pressure prior to bursting or leakage was recorded as the burst

pressure. The entire test was captured on video so that the failure mode could be determined. Each adhesive was tested five times (n = 5).

Oscillatory Shear Rheology

Oscillatory shear rheology data was collected using an AR2000 stress-controlled rheometer (TA Instruments). Polymer samples were collected on a glass slide, transitioned at 37°C for 15 min, and then transferred to a parallel plate geometry (diameter = 8 mm) of the AR2000. Frequency sweeps from 0.01 to 100 Hz were run at a constant 1% strain at 25°C. The storage modulus (G'), loss modulus (G''), and complex viscosity (η*) were recorded as functions of frequency in this test, with tan(δ) was calculated as a ratio of G'' to G'. We thank Dr. Srinivasa Raghavan for allowing us the use of the rheometer in his lab and Nikhil Subraveti from this lab for assistance with the rheological measurements.

Differential Scanning Calorimetry

Neat polymer and drug-loaded polymer samples were sealed in aluminum hermetic pans (TA Instruments) using a sample encapsulation press. DSC measurements were made on a TA Instruments DSC 2500. Samples were held isothermal at −50 °C for 5 min and then heated and cooled from −50 to 80 to −50 °C, at a rate of 3°C/min, ±1 °C amplitude, with a modulation period of 60s for two continuous cycles. Glass-transition temperature (T_g) was calculated using the tangent intersection method.

Mouse Cecal Anastomosis and Ligation Models

All animal procedures were approved by the Children's National Hospital Institutional Animal Care and Use Committee (IACUC protocol #00030703), and the animals were treated in accordance with PHS Policy on Humane Care and Use of laboratory Animals, the National Institute of Health Guide for the Care and Use of Laboratory Animals, and the Animal Welfare Act. Forty, 7-15 week-old C57BL/6 female mice were used (Jackson Laboratory). Mice were randomized into groups based on treatment group. Normal saline injection was used as a negative control, while Seprafilm® (Genzyme) was used as an anti-adhesions control in the cecal anastomosis model, and .1% COG133 dissolved in PBS was used as a drug-only control in the cecal ligation model. Experimental endpoint was 7 days after surgery with a total of five mice (n =5) allocated per group. Polymer solutions of 40k/5k PLCL blend and neat 40k PLCL loaded with either .2% or .4% COG133 were made under sterile conditions in a biosafety cabinet, and later sterilized by UV irradiation in their respective vials. Prior to surgery, a dedicated airbrush was sterilized with ethanol and placed under UV radiation along with polymer solutions.

All mice were anesthetized with a 100 mg kg^{-1} ketamine and 10 mg kg^{-1} xylazine solution (0.1 mL / 10 g mouse mass). After anesthesia, the mice were positioned supine, and skin prepped with betadine solution. In sterile fashion, a 1 cm laparotomy incision was made at the midline. After dissection into the abdominal cavity, the cecum was exposed either ligated with 4-0 Vicryl® Suture (Ethicon) approximately 1cm from distal end in the cecal ligation model or transected to the mesenteric attachment and

then repaired with four symmetrically spaced 7-0 Vicryl® sutures in the cecal anastomosis model. In the case of normal saline injection or .1% COG133 administration, cecum was placed back into the abdominal cavity and 0.1 mL of solution was dripped onto ligated or anastomosed cecum. For the Seprafilm control group, the cecum was placed back into the abdominal cavity and a 1cm square section gently placed on top of either ligated cecum or sutured midline incision of anastomosed cecum. For neat and drug loaded polymer treatment groups, 0.5 mL of solution was sprayed onto ligated cecum or sutured midline incision of anastomosed cecum prior to replacement in abdominal cavity. Upon reinsertion of cecum, skin was closed using 4-0 Vicryl® Suture (Ethicon) in a running fashion, and approximately 0.1 mL buprenorphine was given as an analgesic at the end of the surgery.

Each animal was weighed both pre-operatively and at 7 days after initial surgery prior to euthanasia. After euthanasia, midline laparotomy was performed, and images of the abdominal cavity were taken. The abdominal space was then examined by a surgeon who was blinded to treatment groups and assessed for adhesions formation with scores on a Mazuji-derived scale assigned to each attached organ pair, as well as signs of inflammation and degradation of polymer sample.[212]

Following assessment, cardiac puncture was also performed for serum cytokine assessment. Whole blood was collected via sterile syringe and 25-gauge needle to determine cytokine levels in the serum. In sterile, uncoated vials, blood was allowed to clot over 15 minutes, then serum extracted from supernatant after centrifugation for 15

minutes at 4°C and 2000 RPM. Serum was stored at –80°C until MSD analysis for IFN-γ, IL-1β, IL-2, IL-4, IL-5, IL-6, KC/GRO, IL-10, IL-12p70, and TNF-α. Analysis was performed using an MSD MULTI-SPOT™ Assay kit (Proinflammatory Panel 1 (mouse), V-PLEX, Invitrogen, NY) on serum samples in triplicate. Serum concentrations were interpolated from calibrator standard curves.

Histological Analysis

Ligated and anastomosed cecal tissues were harvested on postoperative day 7 and kept in 10% neutral buffered formalin until histological processing (Histoserv Inc.), then embedded in paraffin wax. Five μm sections were prepared, fixed onto glass slides, and stained with hematoxylin and eosin (H&E). Digital images of the histology slides were taken with TissueScope LE (Huron Digital Pathology) at 5x and 40× magnification then the 40x images were exported for analysis intestinal wall cellularity. One section per mouse, with 5 separate low-powered and high-powered fields of view were imaged per section. Using ImageJ (National Institutes of Health), images were scaled to 1 μm/pixel and converted to an RGB stack. A threshold of 100 was set, and the percent area of the image stained purple was obtained for each image. These percentages were then averaged for each mouse.

Wound Healing Gene Expression

RNA was extracted from frozen cecal tissue using Trizol reagent (Life Technologies, Frederick, MD). In all experiments, 6 μg RNA was used to synthesize first strand cDNA using High-Capacity cDNA Reverse Transcription Kit (Life Technologies).

Real-time PCR was performed using TaqMan® Gene Expression Master Mix (Life Technologies) in a QuantStudio7 Flex RT-PCR system (Thermo Fisher Scientific, Waltham, MA), according to the manufacturer's instructions. Reactions were performed in triplicate, including no template and endogenous control using GAPDH. Gene-specific assays were Mm00434228_m1 for Il1b, Mm0046190_m1 for Il6, Mm00443258_m1 for Tnfa, Mm00437306_m1 for Vegfa, Mm01178820_m1 for Tgfb1, Mm00433287_m1 for Fgf2, Mm00801666_g1 for Col1a1, Mm00802305_g1 for Col3a1, and Mm99999915_g1 for Gapdh (Life Technologies, Thermo Fisher). Changes in relative gene expression normalized to GAPDH levels were determined using the ΔΔCt method. First, the difference between the Ct values (ΔCt) of the gene of interest and the housekeeping gene was calculated for each sample. Then the ΔCt values for the control samples were averaged. The difference in the ΔCt values between each experimental sample and the control sample (ΔΔCt) was calculated. The fold-change in expression of the gene of interest compared to the housekeeping gene for each sample was calculated as $2^{-\Delta\Delta Ct}$, and the results were averaged for graphical representation.

Statistical Analysis

Statistical analysis was performed on Origin (OriginLab). Typically, one-way ANOVA was used to compare group variation, followed by post-hoc pairwise Tukey comparison to determine significant differences between the groups. Typically, averages were plotted with error bars representing standard error. Asterisks are used to indicate statistically significant differences: * = $P < 0.05$, ** = $P < 0.01$, *** = $P < 0.001$. If no

asterisks are shown, there are no significant differences amongst the groups. Real-time PCR results were analyzed using t-tests comparing the ΔΔCt values.

5.3 Results

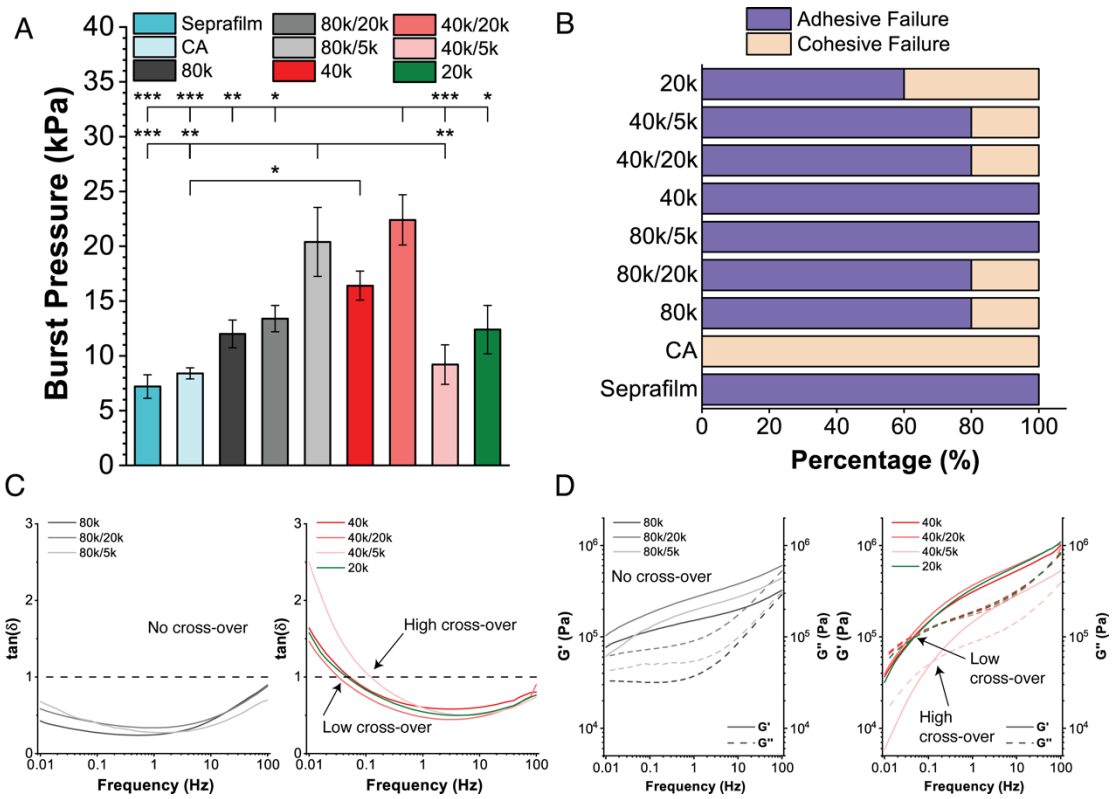

Figure 5.1. Ex vivo porcine intestinal burst pressure and in vitro rheological properties of neat and blend PLCL.
(A) Ex vivo burst pressure on porcine intestine using spray deposited poly(lactide-co-caprolactone) (PLCL) blend, Seprafilm, and cyanoacrylate (CA) as sealant materials (B) Failure mode of samples in burst pressure testing (n=5). (C, D) Oscillatory shear rheology of PLCL blends showing the shift toward liquid-like properties with inclusion of 5k PLCL. (C) Plot of tan(δ) highlights the shift towards a high tack material and ability to flow under pressure at ~0.1 Hz. Storage (G′) and loss (G″) modulus (D) across a frequency range encompassing long time scales (0.1 Hz−1 Hz) and short time scales (1 Hz−100 Hz) qualifying material tack and peel strength, respectively. Data is plotted as mean ± s.e. Asterisks indicate statistical significance: * $p < 0.05$; ** $p < 0.01$; *** $p < 0.001$. Data collected in lab of Dr. Srinivasa Raghavan and initial training by Nikhil Subraveti.

Viscoelastic behavior of PLCL molecular weight blends was studied by SBS deposition of polymer fibers mats and preparation for oscillatory shear rheology, where storage modulus (G'), loss modulus (G''), and tan(δ) (ratio of G'' to G') are reported for a range of frequencies. The same compositions were also tested for sealant efficacy with ex vivo porcine intestine hydrated to 37°C measuring burst pressure of a sealed partial

incision as well as mode of failure. Blending of LMW and HMW PLCL into a composite polymer fiber mat presents an opportunity to concretely tune mechanical properties of cohesive and adhesive strength to clinical need. Our previous work effectively quantified relative differences in both tensile (i.e. cohesive) and pull-apart (i.e. adhesive) strength of neat and blend PLCL.[2] Here we further clinical applicability for a surgical sealant application via burst pressure analysis.

80k/20k and 40k/20k PLCL blends present the highest values of burst pressure across the board (~20 kPa) because of the ability of HMW chains to resist inflationary forces, and the LMW chains to adhere to wet porcine intestinal tissue (**Figure 5.1A,B**) Shear rheology experiments demonstrate that all 80k PLCL containing materials exhibited solid, highly elastic ($\tan(\delta) < 1$) behavior across long and short time scales of shear (**Figure 5.1C,D**). Conversely, 40k PLCL containing blends presented distinct elastic and viscous dominated regimes with a $\tan(\delta)$ transition at 0.07-0.1 Hz, with 40k/5k PLCL presenting a more expansive regime in which viscous, liquid-like forces dominate, as quantitatively expressed through high G'' and low viscosity values (**Table 5.2,5.3**). Such behavior provides rationale as to the lower burst pressure (~9 kPa) presented by 40k/5k PLCL relative to other PLCL blends, but not one that is lower than clinical Seprafilm (~7 kPa) and highly adhesive cyanoacrylate (~8 kPa) controls, providing an avenue for its use in surgery as an adhesion barrier and surgical defect sealant material.

Table 5.2. Tan(δ) values of neat and blend PLCL for select frequencies set in oscillatory shear rheology.

tan(δ) (G''/G')					
	Frequency (Hz)				
PLCL Composition	*0.01*	*0.1*	*1*	*10*	*100*
80k	0.4267	0.2742	0.2454	0.4308	0.8954
80k/20k	0.5847	0.4036	0.3364	0.4574	0.8771
80k/5k	0.6814	0.3951	0.2767	0.3609	0.6986
40k	1.64	0.8512	0.606	0.6047	0.805
40k/20k	1.978	0.8866	0.5075	0.4406	0.6824
40k/5k	2.834	1.306	0.7177	0.5608	0.7267
20k	1.577	0.8311	0.5462	0.5193	0.7659

Table 5.3. Viscosity values of neat and blend PLCL for select frequencies set in oscillatory shear rheology.

Complex Viscosity, η* (Pa•s)					
	Frequency (Hz)				
PLCL Composition	*0.01*	*0.1*	*1*	*10*	*100*
80k	3.08E+08	2.34E+08	3.93E+07	1.70E+07	2.47E+06
80k/20k	1.43E+08	5.46E+07	2.90E+07	4.55E+07	3.01E+05
80k/5k	2.91E+08	2.97E+07	2.16E+07	2.16E+07	1.32E+06
40k	1.41E+07	1.21E+07	1.42E+06	2.86E+07	3.32E+06
40k/20k	7.40E+06	9.92E+06	2.16E+06	1.31E+07	7.85E+05
40k/5k	1.82E+06	4.01E+06	1.86E+06	7.47E+07	1.69E+05
20k	5.38E+06	1.87E+06	1.68E+06	1.83E+07	3.58E+05

In vitro release of COG133 from neat and blend PLCL was studied by loading drug into SBS polymer solution at amounts presenting anti-inflammatory behavior within in vitro cell culture.[234] Drug loaded polymer blends were then spray deposited, sectioned into individual ~10mg discs, and immersed in phosphate buffered saline (PBS) at 37°C within individual wells of a 96 well plate. Supernatant from each well was sampled at select time points over 14 days and tested for COG133 release via a ninhydrin solution measurement of absorbance at 570nm. The objective of this study was to determine

which formulations released an amount of COG133 sufficient to counteract rapid fibrotic tissue deposition presented in adhesion formation.

Depending on initial loading of COG133 into PLCL fiber mats, drug was proportionally released between 200-800 nmol COG133 for 40k-derived blends and 100-400 nmol COG133 for 80k-derived blends per gram of adhesion barrier applied after 14 days (**Figure 5.2B**). A twofold difference in release regimen is best explained through differences in both biodegradation rate as well as viscosity-induced diffusion limitations (**Figure 5.2A**). Biodegradation studies in our recent publication presented a linear biodegradation profile for 80k/5k and 40k/5k PLCL blends with a ~50% mass loss after 14 days.[2] However, all other neat and blend compositions yielded an initial burst in degradation, but effectively plateaued to only ~20% mass loss after 14 days. Diffusion limitations of COG133 through PLCL adhesion barriers are inferred through differences in complex viscosity at low frequency shear rates, where 80k containing PLCL blends present higher complex viscosity than 40k containing PLCL blends (**Figure 5.1C, Table 5.2**).

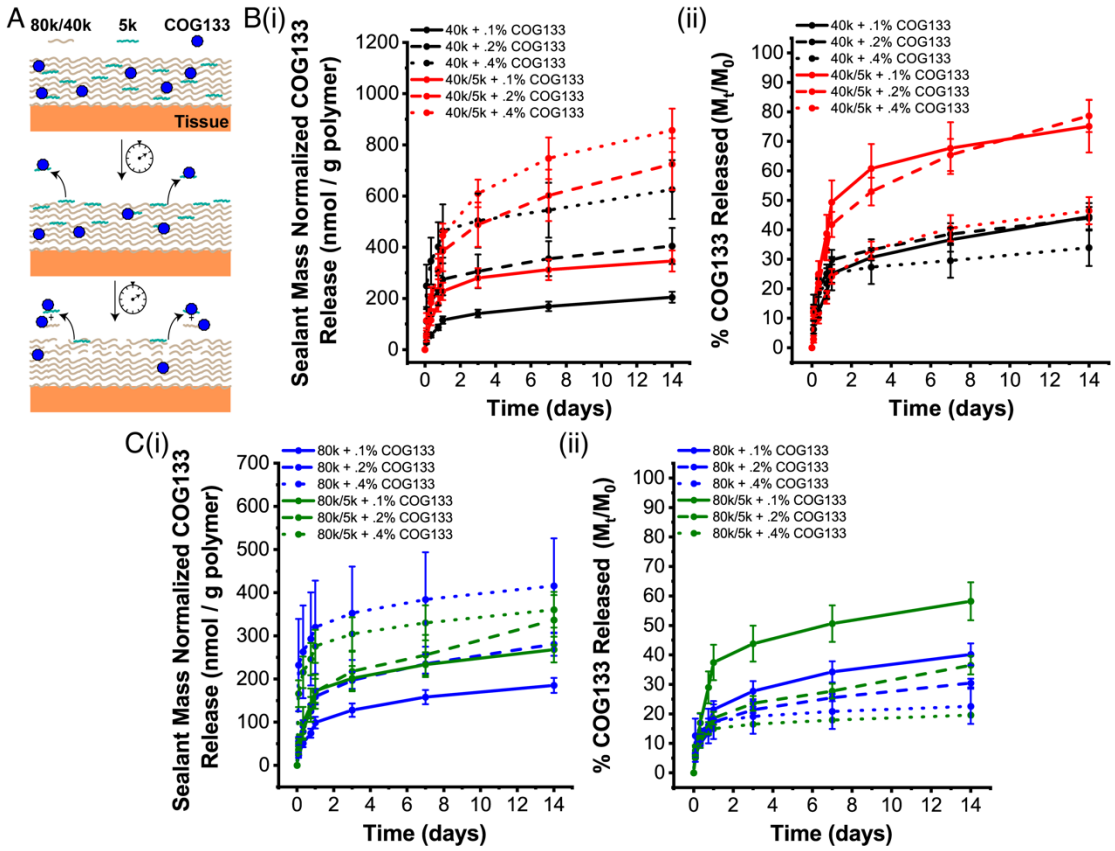

Figure 5.2. In vitro release of COG133 therapeutic from neat and blend PLCL.
(A) Schematic of surface erosion dependent release of COG133 from poly(lactide-co-caprolactone) (PLCL) fiber mats. (B,C) COG133 release over 14d occurs at a rate proportional to both degradation rate of PLCL blend and initial diffusion of drug loaded in fabricated polymer solution. 10mg polymer / sample (normalized) (n=>10) for each time point of release. Data is presented as mean ± s.d. Inclusion of low molecular weight 5k PLCL increased release rate due to increased polymer biodegradation rate. The release has a rapid burst of 20-45% of the loaded COG133 in the first 48h, a critical period in adhesions development.

Addition of COG133 into PLCL solution yields a film-like material– as opposed to a true fiber mat – due to plasticization of the polymer matrix and lowering of polymer glass transition temperature (T_g), thereby promoting cargo transport due to reduced crystallinity (**Figure 5.3-4**). Such a combination of material properties and drug loading amounts lead to large differences in amount of COG133 released from neat and blend PLCL. This is particularly highlighted in two scenarios leading to use of 40k/5k PLCL as a candidate adhesion barrier material : 1) .2% COG133 loading in 80k/5k (~30% at

t=14d) and 40k/5k (~80% at t=14d) PLCL blends, both of which undergo continual biodegradation over 14 days, and 2) .2% COG133 loading in 40k/5k PLCL released a congruent amount of drug after 14 days as comparted to .4% COG133 (~800 nmol / gram of polymer), despite having half the amount of drug in initial solution.

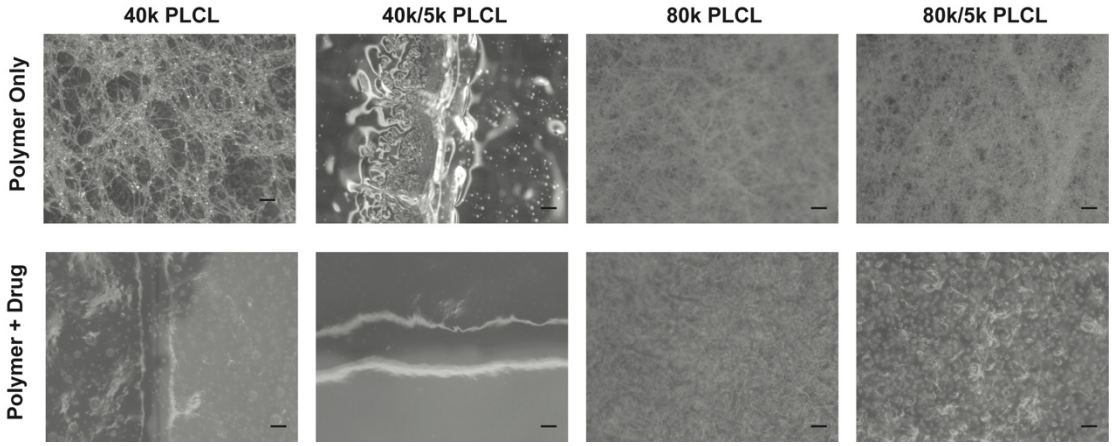

Figure 5.3. Optical microscopy of neat and blend PLCL containing .2% COG133.
Scale bar = 200µm.

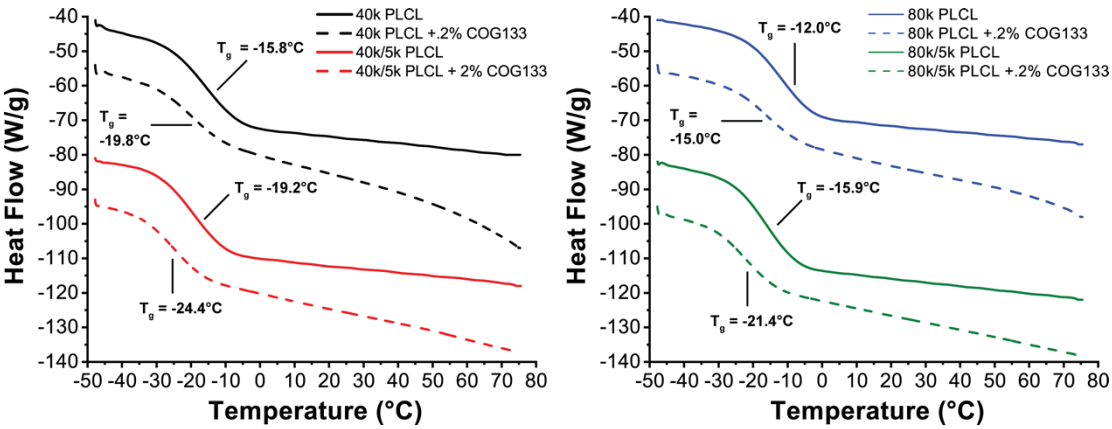

Figure 5.4. Thermal properties of neat and blend PLCL containing .2% COG133 measured via DSC.
Curves have been shifted for clarity of glass transition temperature (T_g).

Achieving biocompatible yet effective dosing of any therapeutic for in vivo applications is a study that need be performed prior to in vivo implantation. Research from our prior work shows an immunosuppressive effect of COG133 on dendritic cells and T-cells for a range of concentrations.[234] In the context of an adhesion barrier application, the effect of COG133 release from PLCL fiber mats on cell viability is imperative in wound healing. We therefore assessed toxicity of COG133 loaded 40k and 40k/5k PLCL blends. L929 mouse fibroblasts were treated with supernatant of degraded polymer-drug hybrid scaffolds. Across both polymer formulations, drug loading amounts there was no effect on cell viability, thereby indicating such compositions could be safely applied for an in vivo adhesion barrier application (**Figure 5.5A**).

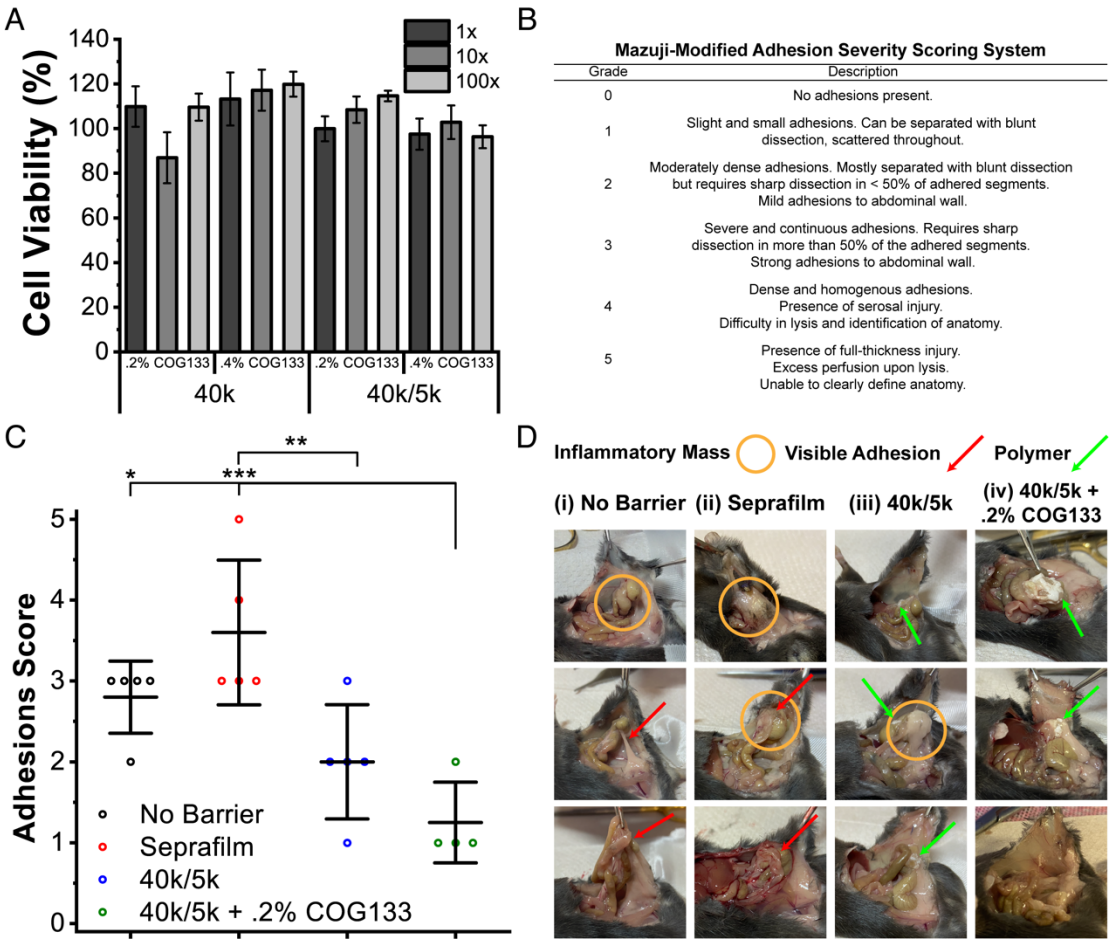

Figure 5.5. Severity scoring comparison of clinical Seprafilm control to neat and blend PLCL/COG133 in mouse cecal anastomosis model of abdominal adhesions.
(A) L929 mouse fibroblast cell viability (versus media only control) of neat and blended poly(L-lactide-co-caprolactone) (PLCL) containing COG133 for 1x, 10x, and 100x dilutions of treatment media. (B) Mazuji-derived adhesion scoring rubric used in clinical assessment. (C) clinical scores and (D) gross pathology for no barrier, Seprafilm, PLCL, and PLCL + COG133 treated groups post-cecal anastomosis at t = 7 d (n=5). 500 µL polymer solution / sample. Data is plotted as mean ± s.e. Asterisks indicate statistical significance: * $p < 0.05$; ** $p < 0.01$; *** $p < 0.001$. PLCL + COG133 groups showed increased significance versus empty and clinical controls in reducing adhesions severity.

Models of adhesion formation need to produce consistent levels of mesothelial tissue disruption. Abrasion of the peritoneum has been proposed as a model to induce adhesions, but is inconsistent due to the variable force applied by the operator.[214] Hence, cecal ligation and anastomosis models were used to explore the intensity of adhesion formation and the effect of barrier deposition in prevention. Following cecal

ligation, mice were treated with liquid droplets of .1% COG133 (free drug control), and SBS deposited 40k and 40k/5k PLCL polymer loaded with either .2% COG133 or .4% COG133 (treatment groups). In the case of cecal anastomosis, mice were treated with either saline (negative control), Seprafilm (clinical control), 40k/5k PLCL blend (polymer only control), or .2% COG133 loaded into 40k/5k PLCL blend (treatment group). In both animal models, adhesion formation and wound healing extent were assessed after 7 days. Mice that did not undergo either cecal ligation or cecal anastomosis were assessed as sham, no wound controls.

Implantation of COG133 loaded PLCL fibers in vivo necessitates toxicity assessment due to a combination of therapeutic concentration and polymer molecular weight dependent toxicity. Supernatant of degraded polymer fiber mats loaded with COG133 was used to treat L929 mouse fibroblasts (**Figure 5.5A**), with >85% cell viability for tested polymer-drug conjugates and their supernatant dilutions. This indicates that .2% and .4% COG133 concentrations loaded into 40k and 40k/5k PLCL solutions exhibit low toxicity and retain clinical utility as both an adhesion barrier and surgical sealant material.

In both mouse cecal ligation and anastomosis animal models, a surgeon was blinded to control and treatment groups, and assessed for adhesion severity using a Mazuji-derived scoring rubric (**Figure 5.5B**). Results of mouse cecal ligation evidenced effectiveness of .2% COG133 loaded into 40k/5k PLCL through a reduction in scored severity versus a .1% COG133 droplet, free drug control (**Figure 5.6**). Difference in

prevention efficacy in this study can be attributed to the controlled, yet nominally high release of COG133 from polymer adhesion barrier (**Figure 5.2B**) caused by favorable film-like morphology (**Figure 5.3**) and thermal properties (**Figure 5.4**), as well as wet tissue adhesive properties previously reported for pure 40k/5k PLCL.[2] This was followed up with a mouse cecal anastomosis model for assessment of both adhesions prevention efficacy and intestinal sealant ability (**Figure 5.5C-D**). Anastomosed mice with a 40k/5k PLCL + .2% COG133 applied barrier displayed a significantly lower score versus both no barrier and Seprafilm treated controls, whereas 40k/5k PLCL polymer-only control exhibited a statistically significant difference versus only Seprafilm treated mice.

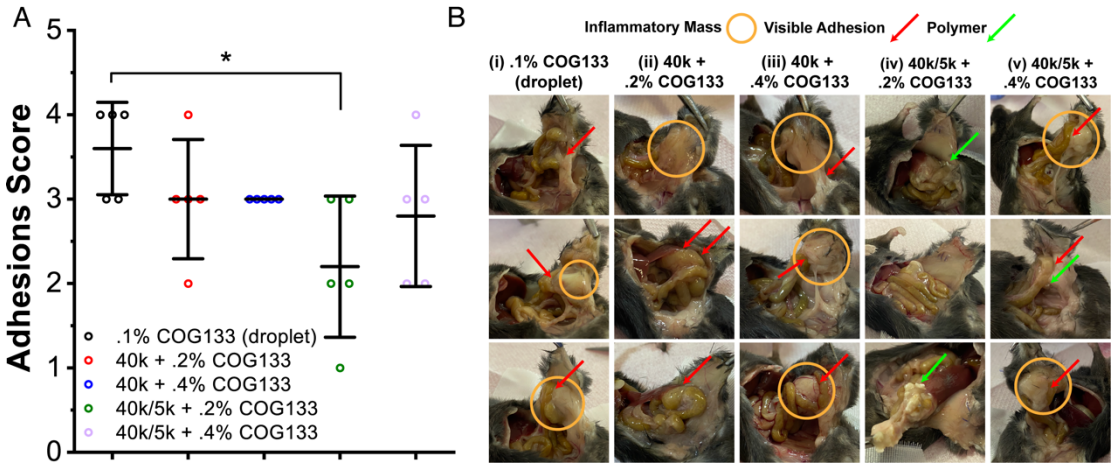

Figure 5.6. Severity scoring comparison of free drug COG133 control to neat and blend PLCL/COG133 in mouse cecal ligation model of abdominal adhesions.
(A) Clinical scores and (B) gross pathology for (i) COG133 only, and (ii-v) poly(L-lactide-co-caprolactone) (PLCL) + COG133 treated groups post-cecal ligation at t = 7 days. Data is plotted as mean ± s.e. Asterisks indicate statistical significance: * $p < 0.05$; ** $p < 0.01$; *** $p < 0.001$.

Adhesion formation is a process akin to wound healing through deposition of fibrotic scar tissue, thereby providing an avenue for additional severity assessment through

histology, gene expression, and cytokine analysis.[188–190] Cecal tissue was harvested as part of anastomosis studies at Day 7 and assessed for markers of inflammation concurrent with fibrosis and adhesion formation. Histological cross sections of harvested tissue presented markers of cellular infiltration across all control and treatment groups (**Figure 5.7A,B, 5.8**). Cellularity – a quantitative metric of inflammation – presented equivalent values for normal saline, Seprafilm, polymer only, and polymer with drug groups. However, all groups were markedly higher than the sham surgery groups as expected due to a foreign body response characteristic of biomaterials implanted in vivo.

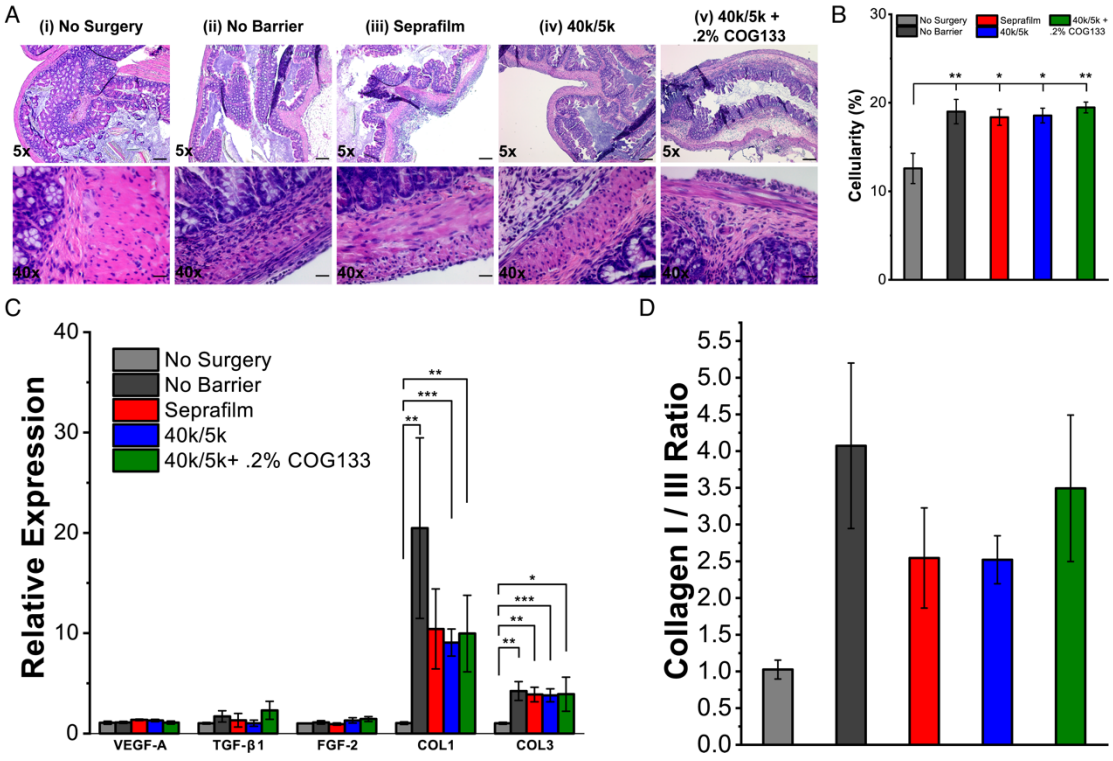

Figure 5.7. Histological image and wound healing gene expression comparison of clinical Seprafilm control to neat and blend PLCL/COG133 in mouse cecal anastomosis model of abdominal adhesions.

(A) Histological cross-sections and (B) cellularity of mouse cecum, and (C) mRNA expression levels measured via RT-PCR of vascular endothelial growth factor (VEGF-A), transforming growth factor-β1 (TGF-β1), fibroblast growth factor-2 (FGF-2), collagen I (COL1), and collagen III (COL3) wound

healing gene markers and (D) ratio of collagen I to III expression for (i) no surgery, (ii) no barrier, (iii) Seprafilm, (iv) poly(lactide-co-caprolactone) (PLCL) polymer-only treated, and (v) COG133 loaded PLCL groups post-cecal anastomosis at t = 7 days (n = 4–5). Scale bars = 200 μm (top row) and 20 μm (bottom row). Data are plotted as mean ± SE. Asterisks indicate statistical significance: *p < 0.05; **p < 0.01; ***p < 0.001.

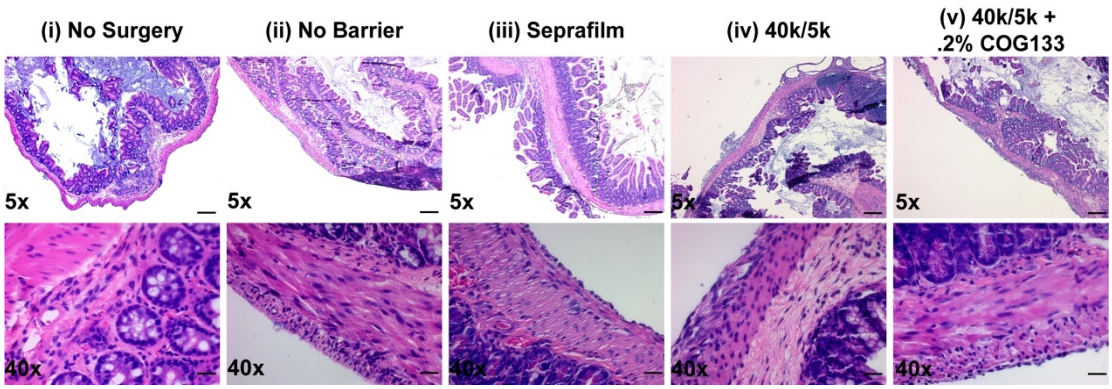

Figure 5.8. Supplementary histological image comparison of clinical Seprafilm control to neat and blend PLCL/COG133 in mouse cecal anastomosis model of abdominal adhesions.
Additional histological cross sections of mouse cecum for (i) no surgery, (ii) no barrier, (iii) Seprafilm, (iv) poly(L-lactide-co-caprolactone) (PLCL) only, and (v) PLCL + COG133 treated groups post-cecal anastomosis at t = 7 days. Scale bars = 200μm (top row) and 20μm (bottom row).

Further quantitative comparison of immune response to implanted Seprafilm, polymer only, and polymer with drug adhesion barriers to no treatment saline was studied in gene expression and cytokine levels. Wound healing gene expression of IL-6, TNF-α, VEGF-A, TGF-β1, FGF-2, collagen I, collagen III, and IL-1β were measured for cecum harvested from anastomosed mice at t = 7d via real-time PCR and compared to tissue from normal ("no surgery") mice (**Figure 5.7C, 5.10**). Levels of angiogenic (VEGF-A) and fibrogenic (TGF-β1, FGF-2) growth factors displayed no significant differences across control and treatment groups. Collagen I to Collagen III ratio is an indication of tendency to form rigid scar tissue through numerical comparison of ordered-to-disordered collagen fibrils, with values consistent across all groups (**Figure 5.7D**). Elevated levels of IL-6 and TNF-α – characteristic markers of inflammation – were particularly elevated in Seprafilm treated groups (**Figure 5.10**) and could provide

rationale into their higher score in clinical assessment (**Figure 5.5C**). Serum levels of inflammatory cytokines in IFN-γ, IL-1β, IL-2, IL-4, IL-5, IL-6, KC/GRO, IL-10, IL-12p70, and TNF-α was measured via MSD, displaying elevated levels of IL-6 and reduced levels of TNF-α for polymer only and drug loaded polymer adhesion barrier versus no barrier and Seprafilm treated mice (**Figure 5.9**). Elevated levels of IL-6 are expected for groups with deposited polymer, as IL-6 is a cytokine with implications in host defense and foreign body response.[235,236]

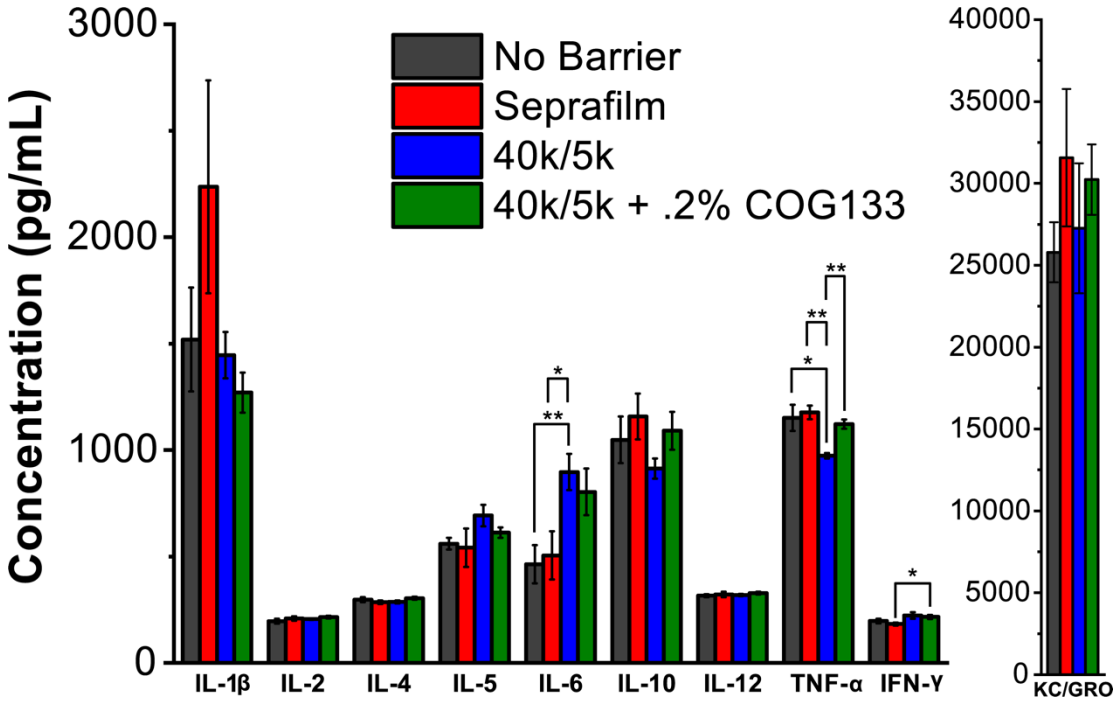

Figure 5.9. Serum cytokine comparison of clinical Seprafilm control to neat and blend PLCL/COG133 in mouse cecal ligation model of abdominal adhesions.
Serum concentrations of inflammatory cytokines measured via ELISA in no barrier, Seprafilm, PLCL, and PLCL + COG133 treated groups post-cecal anastomosis at t = 7 days (n=5). Data is plotted as mean ± s.e. * $p < 0.05$; ** $p < 0.01$; *** $p < 0.001$.

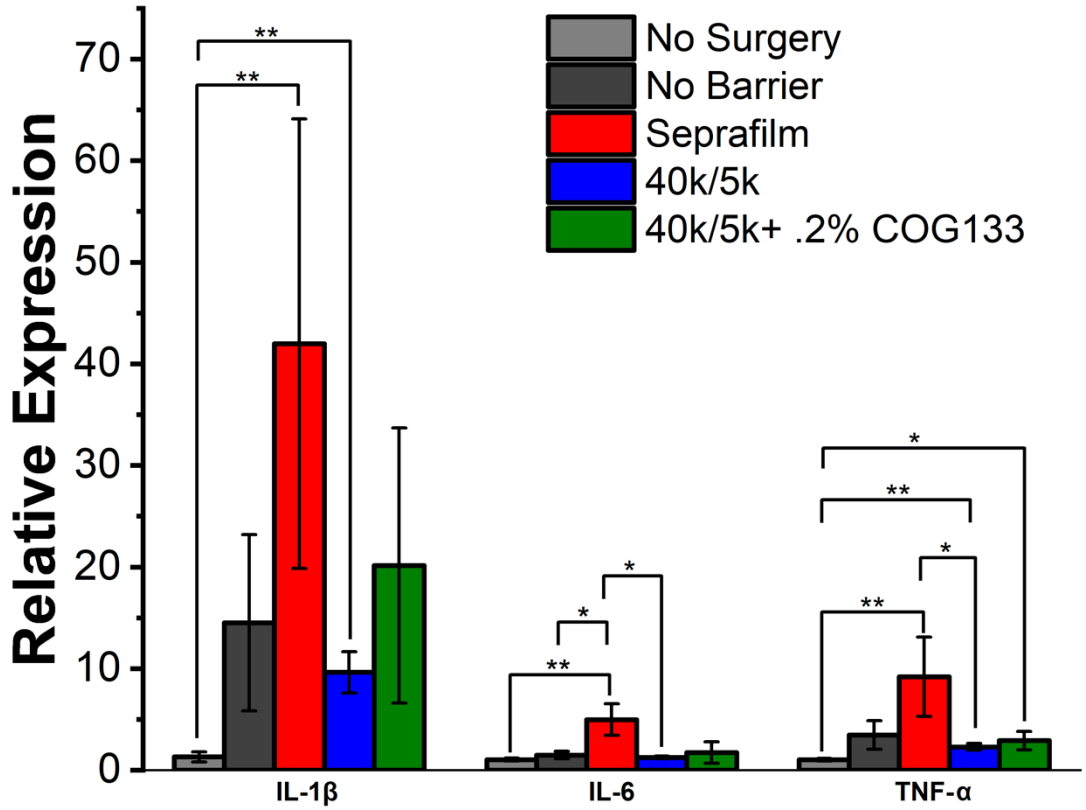

Figure 5.10. Supplementary wound healing gene expression comparison of clinical Seprafilm control to neat and blend PLCL in mouse cecal anastomosis model of abdominal adhesions. mRNA expression levels measured via RT-PCR of interleukin-1β (IL-1β), interleukin-6 (IL-6) and tumor necrosis factor-α (TNF-α) for no surgery, no barrier, Seprafilm, and poly(L-lactide-co-caprolactone) (PLCL) treated groups post-cecal ligation at t = 7 days (n = 4-5). Data is plotted as mean ± s.e. Asterisks indicate statistical significance: * $p < 0.05$; ** $p < 0.01$; *** $p < 0.001$.

5.4 Discussion

An optimal adhesion barrier is one that prevents deposition and maturation of inflammatory scar tissue, does not impair wound healing, and maintains mechanical properties necessary to remain at the site of application in vivo. Spray deposition of PLCL fiber mats provides an inherent clinical advantage versus a currently adopted material in Seprafilm, a pre-fabricated, dried hydrogel sheet. While interfacial lubrication is the proposed mechanism of prevention for the barrier, Seprafilm is brittle,

sticky and difficult to precisely place during surgery. Use of SBS allows for an operator to deposit flexible, polymer fibers with high conformability and adhesion to diverse tissue surfaces.

In this work we demonstrate the ability of a molecular weight blend of PLCL with tunable surface erosion behavior to release an immunomodulatory agent. Neat and blend PLCL compositions display a range of viscoelastic properties dictated by presence of HMW and LMW constituents. While LMW PLCL chains in the deposited fiber mat increase tackifying ability and spreadability across tissue substrates, they do not retain cohesive strength presented with HMW PLCL sufficient for in vivo implantation and retention at the site of application (**Figure 5.1B**). This leads to a range of burst pressure values for SBS deposited materials, but none lower than that of clinical Seprafilm or adhesive, toxic cyanoacrylate control (**Figure 5.1A**). The combination of favorable solid-like and liquid like-behavior lends itself to applications in which sealant efficacy is required.

A linear biodegradation profile is critical – rather than one that plateaus following an initial burst – for a drug eluting material in which surface erosion is a driving mechanism. Such behavior provides for continual release of therapeutic over the 14-days in which adhesion formation occurs. While previous research demonstrates an ability of select PLCL blends to consistently release polymer fragments and drug from its surface, viscosity-induced diffusion limitations also come under consideration.[2] Through diffusion of drug in the polymer matrix and degradation of the matrix itself,

drug release rate over a 14-day period is tunable through alternation of HMW and LMW molecular weight components (**Figure 5.2A**). Compositions containing 80k PLCL release half the nominal amount of drug relative to compositions containing 40k PLCL after 14 days (**Figure 5.2B,C**). Initial loading of COG133 also is found to play a role in the amount released, with .2% and .4% COG133 loading into 40k/5k PLCL blend releasing nearly the same nominal amount of drug after 14 days (**Figure 5.2B**). Such tunability in release profiles provides for an avenue of favorable adhesion barrier materials with an active mechanism of preventing adhesions as opposed to dropwise, topical administration of a drug in solution.

40k/5k PLCL blend loaded with .2% COG133 presented an ability to significantly reduce abdominal adhesion severity in a cecal ligation mouse model versus a free drug control (**Figure 5.6**), leading to its exploration in an additional mouse model. In a cecal anastomosis mouse model, pure 40k/5k PLCL and 40k/5k PLCL blend loaded with .2% COG133 both significantly reduced adhesion severity versus saline and Seprafilm treated controls, with the drug loaded polymer adhesion barrier in particular demonstrating a highly statistically significant decrease (**Figure 5.5C**). Follow up studies assessing expression of wound healing genes (**Figure 5.7**) and cytokines (**Figure 5.9**) present a similar response for saline, Seprafilm, polymer only, and drug loaded polymer groups. Although the findings of the molecular immune response studies and their implications on adhesion formation are not different between the groups, it is possible that the majority of fibrous matrix deposition and maturation has occurred when assessed at t = 7d.

5.5 Conclusions

Commonly deployed adhesion barriers in surgery, like Seprafilm, suffer from poor mechanical properties limiting their translational efficacy. As Seprafilm often fractures upon application to injured mesothelial tissue, it is uncertain whether the proposed mechanism of adhesion prevention is effectively facilitated. The findings reported here demonstrates that release of an anti-inflammatory therapeutic can be controlled through molecular weight blends of a surface eroding polymer in PLCL. Spray deposition of PLCL fiber mats not only provides for a material with a balance of solid-like and liquid-like behavior promoting high tissue adherence and ability to seal sites of adhesion formation, but also a host matrix for drug release that is easily tuned through material composition of SBS solution. Effectiveness of drug loaded polymer materials was exhibited in two distinct, high impact animal models for adhesion formation. Future studies should focus on use of different therapeutics for prevention of asymmetric scar tissue, assuring that a biocompatible, yet effective, release profile is achieved prior to in vivo implantation.

Chapter 6: Future Directions

Optimization of surface eroding polymer scaffolds for adhesion prevention and therapeutic release

Protein adsorption behavior of poly(lactide co caprolactone) molecular weight blends

Rapid, surface eroding polymers can not only provide the ideal release window for administration of anti-inflammatory therapeutics, but also limit adhesion formation through a desorption mechanism. Surface eroding polymers such as PLCL, versus bulk degrading polymers like PLGA, can prevent long term protein adsorption due to the ability to release polymer adsorbent fibro- and angio- genic molecules from the material surface prior to proliferation at site of mesothelial tissue injury. Preliminary results in **Figure 6.1** exhibit the ability of surface eroding PLCL blends to resist the adherence of a fluorescently labeled blood protein as compared to bulk eroding PLGA.

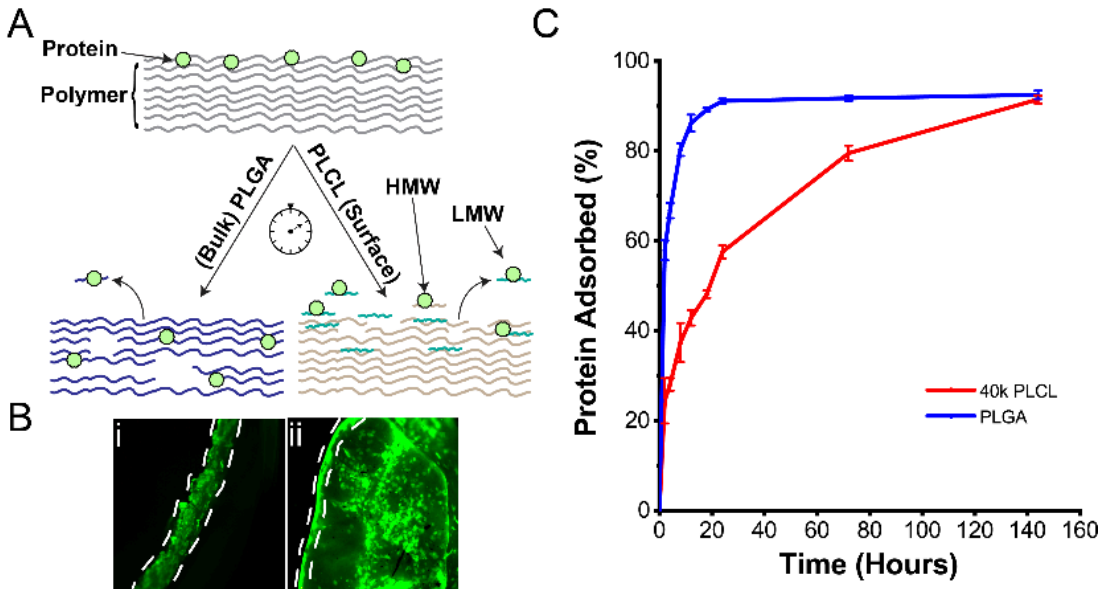

Figure 6.1. Fluorescent albumin protein adsorption to neat blend PLCL.
(A) Illustration of protein adsorption in PLGA and PLCL. HMW = "high" molecular weight. LMW = "low" molecular weight. (B) Fluorescent microscopy of (i) PLGA and (ii) 40k PLCL at t = 24h (n=1). (C) Percent of fluorescent albumin adsorption onto polymer (n=3 / time point). 10mg polymer / sample (normalized). Data is plotted as mean ± s.e.

While an ability to delay rapid albumin — a common blood protein — adsorption is exhibited through use of neat high molecular weight PLCL, it is not the candidate blend of 40k/5k PLCL deployed in adhesions prevention studies. Hence, protein adsorption phenomena of additional neat 80k PLCL and blended 80k/20k, 80k/5k, 40k/20k, and 40k/5k need be explored. Polymer solutions will be deposited onto glass slides via solution blow spinning and divided into 10mg pieces (n=5). As done above in **Figure 6.1.**, polymer masses will then be pre-conditioned in .5% albumin-fluorescein isothiocyanate (FITC-Albumin) solution for three hours at 37°C in an oven and washed three times with PBS prior to overnight vacuum desiccation to remove non-adsorbed protein. Individual wells of a well plate containing polymer will be replenished with PBS. Supernatant of each sample well will then be extracted and measured for

fluorescent intensity (RFU) at excitation and emission wavelengths of 495 and 525nm, respectively. Concentration of protein within the sampled supernatant at each time point is calculated via a standard curve, and using the amount of volume sampled, the mass of suspended protein. This value is then subtracted from the mass of protein loaded into initial stock solution as to obtain amount of protein adsorbed onto polymer at the select timepoint.

Additional proteins characteristic of fibrosis and vascular tissue deposition need be tested as to assess directly implicated proteins in adhesion formation. Fluorescently labeled fibrinogen is readily available and thereby presents a more biologically relevant lens. However, it's high cost deters ordering as-synthesized from a vendor, and encourages novel techniques for conjugating a fluorophore onto a native blood protein through complementary binding with reactive amino residues expressed within the protein.[237]

Fluorescence based techniques impose technical limitations due to light sensitivity of conjugated fluorophores. FITC loses its fluorescence in the presence of light at 495nm due a photobleaching affect. This creates a necessity to operate in dark conditions and wrap well plates in aluminum foil. Absorbance based measurement of protein concentration, such as that done with bicinchoninic acid assay (BCA), presents a more accurate and pragmatic approach to studying protein adsorption onto PLCL fiber mats.

Controlled release of small molecule therapeutics from surface eroding polymer molecular weight blends

The incorporation of COG133 into PLCL blend allows for local release at a surgical site and imparts an immunomodulatory effect preventing severe grade adhesion formation, or formation altogether. Since it is a simple oligopeptide, it can be dissolved in the pre-application solution without denaturing or a loss in bioactivity. Release rate is then tuned by changing the relative ratios of polymer molecular weights in the surgical sealant as well as the initial amount of COG133 loaded. A therapeutic release platform with simple synthesis and application harbors great clinical potential in adhesion prevention, as it can be extended to other anti-inflammatory agents. Additional future work should accurately characterize release kinetics in vivo in an indirect fashion, either photometrically through relative intensity of fluorecently tagged therapeutic or immunologically through relative cytokine epxression over clinical time course. An in vivo, cumulative release profile is hypothesized to be slightly reduced in amount as compared to in vitro work due to dynamic and aqueous nature of peritoneal space.

Work in our lab completed by an undergraduate research team studied incorporation and release of chemotherapeutic agent from PLCL for improved treatment of colorectal cancer.[238] Current treatment methods include a combination of resection, anastomosis, and chemotherapy of affected tumor.[239] Neither treatment approach is deemed effective due to numerous side effects and high reoccurrence rates.[240] Controllably releasing therapeutic from PLCL fiber mats introduces a novel avenue for tempering rapid tumorigenesis, whilst also acting as a site-specific tissue sealant. In vitro release of

prevalent drugs in 5-fluorouracil (5-FU), oxaliplatin, and capecitabine from 80k and 40k PLCL showed a combination of burst and delayed profiles over a 90-day period. Given the ability of chemotherapeutics to temper rapid collagen synthesis characteristic of tumorigenesis, tuning therapeutic release of chemotherapeutic eluting scaffolds has the potential to improve treatment efficacy.[241,242]

Drug solutions of each 5-FU, oxaliplatin, and capecitabine will be made in acetone at IC_{50} concentrations of 24.2 μM, 24.2 μM, and 0.97 μM, respectively. Standard curves for each drug solution are created by measuring the wavelength of maximum absorbance at various concentrations in a PBS serial dilution starting from the IC_{50} value. 1g of either neat (80k, 40k) or blend (80k/20k, 80k/5k, 40k/20k, 40k/5k) will be added to each drug solution, deposited via SBS onto glass slides, sectioned into ~10mg masses, and placed into individual wells of a 96 well plate. 200μL of PBS is then pipetted into each well, followed by sealing of the plate with parafilm and electrical tape, and placed in a 37°C oven for 2 hours. After this time period, the plate is then removed from the oven and 100μL of supernatant - containing degraded PLCL and eluted drug - transferred to a separate 96 well plate and remaining supernatant in sample wells discarded. 200μL of PBS was then replenished in each sample well, the plate sealed in the same fashion, and placed back in a 37°C oven for testing release at later time points. Oxaliplatin elutions are treated with Iron (III) Chloride in the presence of phenanthroline as to shift the lambda max and appear visible with spectrophotometry.[243] 5-FU and capecitabine elutions are left as is. These steps are then repeated as above for additional time point of 8 hours, 18 hours, 24 hours, 3 days, 7

days, 14 days, and 28 days. As to subtract background noise in absorbance spectra, analogous samples of PLCL without drug are performed exactly as above and absorbance curves obtained.

To calculate release of chemotherapeutic from PLCL samples, each λ_{max} absorbance value obtained from supernatant is first normalized to mass (g) of polymer, and then multiplied by 2x as to account for the difference in elution (200μL) and sampling (100μL) volume in procedure. Absorbance values for polymer only elutions are then subtracted from drug containing elutions as to obtain a background-subtracted absorbance value. This extrapolated absorbance value is then referenced against the created standard curves created for each drug solution and multiplied by the sample volume (200μL) as to obtain nmol of drug eluted from each PLCL sample, then then averaged (n=>10). Cumulative release and percent release are then plotted as averages and plotted with pooled standard deviations as an error metric.

Early and late-stage adhesion prevention efficacy of surface eroding polymer and drug blends in preclinical mouse model

Peritoneal adhesion formation and maturation is an inflammatory process that occurs over 14 days. In the first 5-7 days following mesothelial injury, cytokines secreted at the tissue site signal for fibrosis and initial deposition of tissue, followed by deposition vascular tissue for up to 14 days. Time dependent pathology for scar tissue deposition thereby necessitates further investigation at both early stage (1 day) and late stage (28 days). Early stage at t=1d is when the wound healing response is greatest, and we would

be able to denote possible differences in inflammatory and wound healing response. Late stage at t=28d is when the material has completely biodegraded, released all therapeutic, lost its mechanical properties, and the peritoneal space has either healed naturally or proceeded through a foreign body response.

Assessment of adhesion pathology and resultant inflammatory response will be studied at both t=1d and t=28d in both mouse cecal ligation and mouse cecal anastomosis models. Previously investigated polymer (40k PLCL, 40k/5k PLCL) and polymer/drug (40k and 40k/4k PLCL with .2% and .4% COG133) blends will be tested, in addition to any novel formulations that arise. Results obtained at both t=1d and t=28d will be compared to in vivo scoring and in vitro wound healing data obtained for studies at t=7d presented in **Chapter 5** and **Chapter 6**. More extensive inflammatory studies will be performed through flow cytometry with fluorescence-activated cell sorting (FACS) to evaluate the cell infiltrate with appropriate antibodies for markers of macrophages (CD11b), neutrophils (Ly-6G), and leukocytes (CD45)36. An ELISA will be used to measure the amount of tissue-type plasminogen activator (tPA) and relevant inflammatory cytokines in homogenized peritoneum samples, while a plasminogen activator functional capacity assay will be used to show impaired fibrinolytic activity associated with peritoneal adhesions.

Translatability of surface eroding polymer and drug blends in preclinical porcine model

Improving translatability of synthesized adhesion barrier materials studied in this dissertation presents an opportunity to research of higher impact and commercial

potential. While both studied and newly proposed mouse models exhibit a threshold of clinical efficacy, it is imperative to test barrier efficacy in larger animals. A piglet model will be used in such studies as it will more accurately represent human physiology than a mouse model.[244] Sterility and stability of polymer-drug solutions need be carefully studied for improved clinical translatability. It is hypothezied that solutions prepared far (> 3 days) in advance of surgery will spray deposit a larger portion of "wet" rather than "dry" fibers. Ethyl acetate and acetone solvents readily evaporate even in a sealed vial, resulting in a more concentrated polymer solution altering end-product fiber morphology. A possible answer to this complication would be to freeze the polymer/drug solution at -20°C as to reduce evaporation rate. However, thermal stability of drug in freeze/thaw cycles need be studied as to ensure bioactivity is retained.

Materials both reported and proposed within this dissertation will tested in piglet models of either sex. Work reported in this dissertation studied adhesion and wound healing pathology with female mice. Difference in hormonal levels between male and female mice and pigs alter wound healing and fibrotically drive processes in vivo, and thus need be carefully considered in future animal studies. Efficacy of PLCL and PLCL/drug fiber mats will be evaluated for sealing of anastomoses sites, but also assessed for prevention of peritoneal adhesion formation and associated complications. Piglets are considered an excellent model for evaluating peritoneal adhesions due to their comparable physiology, size, and capacity to form adhesions.[245]

A chronic porcine small bowel anastomosis model will be used to study adhesion formation. A control non-sealant anastomosis will be compared to polymer only, drug loaded polymer, and commercial sealants. 6 piglets will be used in each group (3 groups) with study endpoints determined at 1 and 8 weeks (n = 6; 36 total piglets). A small midline laparotomy will be performed and short segments of jejunum isolated. An end-to-end anastomosis will be performed with eight Vicryl 4/0 sutures. Suture anastomosis alone will be compared to the same procedure supplemented with blow spun polymer (PLCL or other) with or without drug (COG133 or other) with the best performing clinically available option as determined by mouse models (3 groups). Animals will be allowed to recover, and feedings will be allowed as tolerated. The anastomoses will be evaluated at 1- and 8-weeks following surgery, at which time the animals will be euthanized. Post-operatively the clinical course will be monitored for time to full feeds (ileus), post-operative peritonitis (infection), the abdominal cavity will be inspected for any complications including anastomotic leak, adhesions, perianastomotic abscess formation, or infection. At the time of harvest, the anastomoses will be evaluated for pre-anastomotic dilation. Tissue will be harvested, biologic response via wound healing gene and cytokine expression will be evaluated in accordance with ISO standard 10993-6 (n = 3) and flow cytometry will be used to quantify any elevations in certain cell populations (n = 3).

Chapter 7: Contributions to Research

My research contributions in the Functional Macromolecular Laboratory has resulted in seven publications that are in press, two manuscripts under review, one manuscript in revision, and two manuscripts in preparation:

In Press

1. **Erdi, M.**, Rozyyev, S., Balabhadrapatruni, M., Saruwatari, M. S., Daristotle, J. L., Ayyub, O. B., Sandler, A. D., Kofinas, P. "Sprayable Tissue Adhesive with Biodegradation Tuned for Prevention of Postoperative Abdominal Adhesions." *Bioengineering & Translational Medicine*, e10335. 2022; DOI: https://doi.org/10.1002/btm2.10335
2. Daristotle, J.L.*, **Erdi, M.*** Lau, L.W., Zaki, S., Srinivasan, P., Balabhadrapatruni, M., Ayyub, O.B., Sandler, A.D., Kofinas, P. "Biodegradable, tissue adhesive polyester blend for safe, complete wound healing". *ACS Biomaterials Science and Engineering*. 2021; 7(8), 3908-3916. DOI: https://doi.org/10.1021/acsbiomaterials.1c00865
3. Daristotle, J.L., Lau, L.W., **Erdi, M.**, Hunter, J., Djoum Jr., A., Srinivasan, P., Wu, X., Basu, M., Ayyub, O.B., Sandler, A.D., Kofinas, P. "Sprayable and Biodegradable, Intrinsically Adhesive Wound Dressing with Antimicrobial Properties". *Bioengineering and Translational Medicine*. 2020; 5(1), e10149. DOI: https://doi.org/10.1002/btm2.10149
4. Daristotle, J.L., Zaki, S., Lau, L.W., Ayyub, O.B., Djouini, M., Srinivasan, P., **Erdi, M**., Sandler, A.D., Kofinas, P. "Pressure-Sensitive Tissue Adhesion and Biodegradation of Viscoelastic Polymer Blends". *ACS Applied Materials and Interfaces*. 2020; 12(14), 16050-16057. DOI: https://doi.org/10.1021/acsami.0c00497
5. Carney, B.C., Oliver, M.A., **Erdi, M**., Kirkpatrick, L.D., Tranchina, S.P., Rozyyev, S., Keyloun, J.W., Saruwatari, M.S., Daristotle, J.L., Moffatt, L.T., Kofinas, P., Sandler, A.D., Shupp, J.W. "Evaluation of Healing Outcomes Combining A Novel Polymer Formulation with Autologous Skin Cell Suspension to Treat Deep Partial and Full Thickness Wounds in a Porcine Model". *Burns.* 2022; DOI: https://doi.org/10.1016/j.burns.2022.01.012
6. Widstrom, M.D., Borodin, O., Ludwig, K.B., Matthews, J.E., Bhattacharyya, S., Garaga, M., Cresce, A.V., Jarry, A., **Erdi, M**., Wang, C., Greenbaum, S.G., Kofinas, P. "Water Domain Enabled Transport in Polymer Electrolytes for Lithium-Ion Batteries". *Macromolecules*. 2021. 54(6), 2882–2891 DOI: https://doi.org/10.1021/acs.macromol.0c01960
7. Widstrom, M.D., Ludwig, K.B., Matthews, J., Jarry, A., **Erdi, M.**, Cresce, A.V., Rubloff, G., Kofinas, P. "Enabling High Performance All-Solid-State Lithium Metal Batteries using Solid Polymer Electrolytes Plasticized with Ionic Liquid". *Electrochimica Acta*. 2020; 345, 136156. DOI: https://doi.org/10.1016/j.electacta.2020.136156

Under Review

1. **Erdi, M.**, Saruwatari, M. S., Rozyyev, S., Acha, C., Sandler, A. D., Kofinas, P. "Biodegradation Driven Release of a Therapeutic Peptide in Sprayable Surgical Sealant for Prevention of Postoperative Abdominal Adhesions" *Advanced Healthcare Materials.*
2. **Erdi, M.**, Sandler, A. D., Kofinas, P. "Polymer nanomaterials for use as adjuvant surgical tools" *WIREs Nanomedicine & Nanobiotechnology.*

In Revision

1. Sarker, S., Colton, A., Wen, Z., Xu, X., **Erdi, M.**, Jones, A., Kofinas, P., Tubaldi, E., Walczak, P., Janowski, M., Liang, Y., Sochol, R.D. "3D-Printed Microinjection Needle Arrays via a Hybrid DLP-Direct Laser Writing Strategy" *Advanced Materials Technologies.*

In Preparation

1. Borden, L.K., Kokilpersaud, U.J., **Erdi, M.**, Kofinas, P., Raghavan, S.R. "Electroadhesion to New Classes of Soft Materials: A Review and New Advancements." (*In Prep*)
2. Borden, L.K., Grasso, S., Nader, M., **Erdi, M.**, Kofinas, P., Raghavan, S.R. "Mechanism for Electroadhesion: Why Gels can be Permanently Adhered to Tissues by Applying a DC Electric Field." *(In Prep)*

Aspects of work presented in Chapter 4 and Chapter 5 have been discussed in a provisional patent application titled "Sprayable Tissue Adhesive with Biodegradation Tuned for Prevention of Post-Operative Abdominal Adhesions." I have presented my contributions to research at meetings for the American Chemical Society and Society for Biomaterials. As a result of my research, I have been awarded the Ruth L. Kirschstein National Research Service Award Individual Predoctoral Fellowship from the National Institute of Diabetes and Digestive and Kidney Diseases (F31DK129021). In addition, I co-wrote a recently awarded Research Project Grant from the National Institute of General Medical Sciences (R01GM141132) with my advisor, Dr. Peter Kofinas, and assistant research professor, Dr. Omar B. Ayyub. This project has enabled me to join the Future Faculty and Clark Doctoral Fellows programs through the A. James Clark School of Engineering. With Dr. Kofinas' continued support, I have also had the fortune of mentoring both undergraduate and graduate students in the lab.

The primary goal of my dissertation research was to engineer tissue adhesive materials for biocompatible and effective wound healing. This proved to be challenging given the complexity of fibrosis as a physical and biologically derived process. Specifically work contained in Chapter 4 and Chapter 5 harbor great potential to improve treatment of atypical tissue deposition resultant of tissue injury in a wide variety of clinical interventions.

Chapter 8: References

1. Daristotle JL, Erdi M, Lau LW, Zaki ST, Srinivasan P, Balabhadrapatruni M, Ayyub OB, Sandler AD, Kofinas P. Biodegradable, Tissue Adhesive Polyester Blends for Safe, Complete Wound Healing. *ACS Biomaterials Science & Engineering*. 2021;7(8):3908-3916. doi:10.1021/acsbiomaterials.1c00865

2. Erdi M, Rozyyev S, Balabhadrapatruni M, Saruwatari MS, Daristotle JL, Ayyub OB, Sandler AD, Kofinas P. Sprayable tissue adhesive with biodegradation tuned for prevention of postoperative abdominal adhesions. *Bioengineering & Translational Medicine*. Published online May 23, 2022:e10335. doi:10.1002/btm2.10335

3. Daristotle JL, Behrens AM, Sandler AD, Kofinas P. A Review of the Fundamental Principles and Applications of Solution Blow Spinning. *ACS Applied Materials & Interfaces*. 2016;8(51):34951-34963. doi:10.1021/acsami.6b12994

4. Medeiros ES, Glenn GM, Klamczynski AP, Orts WJ, Mattoso LHC. Solution blow spinning: A new method to produce micro- and nanofibers from polymer solutions. *Journal of Applied Polymer Science*. 2009;113(4):2322-2330. doi:10.1002/app.30275

5. Polat Y, Pampal ES, Stojanovska E, Simsek R, Hassanin A, Kilic A, Demir A, Yilmaz S. Solution blowing of thermoplastic polyurethane nanofibers: A facile method to produce flexible porous materials. *Journal of Applied Polymer Science*. 2016;133(9). doi:10.1002/app.43025

6. Tutak W, Sarkar S, Lin-Gibson S, Farooque TM, Jyotsnendu G, Wang D, Kohn J, Bolikal D, Simon CG. The support of bone marrow stromal cell differentiation by airbrushed nanofiber scaffolds. *Biomaterials*. 2013;34(10):2389-2398. doi:10.1016/j.biomaterials.2012.12.020

7. Greiner A, Wendorff JH. Electrospinning: A Fascinating Method for the Preparation of Ultrathin Fibers. *Angewandte Chemie International Edition*. 2007;46(30):5670-5703. doi:10.1002/anie.200604646

8. Junker JP, Kamel RA, Caterson EJ, Eriksson E. Clinical Impact Upon Wound Healing and Inflammation in Moist, Wet, and Dry Environments. *Adv Wound Care (New Rochelle)*. 2013;2(7):348-356. doi:10.1089/wound.2012.0412

9. Field CK, Kerstein MD. Overview of wound healing in a moist environment. *The American Journal of Surgery*. 1994;167(1):S2-S6. doi:10.1016/0002-9610(94)90002-7

10. Singh A, Halder S, Chumber S, Misra MC, Sharma LK, Srivastava A, Menon GR. Meta-analysis of Randomized Controlled Trials on Hydrocolloid Occlusive

Dressing Versus Conventional Gauze Dressing in the Healing of Chronic Wounds. *Asian Journal of Surgery*. 2004;27(4):326-332. doi:10.1016/S1015-9584(09)60061-0

11. Church D, Elsayed S, Reid O, Winston B, Lindsay R. Burn Wound Infections. *CLIN MICROBIOL REV*. 2006;19:32.

12. Daristotle JL, Lau LW, Erdi M, Hunter J, Djoum A, Srinivasan P, Wu X, Basu M, Ayyub OB, Sandler AD, Kofinas P. Sprayable and biodegradable, intrinsically adhesive wound dressing with antimicrobial properties. *Bioengineering & Translational Medicine*. 2020;5(1). doi:10.1002/btm2.10149

13. Ahmed R, Tariq M, Ali I, Asghar R, Noorunnisa Khanam P, Augustine R, Hasan A. Novel electrospun chitosan/polyvinyl alcohol/zinc oxide nanofibrous mats with antibacterial and antioxidant properties for diabetic wound healing. *International Journal of Biological Macromolecules*. 2018;120:385-393. doi:10.1016/j.ijbiomac.2018.08.057

14. He M, Sun L, Fu X, McDonough SP, Chu CC. Biodegradable amino acid-based poly(ester amine) with tunable immunomodulating properties and their in vitro and in vivo wound healing studies in diabetic rats' wounds. *Acta Biomaterialia*. 2019;84:114-132. doi:10.1016/j.actbio.2018.11.053

15. Wang J, Li Y, Han X, Zhang H, Fan A, Yao X, Tang B, Zhang X. Light-Triggered Antibacterial Hydrogels Containing Recombinant Growth Factor for Treatment of Bacterial Infections and Improved Wound Healing. *ACS Biomaterials Science & Engineering*. 2021;7(4):1438-1449. doi:10.1021/acsbiomaterials.0c01588

16. Huang Y, Zhao X, Zhang Z, Liang Y, Yin Z, Chen B, Bai L, Han Y, Guo B. Degradable Gelatin-Based IPN Cryogel Hemostat for Rapidly Stopping Deep Noncompressible Hemorrhage and Simultaneously Improving Wound Healing. *Chemistry of Materials*. 2020;32(15):6595-6610. doi:10.1021/acs.chemmater.0c02030

17. Han L, Yan L, Wang K, Fang L, Zhang H, Tang Y, Ding Y, Weng L tao, Xu J, Weng J, Liu Y, Ren F, Lu X. Tough, self-healable and tissue-adhesive hydrogel with tunable multifunctionality. *NPG Asia Materials*. 2017;9(4):n/a. doi:http://dx.doi.org/10.1038/am.2017.33

18. Behrens AM, Lee NG, Casey BJ, Srinivasan P, Sikorski MJ, Daristotle JL, Sandler AD, Kofinas P. Biodegradable-Polymer-Blend-Based Surgical Sealant with Body-Temperature-Mediated Adhesion. *Advanced Materials*. 2015;27(48):8056-8061. doi:10.1002/adma.201503691

19. Amiri N, Ajami S, Shahroodi A, Jannatabadi N, Amiri Darban S, Fazly Bazzaz BS, Pishavar E, Kalalinia F, Movaffagh J. Teicoplanin-loaded chitosan-PEO nanofibers for local antibiotic delivery and wound healing. *International Journal*

of Biological Macromolecules. 2020;162:645-656. doi:10.1016/j.ijbiomac.2020.06.195

20. Dunn LL, de Valence S, Tille JC, Hammel P, Walpoth BH, Stocker R, Imhof BA, Miljkovic-Licina M. Biodegradable and plasma-treated electrospun scaffolds coated with recombinant Olfactomedin-like 3 for accelerating wound healing and tissue regeneration: Matricellular protein olfactomedin-like 3 promotes neovascularization. *Wound Repair and Regeneration*. 2016;24(6):1030-1035. doi:10.1111/wrr.12485

21. Ju HW, Lee OJ, Lee JM, Moon BM, Park HJ, Park YR, Lee MC, Kim SH, Chao JR, Ki CS, Park CH. Wound healing effect of electrospun silk fibroin nanomatrix in burn-model. *International Journal of Biological Macromolecules*. 2016;85:29-39. doi:10.1016/j.ijbiomac.2015.12.055

22. Xie Z, Paras CB, Weng H, Punnakitikashem P, Su LC, Vu K, Tang L, Yang J, Nguyen KT. Dual growth factor releasing multi-functional nanofibers for wound healing. *Acta Biomaterialia*. 2013;9(12):9351-9359. doi:10.1016/j.actbio.2013.07.030

23. Zhang K, Lv H, Zheng Y, Yao Y, Li X, Yu J, Ding B. Nanofibrous hydrogels embedded with phase-change materials: Temperature-responsive dressings for accelerating skin wound healing. *Composites Communications*. 2021;25:100752. doi:10.1016/j.coco.2021.100752

24. Zhao X, Sun X, Yildirimer L, Lang Q, Lin ZY (William), Zheng R, Zhang Y, Cui W, Annabi N, Khademhosseini A. Cell infiltrative hydrogel fibrous scaffolds for accelerated wound healing. *Acta Biomaterialia*. 2017;49:66-77. doi:10.1016/j.actbio.2016.11.017

25. Ryu JH, Messersmith PB, Lee H. Polydopamine Surface Chemistry: A Decade of Discovery. *ACS Applied Materials & Interfaces*. 2018;10(9):7523-7540. doi:10.1021/acsami.7b19865

26. GhavamiNejad A, Park CH, Kim CS. In Situ Synthesis of Antimicrobial Silver Nanoparticles within Antifouling Zwitterionic Hydrogels by Catecholic Redox Chemistry for Wound Healing Application. *Biomacromolecules*. 2016;17(3):1213-1223. doi:10.1021/acs.biomac.6b00039

27. Liang Y, Zhao X, Hu T, Han Y, Guo B. Mussel-inspired, antibacterial, conductive, antioxidant, injectable composite hydrogel wound dressing to promote the regeneration of infected skin. *Journal of Colloid and Interface Science*. 2019;556:514-528. doi:10.1016/j.jcis.2019.08.083

28. Wang L, Zhang X, Yang K, Fu YV, Xu T, Li S, Zhang D, Wang L, Lee C. A Novel Double-Crosslinking-Double-Network Design for Injectable Hydrogels with Enhanced Tissue Adhesion and Antibacterial Capability for Wound

Treatment. *Advanced Functional Materials*. 2020;30(1):1904156. doi:10.1002/adfm.201904156

29. Zhao X, Liang Y, Huang Y, He J, Han Y, Guo B. Physical Double-Network Hydrogel Adhesives with Rapid Shape Adaptability, Fast Self-Healing, Antioxidant and NIR/pH Stimulus-Responsiveness for Multidrug-Resistant Bacterial Infection and Removable Wound Dressing. *Advanced Functional Materials*. 2020;30(17):1910748. doi:10.1002/adfm.201910748

30. Chen T, Chen Y, Rehman HU, Chen Z, Yang Z, Wang M, Li H, Liu H. Ultratough, Self-Healing, and Tissue-Adhesive Hydrogel for Wound Dressing. *ACS Applied Materials & Interfaces*. 2018;10(39):33523-33531. doi:10.1021/acsami.8b10064

31. Han L, Zhang Y, Lu X, Wang K, Wang Z, Zhang H. Polydopamine Nanoparticles Modulating Stimuli-Responsive PNIPAM Hydrogels with Cell/Tissue Adhesiveness. *ACS Applied Materials & Interfaces*. 2016;8(42):29088-29100. doi:10.1021/acsami.6b11043

32. Blacklow SO, Li J, Freedman BR, Zeidi M, Chen C, Mooney DJ. Bioinspired mechanically active adhesive dressings to accelerate wound closure. *Science Advances*. 2019;5(7):eaaw3963. doi:10.1126/sciadv.aaw3963

33. Chen G, Yu Y, Wu X, Wang G, Ren J, Zhao Y. Bioinspired Multifunctional Hybrid Hydrogel Promotes Wound Healing. *Advanced Functional Materials*. 2018;28(33):1801386. doi:10.1002/adfm.201801386

34. Gan D, Xu T, Xing W, Ge X, Fang L, Wang K, Ren F, Lu X. Mussel-Inspired Contact-Active Antibacterial Hydrogel with High Cell Affinity, Toughness, and Recoverability. *Advanced Functional Materials*. 2019;29(1):1805964. doi:10.1002/adfm.201805964

35. Griffin DR, Weaver WM, Scumpia PO, Di Carlo D, Segura T. Accelerated wound healing by injectable microporous gel scaffolds assembled from annealed building blocks. *Nature Materials*. 2015;14(7):737-744. doi:10.1038/nmat4294

36. He J, Shi M, Liang Y, Guo B. Conductive adhesive self-healing nanocomposite hydrogel wound dressing for photothermal therapy of infected full-thickness skin wounds. *Chemical Engineering Journal*. 2020;394:124888. doi:10.1016/j.cej.2020.124888

37. Guo S, Yao M, Zhang D, He Y, Chang R, Ren Y, Guan F. One-Step Synthesis of Multifunctional Chitosan Hydrogel for Full-Thickness Wound Closure and Healing. *Advanced Healthcare Materials*. 2022;11(4):2101808. doi:10.1002/adhm.202101808

38. Liang Y, Chen B, Li M, He J, Yin Z, Guo B. Injectable Antimicrobial Conductive Hydrogels for Wound Disinfection and Infectious Wound Healing. *Biomacromolecules*. 2020;21(5):1841-1852. doi:10.1021/acs.biomac.9b01732

39. Lokhande G, Carrow JK, Thakur T, Xavier JR, Parani M, Bayless KJ, Gaharwar AK. Nanoengineered injectable hydrogels for wound healing application. *Acta Biomaterialia*. 2018;70:35-47. doi:10.1016/j.actbio.2018.01.045

40. Ma R, Wang Y, Qi H, Shi C, Wei G, Xiao L, Huang Z, Liu S, Yu H, Teng C, Liu H, Murugadoss V, Zhang J, Wang Y, Guo Z. Nanocomposite sponges of sodium alginate/graphene oxide/polyvinyl alcohol as potential wound dressing: In vitro and in vivo evaluation. *Composites Part B: Engineering*. 2019;167:396-405. doi:10.1016/j.compositesb.2019.03.006

41. Qu J, Zhao X, Liang Y, Zhang T, Ma PX, Guo B. Antibacterial adhesive injectable hydrogels with rapid self-healing, extensibility and compressibility as wound dressing for joints skin wound healing. *Biomaterials*. 2018;183:185-199. doi:10.1016/j.biomaterials.2018.08.044

42. Tang X, Gu X, Wang Y, Chen X, Ling J, Yang Y. Stable antibacterial polysaccharide-based hydrogels as tissue adhesives for wound healing. *RSC Advances*. 2020;10(29):17280-17287. doi:10.1039/D0RA02017F

43. Ying H, Zhou J, Wang M, Su D, Ma Q, Lv G, Chen J. In situ formed collagen-hyaluronic acid hydrogel as biomimetic dressing for promoting spontaneous wound healing. *Materials Science and Engineering: C*. 2019;101:487-498. doi:10.1016/j.msec.2019.03.093

44. Zhao X, Wu H, Guo B, Dong R, Qiu Y, Ma PX. Antibacterial anti-oxidant electroactive injectable hydrogel as self-healing wound dressing with hemostasis and adhesiveness for cutaneous wound healing. *Biomaterials*. 2017;122:34-47. doi:10.1016/j.biomaterials.2017.01.011

45. Li S, Zhou J, Huang Y, Roy J, Zhou N, Yum K, Sun X, Tang L. Injectable Click Chemistry-based Bioadhesives for Accelerated Wound Closure. *Acta Biomaterialia*. 2020;110:95-104. doi:10.1016/j.actbio.2020.04.004

46. Zhu J, Li F, Wang X, Yu J, Wu D. Hyaluronic Acid and Polyethylene Glycol Hybrid Hydrogel Encapsulating Nanogel with Hemostasis and Sustainable Antibacterial Property for Wound Healing. *ACS Applied Materials & Interfaces*. 2018;10(16):13304-13316. doi:10.1021/acsami.7b18927

47. Huang W, Wang Y, Huang Z, Wang X, Chen L, Zhang Y, Zhang L. On-Demand Dissolvable Self-Healing Hydrogel Based on Carboxymethyl Chitosan and Cellulose Nanocrystal for Deep Partial Thickness Burn Wound Healing. *ACS Applied Materials & Interfaces*. 2018;10(48):41076-41088. doi:10.1021/acsami.8b14526

48. Liang Y, Zhao X, Hu T, Chen B, Yin Z, Ma PX, Guo B. Adhesive Hemostatic Conducting Injectable Composite Hydrogels with Sustained Drug Release and Photothermal Antibacterial Activity to Promote Full-Thickness Skin Regeneration During Wound Healing. *Small*. 2019;15(12):1900046. doi:10.1002/smll.201900046

49. Lu Z, Gao J, He Q, Wu J, Liang D, Yang H, Chen R. Enhanced antibacterial and wound healing activities of microporous chitosan-Ag/ZnO composite dressing. *Carbohydrate Polymers*. 2017;156:460-469. doi:10.1016/j.carbpol.2016.09.051

50. Turabee MdH, Thambi T, Lee DS. Development of an Injectable Tissue Adhesive Hybrid Hydrogel for Growth Factor-Free Tissue Integration in Advanced Wound Regeneration. *ACS Applied Bio Materials*. 2019;2(6):2500-2510. doi:10.1021/acsabm.9b00204

51. Singer AJ, Perry LC, Allen Jr RL. In Vivo Study of Wound Bursting Strength and Compliance of Topical Skin Adhesives. *Academic Emergency Medicine*. 2008;15(12):1290-1294. doi:10.1111/j.1553-2712.2008.00273.x

52. Singer AJ, Quinn JV, Hollander JE. The cyanoacrylate topical skin adhesives. *The American Journal of Emergency Medicine*. 2008;26(4):490-496. doi:10.1016/j.ajem.2007.05.015

53. Deng X. Progress on rubber-based pressure-sensitive adhesives. *The Journal of Adhesion*. 2018;94(2):77-96. doi:10.1080/00218464.2016.1249573

54. Shin J, Martello MT, Shrestha M, Wissinger JE, Tolman WB, Hillmyer MA. Pressure-Sensitive Adhesives from Renewable Triblock Copolymers. *Macromolecules*. 2011;44(1):87-94. doi:10.1021/ma102216d

55. Falsafi A, Tirrell M, Pocius AV. Compositional Effects on the Adhesion of Acrylic Pressure Sensitive Adhesives. *Langmuir*. 2000;16(4):1816-1824. doi:10.1021/la990345z

56. Nam S, Mooney D. Polymeric Tissue Adhesives. *Chemical Reviews*. 2021;121(18):11336-11384. doi:10.1021/acs.chemrev.0c00798

57. Daristotle JL, Zaki ST, Lau LW, Ayyub OB, Djouini M, Srinivasan P, Erdi M, Sandler AD, Kofinas P. Pressure-Sensitive Tissue Adhesion and Biodegradation of Viscoelastic Polymer Blends. *ACS Applied Materials & Interfaces*. 2020;12(14):16050-16057. doi:10.1021/acsami.0c00497

58. Jeon EY, Lee J, Kim BJ, Joo KI, Kim KH, Lim G, Cha HJ. Bio-inspired swellable hydrogel-forming double-layered adhesive microneedle protein patch for regenerative internal/external surgical closure. *Biomaterials*. 2019;222:119439. doi:10.1016/j.biomaterials.2019.119439

59. Kelmansky R, McAlvin BJ, Nyska A, Dohlman JC, Chiang HH, Hashimoto M, Kohane DS, Mizrahi B. Strong tissue glue with tunable elasticity. *Acta Biomaterialia*. 2017;53:93-99. doi:10.1016/j.actbio.2017.02.009

60. Zhang W, Ji T, Lyon S, Mehta M, Zheng Y, Deng X, Liu A, Shagan A, Mizrahi B, Kohane DS. Functionalized Multiarmed Polycaprolactones as Biocompatible Tissue Adhesives. *ACS Applied Materials & Interfaces*. 2020;12(15):17314-17320. doi:10.1021/acsami.0c03478

61. Yuk H, Varela CE, Nabzdyk CS, Mao X, Padera RF, Roche ET, Zhao X. Dry double-sided tape for adhesion of wet tissues and devices. *Nature*. 2019;575(7781):169-174. doi:10.1038/s41586-019-1710-5

62. Peppas NA, Buri PA. Surface, interfacial and molecular aspects of polymer bioadhesion on soft tissues. *Journal of Controlled Release*. 1985;2:257-275. doi:10.1016/0168-3659(85)90050-1

63. Felton L. Influence of plasticizers on the adhesive properties of an acrylic resin copolymer to hydrophilic and hydrophobic tablet compacts. *International Journal of Pharmaceutics*. 1997;154(2):167-178. doi:10.1016/S0378-5173(97)00133-6

64. Kinloch AJ. The science of adhesion. *Journal of Materials Science*. 1980;15(9):2141-2166. doi:10.1007/BF00552302

65. Kim YS. Human Tissues: Chemical Composition and Photon Dosimetry Data. *Radiation Research*. 1974;57(1):38. doi:10.2307/3573753

66. Kord Forooshani P, Lee BP. Recent approaches in designing bioadhesive materials inspired by mussel adhesive protein. *Journal of Polymer Science Part A: Polymer Chemistry*. 2017;55(1):9-33. doi:10.1002/pola.28368

67. Chen W, Wang R, Xu T, Ma X, Yao Z, Chi B, Xu H. A mussel-inspired poly(γ-glutamic acid) tissue adhesive with high wet strength for wound closure. *J Mater Chem B*. 2017;5(28):5668-5678. doi:10.1039/C7TB00813A

68. Fan C, Fu J, Zhu W, Wang DA. A mussel-inspired double-crosslinked tissue adhesive intended for internal medical use. *Acta Biomaterialia*. 2016;33:51-63. doi:10.1016/j.actbio.2016.02.003

69. Han L, Wang M, Li P, Gan D, Yan L, Xu J, Wang K, Fang L, Chan CW, Zhang H, Yuan H, Lu X. Mussel-Inspired Tissue-Adhesive Hydrogel Based on the Polydopamine–Chondroitin Sulfate Complex for Growth-Factor-Free Cartilage Regeneration. *ACS Applied Materials & Interfaces*. 2018;10(33):28015-28026. doi:10.1021/acsami.8b05314

70. He X, Liu L, Han H, Shi W, Yang W, Lu X. Bioinspired and Microgel-Tackified Adhesive Hydrogel with Rapid Self-Healing and High Stretchability. *Macromolecules*. 2019;52(1):72-80. doi:10.1021/acs.macromol.8b01678

71. Liu Y, Meng H, Konst S, Sarmiento R, Rajachar R, Lee BP. Injectable Dopamine-Modified Poly(ethylene glycol) Nanocomposite Hydrogel with Enhanced Adhesive Property and Bioactivity. *ACS Applied Materials & Interfaces*. 2014;6(19):16982-16992. doi:10.1021/am504566v

72. Pinnaratip R, Meng H, Rajachar RM, Lee BP. Effect of incorporating clustered silica nanoparticles on the performance and biocompatibility of catechol-containing PEG-based bioadhesive. *Biomedical Materials*. 2018;13(2):025003. doi:10.1088/1748-605X/aa985d

73. Li M, Zhang Z, Liang Y, He J, Guo B. Multifunctional Tissue-Adhesive Cryogel Wound Dressing for Rapid Nonpressing Surface Hemorrhage and Wound Repair. *ACS Applied Materials & Interfaces*. 2020;12(32):35856-35872. doi:10.1021/acsami.0c08285

74. Suneetha M, Rao KM, Han SS. Mussel-Inspired Cell/Tissue-Adhesive, Hemostatic Hydrogels for Tissue Engineering Applications. *ACS Omega*. 2019;4(7):12647-12656. doi:10.1021/acsomega.9b01302

75. Hermanson GT. *Bioconjugate Techniques*. Third edition. Elsevier/AP; 2013.

76. Hanthamrongwit M, Reid WH, Grant MH. Chondroitin-6-sulphate incorporated into collagen gels for the growth of human keratinocytes: the effect of cross-linking agents and diamines. *Biomaterials*. 1996;17(8):775-780. doi:10.1016/0142-9612(96)81414-1

77. Powell HM, Boyce ST. EDC cross-linking improves skin substitute strength and stability. *Biomaterials*. 2006;27(34):5821-5827. doi:10.1016/j.biomaterials.2006.07.030

78. Zhang H, Zhao T, Duffy P, Dong Y, Annaidh AN, O'Cearbhaill E, Wang W. Hydrolytically Degradable Hyperbranched PEG-Polyester Adhesive with Low Swelling and Robust Mechanical Properties. *Advanced Healthcare Materials*. 2015;4(15):2260-2268. doi:10.1002/adhm.201500406

79. Sun F, Bu Y, Chen Y, Yang F, Yu J, Wu D. An Injectable and Instant Self-Healing Medical Adhesive for Wound Sealing. *ACS Applied Materials & Interfaces*. 2020;12(8):9132-9140. doi:10.1021/acsami.0c01022

80. Bu Y, Zhang L, Sun G, Sun F, Liu J, Yang F, Tang P, Wu D. Tetra-PEG Based Hydrogel Sealants for In Vivo Visceral Hemostasis. *Advanced Materials*. 2019;31(28):1901580. doi:10.1002/adma.201901580

81. Lee Y, Xu C, Sebastin M, Lee A, Holwell N, Xu C, Miranda Nieves D, Mu L, Langer RS, Lin C, Karp JM. Bioinspired Nanoparticulate Medical Glues for Minimally Invasive Tissue Repair. *Advanced Healthcare Materials*. 2015;4(16):2587-2596. doi:10.1002/adhm.201500419

82. Lee JN, Lee SY, Park WH. Bioinspired Self-Healable Polyallylamine-Based Hydrogels for Wet Adhesion: Synergistic Contributions of Catechol-Amino Functionalities and Nanosilicate. *ACS Applied Materials & Interfaces*. 2021;13(15):18324-18337. doi:10.1021/acsami.1c02141

83. Lang N, Pereira MJ, Lee Y, Friehs I, Vasilyev NV, Feins EN, Ablasser K, O'Cearbhaill ED, Xu C, Fabozzo A, Padera R, Wasserman S, Freudenthal F, Ferreira LS, Langer R, Karp JM, del Nido PJ. A Blood-Resistant Surgical Glue for Minimally Invasive Repair of Vessels and Heart Defects. *Science Translational Medicine*. 2014;6(218). doi:10.1126/scitranslmed.3006557

84. Nishiguchi A, Taguchi T. Designing an anti-inflammatory and tissue-adhesive colloidal dressing for wound treatment. *Colloids and Surfaces B: Biointerfaces*. Published online January 2020:110737. doi:10.1016/j.colsurfb.2019.110737

85. Okada M, Nakai A, Hara ES, Taguchi T, Nakano T, Matsumoto T. Biocompatible nanostructured solid adhesives for biological soft tissues. *Acta Biomaterialia*. 2017;57:404-413. doi:10.1016/j.actbio.2017.05.014

86. Shirzaei Sani E, Kheirkhah A, Rana D, Sun Z, Foulsham W, Sheikhi A, Khademhosseini A, Dana R, Annabi N. Sutureless repair of corneal injuries using naturally derived bioadhesive hydrogels. *Science Advances*. 2019;5(3):eaav1281. doi:10.1126/sciadv.aav1281

87. Wang Z, He X, He T, Zhao J, Wang S, Peng S, Yang D, Ye L. Polymer Network Editing of Elastomers for Robust Underwater Adhesion and Tough Bonding to Diverse Surfaces. *ACS Applied Materials & Interfaces*. 2021;13(30):36527-36537. doi:10.1021/acsami.1c09239

88. Zhou L, Dai C, Fan L, Jiang Y, Liu C, Zhou Z, Guan P, Tian Y, Xing J, Li X, Luo Y, Yu P, Ning C, Tan G. Injectable Self-Healing Natural Biopolymer-Based Hydrogel Adhesive with Thermoresponsive Reversible Adhesion for Minimally Invasive Surgery. *Advanced Functional Materials*. 2021;31(14):2007457. doi:10.1002/adfm.202007457

89. Annabi N, Zhang YN, Assmann A, Sani ES, Cheng G, Lassaletta AD, Vegh A, Dehghani B, Ruiz-Esparza GU, Wang X, Gangadharan S, Weiss AS, Khademhosseini A. Engineering a highly elastic human protein–based sealant for surgical applications. *Science Translational Medicine*. 2017;9(410):eaai7466. doi:10.1126/scitranslmed.aai7466

90. Anthis AHC, Hu X, Matter MT, Neuer AL, Wei K, Schlegel AA, Starsich FHL, Herrmann IK. Chemically Stable, Strongly Adhesive Sealant Patch for Intestinal Anastomotic Leakage Prevention. *Advanced Functional Materials*. 2021;31(16):2007099. doi:10.1002/adfm.202007099

91. Assmann A, Vegh A, Ghasemi-Rad M, Bagherifard S, Cheng G, Sani ES, Ruiz-Esparza GU, Noshadi I, Lassaletta AD, Gangadharan S, Tamayol A, Khademhosseini A, Annabi N. A highly adhesive and naturally derived sealant. *Biomaterials*. 2017;140:115-127. doi:10.1016/j.biomaterials.2017.06.004

92. Du X, Liu Y, Yan H, Rafique M, Li S, Shan X, Wu L, Qiao M, Kong D, Wang L. Anti-Infective and Pro-Coagulant Chitosan-Based Hydrogel Tissue Adhesive for Sutureless Wound Closure. *Biomacromolecules*. 2020;21(3):1243-1253. doi:10.1021/acs.biomac.9b01707

93. Hong Y, Zhou F, Hua Y, Zhang X, Ni C, Pan D, Zhang Y, Jiang D, Yang L, Lin Q, Zou Y, Yu D, Arnot DE, Zou X, Zhu L, Zhang S, Ouyang H. A strongly adhesive hemostatic hydrogel for the repair of arterial and heart bleeds. *Nature Communications*. 2019;10(1):2060. doi:10.1038/s41467-019-10004-7

94. Kim HJ, Hwang BH, Lim S, Choi BH, Kang SH, Cha HJ. Mussel adhesion-employed water-immiscible fluid bioadhesive for urinary fistula sealing. *Biomaterials*. 2015;72:104-111. doi:10.1016/j.biomaterials.2015.08.055

95. Bai S, Zhang X, Cai P, Huang X, Huang Y, Liu R, Zhang M, Song J, Chen X, Yang H. A silk-based sealant with tough adhesion for instant hemostasis of bleeding tissues. *Nanoscale Horizons*. 2019;4(6):1333-1341. doi:10.1039/C9NH00317G

96. Spotnitz WD. Fibrin Sealant: Past, Present, and Future: A Brief Review. *World Journal of Surgery*. 2010;34(4):632-634. doi:10.1007/s00268-009-0252-7

97. Spotnitz WD, Burks S. Hemostats, sealants, and adhesives III: a new update as well as cost and regulatory considerations for components of the surgical toolbox. *Transfusion*. 2012;52(10):2243-2255. doi:10.1111/j.1537-2995.2012.03707.x

98. Wallace DG, Cruise GM, Rhee WM, Schroeder JA, Prior JJ, Ju J, Maroney M, Duronio J, Ngo MH, Estridge T, others. A tissue sealant based on reactive multifunctional polyethylene glycol. *Journal of Biomedical Materials Research*. 2001;58(5):545-555.

99. Kern NG, Behrens AM, Srinivasan P, Rossi CT, Daristotle JL, Kofinas P, Sandler AD. Solution blow spun polymer: A novel preclinical surgical sealant for bowel anastomoses. *Journal of Pediatric Surgery*. 2017;52(8):1308-1312. doi:10.1016/j.jpedsurg.2016.11.044

100. Daristotle JL, Zaki ST, Lau LW, Torres L, Zografos A, Srinivasan P, Ayyub OB, Sandler AD, Kofinas P. Improving the adhesion, flexibility, and hemostatic efficacy of a sprayable polymer blend surgical sealant by incorporating silica particles. *Acta Biomaterialia*. 2019;90:205-216. doi:10.1016/j.actbio.2019.04.015

101. Fernandez JG, Seetharam S, Ding C, Feliz J, Doherty E, Ingber DE. Direct Bonding of Chitosan Biomaterials to Tissues Using Transglutaminase for Surgical Repair or Device Implantation. *Tissue Engineering Part A*. 2017;23(3-4):135-142. doi:10.1089/ten.tea.2016.0266

102. Ryu JH, Kim HJ, Kim K, Yoon G, Wang Y, Choi G, Lee H, Park JS. Multipurpose Intraperitoneal Adhesive Patches. *Advanced Functional Materials*. 2019;29(29):1900495. doi:10.1002/adfm.201900495

103. Luo JW, Liu C, Wu JH, Lin LX, Fan HM, Zhao DH, Zhuang YQ, Sun YL. In situ injectable hyaluronic acid/gelatin hydrogel for hemorrhage control. *Materials Science and Engineering: C*. 2019;98:628-634. doi:10.1016/j.msec.2019.01.034

104. Shimony N, Shagan A, Eylon B, Nyska A, Gross A, Mizrahi B. Liquid Copolymers as Biodegradable Surgical Sealant. *Advanced Healthcare Materials*. 2021;10(19):2100803. doi:10.1002/adhm.202100803

105. Zhang Z, Wang X, Wang Y, Hao J. Rapid-Forming and Self-Healing Agarose-Based Hydrogels for Tissue Adhesives and Potential Wound Dressings. *Biomacromolecules*. 2018;19(3):980-988. doi:10.1021/acs.biomac.7b01764

106. Evans JA, van Wessem KJP, McDougall D, Lee KA, Lyons T, Balogh ZJ. Epidemiology of Traumatic Deaths: Comprehensive Population-Based Assessment. *World Journal of Surgery*. 2010;34(1):158-163. doi:10.1007/s00268-009-0266-1

107. Kelly JF, Ritenour AE, McLaughlin DF, Bagg KA, Apodaca AN, Mallak CT, Pearse L, Lawnick MM, Champion HR, Wade CE, Holcomb JB. Injury Severity and Causes of Death From Operation Iraqi Freedom and Operation Enduring Freedom: 2003–2004 Versus 2006. *Journal of Trauma: Injury, Infection & Critical Care*. 2008;64(2):S21-S27. doi:10.1097/TA.0b013e318160b9fb

108. Deuling J h. h., Vermeulen R p., Anthonio R a., van den Heuvel A f. m., Jaarsma T, Jessurun G, de Smet B j. g. l., Tan E s., Zijlstra F. Closure of the femoral artery after cardiac catheterization: A comparison of Angio-Seal, StarClose, and manual compression. *Catheterization and Cardiovascular Interventions*. 2008;71(4):518-523. doi:10.1002/ccd.21429

109. Fuller C. Reduction of intraoperative air leaks with Progel in pulmonary resection: a comprehensive review. *Journal of Cardiothoracic Surgery*. 2013;8(1):90. doi:10.1186/1749-8090-8-90

110. Behrens AM, Sikorski MJ, Li T, Wu ZJ, Griffith BP, Kofinas P. Blood-aggregating hydrogel particles for use as a hemostatic agent. *Acta Biomaterialia*. 2014;10(2):701-708. doi:10.1016/j.actbio.2013.10.029

111. Fathi P, Sikorski M, Christodoulides K, Langan K, Choi YS, Titcomb M, Ghodasara A, Wonodi O, Thaker H, Vural M, Behrens A, Kofinas P. Zeolite-loaded alginate-chitosan hydrogel beads as a topical hemostat: Zeolite-loaded alginate-chitosan hydrogel. *Journal of Biomedical Materials Research Part B: Applied Biomaterials*. 2018;106(5):1662-1671. doi:10.1002/jbm.b.33969

112. Xuan C, Hao L, Liu X, Zhu Y, Yang H, Ren Y, Wang L, Fujie T, Wu H, Chen Y, Shi X, Mao C. Wet-adhesive, haemostatic and antimicrobial bilayered composite nanosheets for sealing and healing soft-tissue bleeding wounds. *Biomaterials*. 2020;252:120018. doi:10.1016/j.biomaterials.2020.120018

113. Lan G, Lu B, Wang T, Wang L, Chen J, Yu K, Liu J, Dai F, Wu D. Chitosan/gelatin composite sponge is an absorbable surgical hemostatic agent. *Colloids and Surfaces B: Biointerfaces*. 2015;136:1026-1034. doi:10.1016/j.colsurfb.2015.10.039

114. Liu C, Liu X, Liu C, Wang N, Chen H, Yao W, Sun G, Song Q, Qiao W. A highly efficient, in situ wet-adhesive dextran derivative sponge for rapid hemostasis. *Biomaterials*. 2019;205:23-37. doi:10.1016/j.biomaterials.2019.03.016

115. Wang, Liu, Cherng, Lin, Chang, Hong, Liu, Chiu, Hsu, Chang. Biological Effects of Chitosan-Based Dressing on Hemostasis Mechanism. *Polymers*. 2019;11(11):1906. doi:10.3390/polym11111906

116. Ostomel TA, Shi Q, Stoimenov PK, Stucky GD. Metal Oxide Surface Charge Mediated Hemostasis. *Langmuir*. 2007;23(22):11233-11238. doi:10.1021/la701281t

117. Chan LW, Wang X, Wei H, Pozzo LD, White NJ, Pun SH. A synthetic fibrin cross-linking polymer for modulating clot properties and inducing hemostasis. *Science Translational Medicine*. 2015;7(277). doi:10.1126/scitranslmed.3010383

118. Hsu BB, Conway W, Tschabrunn CM, Mehta M, Perez-Cuevas MB, Zhang S, Hammond PT. Clotting Mimicry from Robust Hemostatic Bandages Based on Self-Assembling Peptides. *ACS Nano*. 2015;9(9):9394-9406. doi:10.1021/acsnano.5b02374

119. Hoque J, Prakash RG, Paramanandham K, Shome BR, Haldar J. Biocompatible Injectable Hydrogel with Potent Wound Healing and Antibacterial Properties. *Molecular Pharmaceutics*. 2017;14(4):1218-1230. doi:10.1021/acs.molpharmaceut.6b01104

120. Han L, Lu X, Liu K, Wang K, Fang L, Weng LT, Zhang H, Tang Y, Ren F, Zhao C, Sun G, Liang R, Li Z. Mussel-Inspired Adhesive and Tough Hydrogel Based on Nanoclay Confined Dopamine Polymerization. *ACS Nano*. 2017;11(3):2561-2574. doi:10.1021/acsnano.6b05318

121. Liu C, Yao W, Tian M, Wei J, Song Q, Qiao W. Mussel-inspired degradable antibacterial polydopamine/silica nanoparticle for rapid hemostasis. *Biomaterials*. 2018;179:83-95. doi:10.1016/j.biomaterials.2018.06.037

122. Dowling MB, Smith W, Balogh P, Duggan MJ, MacIntire IC, Harris E, Mesar T, Raghavan SR, King DR. Hydrophobically-modified chitosan foam: description and hemostatic efficacy. *Journal of Surgical Research*. 2015;193(1):316-323. doi:10.1016/j.jss.2014.06.019

123. Yan T, Cheng F, Wei X, Huang Y, He J. Biodegradable collagen sponge reinforced with chitosan/calcium pyrophosphate nanoflowers for rapid hemostasis. *Carbohydrate Polymers*. 2017;170:271-280. doi:10.1016/j.carbpol.2017.04.080

124. Chen S, Carlson MA, Zhang YS, Hu Y, Xie J. Fabrication of injectable and superelastic nanofiber rectangle matrices ("peanuts") and their potential applications in hemostasis. *Biomaterials*. 2018;179:46-59. doi:10.1016/j.biomaterials.2018.06.031

125. Yuan H, Chen L, Hong FF. A Biodegradable Antibacterial Nanocomposite Based on Oxidized Bacterial Nanocellulose for Rapid Hemostasis and Wound Healing. *ACS Applied Materials & Interfaces*. 2020;12(3):3382-3392. doi:10.1021/acsami.9b17732

126. Yu L, Shang X, Chen H, Xiao L, Zhu Y, Fan J. A tightly-bonded and flexible mesoporous zeolite-cotton hybrid hemostat. *Nature Communications*. 2019;10(1):1932. doi:10.1038/s41467-019-09849-9

127. Menzies D. Peritoneal adhesions. Incidence, cause, and prevention. *Surgery Annual*. 1992;24 Pt 1:27-45.

128. Menzies D. Postoperative adhesions: their treatment and relevance in clinical practice. *Annals of the Royal College of Surgeons of England*. 1993;75(3):147-153.

129. Moscowitz I, Wexner SD. Contributions of Adhesions to the Cost of Healthcare. In: diZerega GS, ed. *Peritoneal Surgery*. Springer New York; 2000:335-342. doi:10.1007/978-1-4612-1194-5_30

130. Menzies D, Ellis H. Intestinal obstruction from adhesions--how big is the problem? *Annals of The Royal College of Surgeons of England*. 1990;72(1):60-63.

131. On Behalf of the World Society of Emergency Surgery, Catena F, Ansaloni L, Di Saverio S, Pinna AD. P.O.P.A. Study: Prevention of Postoperative Abdominal Adhesions by Icodextrin 4% Solution After Laparotomy for Adhesive Small Bowel Obstruction. A Prospective Randomized Controlled Trial. *Journal of Gastrointestinal Surgery*. 2012;16(2):382-388. doi:10.1007/s11605-011-1736-y

132. Chen CH, Chen SH, Shalumon KT, Chen JP. Prevention of peritendinous adhesions with electrospun polyethylene glycol/polycaprolactone nanofibrous membranes. *Colloids and Surfaces B: Biointerfaces*. 2015;133:221-230. doi:10.1016/j.colsurfb.2015.06.012

133. Stapleton LM, Steele AN, Wang H, Lopez Hernandez H, Yu AC, Paulsen MJ, Smith AAA, Roth GA, Thakore AD, Lucian HJ, Totherow KP, Baker SW, Tada Y, Farry JM, Eskandari A, Hironaka CE, Jaatinen KJ, Williams KM, Bergamasco H, Marschel C, et al. Use of a supramolecular polymeric hydrogel as an effective post-operative pericardial adhesion barrier. *Nature Biomedical Engineering*. 2019;3(8):611-620. doi:10.1038/s41551-019-0442-z

134. Stapleton LM, Lucian HJ, Grosskopf AK, Smith AAA, Totherow KP, Woo YJ, Appel EA. Dynamic Hydrogels for Prevention of Post-Operative Peritoneal Adhesions. *Advanced Therapeutics*. 2021;4(3):2000242. doi:10.1002/adtp.202000242

135. Song L, Li L, He T, Wang N, Yang S, Yang X, Zeng Y, Zhang W, Yang L, Wu Q, Gong C. Peritoneal adhesion prevention with a biodegradable and injectable N,O-carboxymethyl chitosan-aldehyde hyaluronic acid hydrogel in a rat repeated-injury model. *Scientific Reports*. 2016;6(1):37600. doi:10.1038/srep37600

136. Li J, Xu W, Chen J, Li D, Zhang K, Liu T, Ding J, Chen X. Highly Bioadhesive Polymer Membrane Continuously Releases Cytostatic and Anti-Inflammatory Drugs for Peritoneal Adhesion Prevention. *ACS Biomaterials Science & Engineering*. 2018;4(6):2026-2036. doi:10.1021/acsbiomaterials.7b00605

137. Jiang S, Yan H, Fan D, Song J, Fan C. Multi-Layer Electrospun Membrane Mimicking Tendon Sheath for Prevention of Tendon Adhesions. *International Journal of Molecular Sciences*. 2015;16(12):6932-6944. doi:10.3390/ijms16046932

138. Leberfinger A, Hospodiuk M, Pena-Francesch A, Ayan B, Ozbolat V, Koduru S, Ozbolat I, Demirel MC, Ravnic D. Squid Ring Teeth-coated Mesh Improves Abdominal Wall Repair. *Plast Reconstr Surg Glob Open*. 2018;6:e1881. doi:10.1101/214114

139. Xia Q, Liu Z, Wang C, Zhang Z, Xu S, Han CC. A Biodegradable Trilayered Barrier Membrane Composed of Sponge and Electrospun Layers: Hemostasis and Antiadhesion. *Biomacromolecules*. 2015;16(9):3083-3092. doi:10.1021/acs.biomac.5b01099

140. Bang S, Lee E, Ko YG, Kim WI, Kwon OH. Injectable pullulan hydrogel for the prevention of postoperative tissue adhesion. *International Journal of Biological Macromolecules*. 2016;87:155-162. doi:10.1016/j.ijbiomac.2016.02.026

141. Cai X, Hu S, Yu B, Cai Y, Yang J, Li F, Zheng Y, Shi X. Transglutaminase-catalyzed preparation of crosslinked carboxymethyl chitosan/carboxymethyl cellulose/collagen composite membrane for postsurgical peritoneal adhesion prevention. *Carbohydrate Polymers*. 2018;201:201-210. doi:10.1016/j.carbpol.2018.08.065

142. Chen CH, Chen SH, Mao SH, Tsai MJ, Chou PY, Liao CH, Chen JP. Injectable thermosensitive hydrogel containing hyaluronic acid and chitosan as a barrier for prevention of postoperative peritoneal adhesion. *Carbohydrate Polymers*. 2017;173:721-731. doi:10.1016/j.carbpol.2017.06.019

143. Li Z, Liu L, Chen Y. Dual dynamically crosslinked thermosensitive hydrogel with self-fixing as a postoperative anti-adhesion barrier. *Acta Biomaterialia*. 2020;110:119-128. doi:10.1016/j.actbio.2020.04.034

144. Mayes SM, Davis J, Scott J, Aguilar V, Zawko SA, Swinnea S, Peterson DL, Hardy JG, Schmidt CE. Polysaccharide-based films for the prevention of unwanted postoperative adhesions at biological interfaces. *Acta Biomaterialia*. 2020;106:92-101. doi:10.1016/j.actbio.2020.02.027

145. Ruiz-Esparza GU, Wang X, Zhang X, Jimenez-Vazquez S, Diaz-Gomez L, Lavoie AM, Afewerki S, Fuentes-Baldemar AA, Parra-Saldivar R, Jiang N, Annabi N, Saleh B, Yetisen AK, Sheikhi A, Jozefiak TH, Shin SR, Dong N, Khademhosseini A. Nanoengineered Shear-Thinning Hydrogel Barrier for Preventing Postoperative Abdominal Adhesions. *Nano-Micro Letters*. 2021;13(1):212. doi:10.1007/s40820-021-00712-5

146. Sakai S, Ueda K, Taya M. Peritoneal adhesion prevention by a biodegradable hyaluronic acid-based hydrogel formed in situ through a cascade enzyme reaction initiated by contact with body fluid on tissue surfaces. *Acta Biomaterialia*. 2015;24:152-158. doi:10.1016/j.actbio.2015.06.023

147. Sultana T, Gwon JG, Lee BT. Thermal stimuli-responsive hyaluronic acid loaded cellulose based physical hydrogel for post-surgical de novo peritoneal adhesion prevention. *Materials Science and Engineering: C*. Published online January 2020:110661. doi:10.1016/j.msec.2020.110661

148. Sultana T, Van Hai H, Abueva C, Kang HJ, Lee SY, Lee BT. TEMPO oxidized nano-cellulose containing thermo-responsive injectable hydrogel for post-surgical peritoneal tissue adhesion prevention. *Materials Science and Engineering: C*. 2019;102:12-21. doi:10.1016/j.msec.2019.03.110

149. Yang Y, Liu X, Li Y, Wang Y, Bao C, Chen Y, Lin Q, Zhu L. A postoperative anti-adhesion barrier based on photoinduced imine-crosslinking hydrogel with tissue-adhesive ability. *Acta Biomaterialia*. 2017;62:199-209. doi:10.1016/j.actbio.2017.08.047

150. Yu J, Wang K, Fan C, Zhao X, Gao J, Jing W, Zhang X, Li J, Li Y, Yang J, Liu W. An Ultrasoft Self-Fused Supramolecular Polymer Hydrogel for Completely Preventing Postoperative Tissue Adhesion. *Advanced Materials*. 2021;33(16):2008395. doi:10.1002/adma.202008395

151. Zhang E, Li J, Zhou Y, Che P, Ren B, Qin Z, Ma L, Cui J, Sun H, Yao F. Biodegradable and injectable thermoreversible xyloglucan based hydrogel for prevention of postoperative adhesion. *Acta Biomaterialia*. 2017;55:420-433. doi:10.1016/j.actbio.2017.04.003

152. diZerega GS. Peritoneal repair and post-surgical adhesion formation. *Human Reproduction Update*. 2001;7(6):547-555. doi:10.1093/humupd/7.6.547

153. Widman TJ, Oostman H, Storrs FJ. Allergic Contact Dermatitis from Medical Adhesive Bandages in Patients Who Report Having a Reaction to Medical Bandages: *Dermatitis*. 2008;19(1):32-37. doi:10.2310/6620.2008.07053

154. Waring M, Bielfeldt S, Mätzold K, Wilhelm KP, Butcher M. An evaluation of the skin stripping of wound dressing adhesives. *Journal of Wound Care*. 2011;20(9):412, 414, 416-422. doi:10.12968/jowc.2011.20.9.412

155. Wiegand C, Abel M, Hipler UC, Elsner P. Effect of non-adhering dressings on promotion of fibroblast proliferation and wound healing in vitro. *Scientific Reports*. 2019;9(1):1-10. doi:10.1038/s41598-019-40921-y

156. Rippon M, White R, Davies P. Skin adhesives and their role in wound dressings. *Wounds UK*. 2007;3(4):76-86.

157. King A, Stellar JJ, Blevins A, Shah KN. Dressings and Products in Pediatric Wound Care. *Advances in Wound Care*. 2014;3(4):324-334. doi:10.1089/wound.2013.0477

158. Pukki T, Tikkanen M, Halonen S. Assessing Mepilex® Border in post-operative wound care. *Wounds UK*. 2010;6(1):30-40.

159. White R. Evidence for atraumatic soft silicone dressing use. *Wounds UK*. 2005;1(3):104-109.

160. Davies P, Rippon M. Evidence review: the clinical benefits of Safetac technology in wound care. *Journal of Wound Care*. 2008;17(Suppl 1):3-31.

161. Lantin A, Diegel C, Scheske J, Brönner A, Jodl H. Mepilex XT in practice: results of a study in German specialist wound care centres. *Clinical Practice*. 2016;7(2):4.

162. Lee BK, Ryu JH, Baek IB, Kim Y, Jang WI, Kim SH, Yoon YS, Kim SH, Hong SG, Byun S, Yu HY. Silicone-Based Adhesives with Highly Tunable Adhesion Force for Skin-Contact Applications. *Advanced Healthcare Materials*. 2017;6(22):1700621. doi:10.1002/adhm.201700621

163. Borde A, Larsson M, Odelberg Y, Hagman J, Löwenhielm P, Larsson A. Increased water transport in PDMS silicone films by addition of excipients. *Acta Biomaterialia*. 2012;8(2):579-588. doi:10.1016/j.actbio.2011.09.022

164. Mecham S, Sentman A, Sambasivam M. Amphiphilic silicone copolymers for pressure sensitive adhesive applications. *Journal of Applied Polymer Science*. 2010;116(6):3265-3270. doi:10.1002/app.31752

165. Deng W, Lei Y, Zhou S, Zhang A, Lin Y. Absorptive supramolecular elastomer wound dressing based on polydimethylsiloxane–(polyethylene glycol)–polydimethylsiloxane copolymer: preparation and characterization. *RSC Advances*. 2016;6(57):51694-51702. doi:10.1039/C6RA07146E

166. Nasiri M, Saxon DJ, Reineke TM. Enhanced Mechanical and Adhesion Properties in Sustainable Triblock Copolymers via Non-covalent Interactions. *Macromolecules*. 2018;51(7):2456-2465. doi:10.1021/acs.macromol.7b02248

167. Czech Z, Wilpiszewska K, Tyliszczak B, Jiang X, Bai Y, Shao L. Biodegradable self-adhesive tapes with starch carrier. *International Journal of Adhesion and Adhesives*. 2013;44:195-199. doi:10.1016/j.ijadhadh.2013.03.002

168. Sood A, Granick MS, Tomaselli NL. Wound Dressings and Comparative Effectiveness Data. *Advances in Wound Care*. 2014;3(8):511-529. doi:10.1089/wound.2012.0401

169. Narayanan A, Kaur S, Peng C, Debnath D, Mishra K, Liu Q, Dhinojwala A, Joy A. Viscosity Attunes the Adhesion of Bioinspired Low Modulus Polyester Adhesive Sealants to Wet Tissues. *Biomacromolecules*. 2019;20(7):2577-2586. doi:10.1021/acs.biomac.9b00383

170. Shagan A, Zhang W, Mehta M, Levi S, Kohane DS, Mizrahi B. Hot Glue Gun Releasing Biocompatible Tissue Adhesive. *Advanced Functional Materials*. 2019;30(18):1900998. doi:10.1002/adfm.201900998

171. Zhang W, Ji T, Lyon S, Mehta M, Zheng Y, Deng X, Liu A, Shagan A, Mizrahi B, Kohane DS. Functionalized Multiarmed Polycaprolactones as Biocompatible Tissue Adhesives. *ACS Applied Materials & Interfaces*. 2020;12(15):17314-17320. doi:10.1021/acsami.0c03478

172. Cohn D, Lando G. Tailoring lactide/caprolactone co-oligomers as tissue adhesives. *Biomaterials*. 2004;25(27):5875-5884. doi:10.1016/j.biomaterials.2004.01.040

173. Behrens AM, Casey BJ, Sikorski MJ, Wu KL, Tutak W, Sandler AD, Kofinas P. In Situ Deposition of PLGA Nanofibers via Solution Blow Spinning. *ACS Macro Letters*. 2014;3(3):249-254. doi:10.1021/mz500049x

174. F04 Committee. *Test Method for Wound Closure Strength of Tissue Adhesives and Sealants*. ASTM International doi:10.1520/F2458-05R15

175. Barnett A, Berkowitz RL, Mills R, Vistnes LM. Comparison of synthetic adhesive moisture vapor permeable and fine mesh gauze dressings for split-thickness skin graft donor sites. *American Journal of Surgery*. 1983;145(3):379-381.

176. Gurtner GC, Werner S, Barrandon Y, Longaker MT. Wound repair and regeneration. *Nature*. 2008;453:314-321. doi:10.1038/nature07039

177. Li J, Zhang YP, Kirsner RS. Angiogenesis in wound repair: Angiogenic growth factors and the extracellular matrix. *Microscopy Research and Technique*. 2003;60(1):107-114. doi:10.1002/jemt.10249

178. Wang W, Liu S, Chen B, Yan X, Li S, Ma X, Yu X. DNA-Inspired Adhesive Hydrogels Based on the Biodegradable Polyphosphoesters Tackified by a Nucleobase. *Biomacromolecules*. 2019;20(10):3672-3683. doi:10.1021/acs.biomac.9b00642

179. Kim HJ, Choi BH, Jun SH, Cha HJ. Sandcastle Worm-Inspired Blood-Resistant Bone Graft Binder Using a Sticky Mussel Protein for Augmented In Vivo Bone Regeneration. *Advanced Healthcare Materials*. 2016;5(24):3191-3202. doi:10.1002/adhm.201601169

180. Grand View Research. *Advanced Wound Dressing Market Size, Share & Trends Report, 2026*.; 2019. Accessed December 28, 2020. https://www.grandviewresearch.com/industry-analysis/advanced-wound-care-dressing-market

181. Grand View Research. *Medical Tapes and Bandages Market Size | Industry Report, 2018-2025*.; 2017. Accessed December 28, 2020. https://www.grandviewresearch.com/industry-analysis/medical-tapes-bandages-market

182. Tam I, Wang JX, De J. Identifying Acrylates in Medical Adhesives. *Dermatitis*. 2020;31(4):e40-e42. doi:10.1097/DER.0000000000000628

183. Spencer A, Gazzani P, Thompson DA. Acrylate and methacrylate contact allergy and allergic contact disease: a 13-year review. *Contact Dermatitis*. 2016;75(3):157-164. doi:https://doi.org/10.1111/cod.12647

184. Norris P, Storrs FJ. Allergic Contact Dermatitis to Adhesive Bandages. *Dermatologic Clinics*. 1990;8(1):147-152. doi:10.1016/S0733-8635(18)30540-0

185. Cheong YC, Laird SM, Li TC, Shelton JB, Ledger WL, Cooke ID. Peritoneal healing and adhesion formation/reformation. *Human Reproduction Update*. 2001;7(6):556-566. doi:10.1093/humupd/7.6.556

186. Monk BJ, Berman ML, Montz FJ. Adhesions after extensive gynecologic surgery: Clinical significance, etiology, and prevention. *American Journal of Obstetrics and Gynecology*. (5).

187. Kamel RM. Prevention of postoperative peritoneal adhesions. *European Journal of Obstetrics & Gynecology and Reproductive Biology*. 2010;150(2):111-118. doi:10.1016/j.ejogrb.2010.02.003

188. Arung W, Meurisse M, Detry O. Pathophysiology and prevention of postoperative peritoneal adhesions. *World Journal of Gastroenterology*. 2011;17(41). doi:10.3748/wjg.v17.i41.4545

189. Attard JAP, MacLean AR. Adhesive small bowel obstruction: epidemiology, biology and prevention. 50(4).

190. diZerega GS. Biochemical events in peritoneal tissue repair. *The European Journal of Surgery Supplement: = Acta Chirurgica Supplement*. 1997;(577):10-16.

191. Buţureanu SA, Buţureanu TAS. Pathophysiology of adhesions. *Chirurgia (Bucharest, Romania : 1990)*. 2014;109(3):293-298.

192. Ward BC, Panitch A. Abdominal Adhesions: Current and Novel Therapies. *Journal of Surgical Research*. 165(1):91-111. doi:10.1016/j.jss.2009.09.015

193. Gutt CN, Oniu T, Schemmer P, Mehrabi A, Büchler MW. Fewer adhesions induced by laparoscopic surgery? *Surgical Endoscopy*. 2004;18(6):898-906. doi:10.1007/s00464-003-9233-3

194. Vrijland WW, Jeekel J, van Geldorp HJ, Swank DJ, Bonjer HJ. Abdominal adhesions: intestinal obstruction, pain, and infertility. *Surgical Endoscopy And Other Interventional Techniques*. 2003;17(7):1017-1022. doi:10.1007/s00464-002-9208-9

195. Ray N. Abdominal Adhesiolysis: Inpatient Care and Expenditures in the United States in 1994. *Journal of the American College of Surgeons*. 1998;186(1):1-9. doi:10.1016/S1072-7515(97)00127-0

196. Sikirica V, Bapat B, Candrilli SD, Davis KL, Wilson M, Johns A. The inpatient burden of abdominal and gynecological adhesiolysis in the US. *BMC Surgery*. 2011;11(1):13. doi:10.1186/1471-2482-11-13

197. Ellis H. The clinical significance of adhesions: focus on intestinal obstruction. *The European Journal of Surgery Supplement: = Acta Chirurgica Supplement*. 1997;(577):5-9.

198. Diamond MP, Burns EL, Accomando B, Mian S, Holmdahl L. Seprafilm® adhesion barrier: (1) a review of preclinical, animal, and human investigational studies. *Gynecological Surgery*. 2012;9(3):237-245. doi:10.1007/s10397-012-0741-9

199. Diamond MP, Burns EL, Accomando B, Mian S, Holmdahl L. Seprafilm® adhesion barrier: (2) a review of the clinical literature on intraabdominal use. *Gynecological Surgery*. 2012;9(3):247-257. doi:10.1007/s10397-012-0742-8

200. Klingler PJ, Floch NR, Seelig MH, Branton SA, Wolfe JT, Metzger PP. Seprafilm®-induced peritoneal inflammation: A previously unknown complication: Report of a case. *Diseases of the Colon & Rectum*. 1999;42(12):1639-1642. doi:10.1007/BF02236221

201. Vrijland WW, Tseng LNL, Eijkman HJM, Hop WCJ, Jakimowicz JJ, Leguit P, Stassen LPS, Swank DJ, Haverlag R, Bonjer HJ, Jeekel H. Fewer Intraperitoneal Adhesions With Use of Hyaluronic Acid–Carboxymethylcellulose Membrane: A Randomized Clinical Trial. *Annals of Surgery*. 2002;235(2):193-199. doi:10.1097/00000658-200202000-00006

202. Mohri Y, Uchida K, Araki T, Inoue Y, Tonouchi H, Miki C, Kusunoki M. Hyaluronic Acid–Carboxycellulose Membrane (Seprafilm) Reduces Early Postoperative Small Bowel Obstruction in Gastrointestinal Surgery. *The American Surgeon*. 2005;71(10):861-863. doi:10.1177/000313480507101014

203. Beck DE, Cohen Z, Fleshman JW, Kaufman HS, van Goor H, Wolff BG. A Prospective, Randomized, Multicenter, Controlled Study of the Safety of Seprafilm® Adhesion Barrier in Abdominopelvic Surgery of the Intestine. *Diseases of the Colon & Rectum*. 2003;46(10):1310-1319. doi:10.1007/s10350-004-6739-2

204. Bachmann B, Spitz S, Schädl B, Teuschl AH, Redl H, Nürnberger S, Ertl P. Stiffness Matters: Fine-Tuned Hydrogel Elasticity Alters Chondrogenic Redifferentiation. *Frontiers in Bioengineering and Biotechnology*. 2020;8:373. doi:10.3389/fbioe.2020.00373

205. Prager J, Adams CF, Delaney AM, Chanoit G, Tarlton JF, Wong LF, Chari DM, Granger N. Stiffness-matched biomaterial implants for cell delivery: clinical, intraoperative ultrasound elastography provides a ‘target’ stiffness for hydrogel

synthesis in spinal cord injury. *Journal of Tissue Engineering*. 2020;11:204173142093480. doi:10.1177/2041731420934806

206. Huang G, Wang L, Wang S, Han Y, Wu J, Zhang Q, Xu F, Lu TJ. Engineering three-dimensional cell mechanical microenvironment with hydrogels. *Biofabrication*. 2012;4(4):042001. doi:10.1088/1758-5082/4/4/042001

207. Taboada GM, Yang K, Pereira MJN, Liu SS, Hu Y, Karp JM, Artzi N, Lee Y. Overcoming the translational barriers of tissue adhesives. *Nature Reviews Materials*. 2020;5(4):310-329. doi:10.1038/s41578-019-0171-7

208. Jesmer AH, Wylie RG. Controlling Experimental Parameters to Improve Characterization of Biomaterial Fouling. *Frontiers in Chemistry*. 2020;8:604236. doi:10.3389/fchem.2020.604236

209. Yu J. Biodegradation-based Polymer Surface Erosion and Surface Renewal for Foul-release at Low Ship Speeds. *Biofouling*. 2003;19(sup1):83-90. doi:10.1080/0892701031000063820

210. *Q3C Impurities: Guideline for Residual Solvents*. The International Council for Harmonisation of Technical Requirements for Pharmaceuticals for Human Use (ICH); 2021:1-7. Accessed April 19, 2022. https://database.ich.org/sites/default/files/ICH_Q3C-R8_Guideline_Step4_2021_0422_1.pdf

211. International Organization for Standardization. *ISO 10993-5:2009 Biological Evaluation of Medical Devices -- Part 5: Tests for in Vitro Cytotoxicity*. 3rd ed. International Organization for Standardization; 2009.

212. Mazuji MK. Prevention of Adhesions With Polyvinylpyrrolidone: Preliminary Report. *Archives of Surgery*. 1964;89(6):1011. doi:10.1001/archsurg.1964.01320060079015

213. Taylor MS, Daniels AU, Andriano KP, Heller J. Six bioabsorbable polymers:In vitro acute toxicity of accumulated degradation products. *Journal of Applied Biomaterials*. 1994;5(2):151-157. doi:10.1002/jab.770050208

214. Oncel M, Remzi FH, Connor J, Fazio VW. Comparison of cecal abrasion and multiple-abrasion models in generating intra-abdominal adhesions for animal studies. *Techniques in Coloproctology*. 2005;9(1):29-33. doi:10.1007/s10151-005-0189-2

215. Caetano GF, Fronza M, Leite MN, Gomes A, Frade MAC. Comparison of collagen content in skin wounds evaluated by biochemical assay and by computer-aided histomorphometric analysis. *Pharmaceutical Biology*. 2016;54(11):2555-2559. doi:10.3109/13880209.2016.1170861

216. Friedman S. Cytokines and Fibrogenesis. *Seminars in Liver Disease*. 1999;19(02):129-140. doi:10.1055/s-2007-1007105

217. Rodgers KE. Nonsteroidal anti-inflammatory drugs (NSAIDs) in the treatment of postsurgical adhesion. *Progress in Clinical and Biological Research*. 1990;358:119-129.

218. Mais V. Peritoneal adhesions after laparoscopic gastrointestinal surgery. *World Journal of Gastroenterology : WJG*. 2014;20(17):4917-4925. doi:10.3748/wjg.v20.i17.4917

219. Glucksman DL, Warren WD. The effect of topically applied corticosteroids in the prevention of peritoneal adhesions. An experimental approach with a review of the literature. *Surgery*. 1966;60(2):352-360.

220. On Behalf of the World Society of Emergency Surgery, Catena F, Ansaloni L, Di Saverio S, Pinna AD. P.O.P.A. Study: Prevention of Postoperative Abdominal Adhesions by Icodextrin 4% Solution After Laparotomy for Adhesive Small Bowel Obstruction. A Prospective Randomized Controlled Trial. *Journal of Gastrointestinal Surgery*. 2012;16(2):382-388. doi:10.1007/s11605-011-1736-y

221. Holtz G. Failure of a nonsteroidal anti-inflammatory agent (ibuprofen) to inhibit peritoneal adhesion reformation after lysis. *Fertility and Sterility*. 1982;37(4):582-583. doi:10.1016/S0015-0282(16)46171-6

222. Watson A, Vandekerckhove P, Lilford R. Liquid and fluid agents for preventing adhesions after surgery for subfertility. In: The Cochrane Collaboration, ed. *The Cochrane Database of Systematic Reviews*. John Wiley & Sons, Ltd; 2000:CD001298. doi:10.1002/14651858.CD001298

223. Metwally M, Watson A, Lilford R, Vanderkerchove P. Fluid and pharmacological agents for adhesion prevention after gynaecological surgery. In: The Cochrane Collaboration, ed. *Cochrane Database of Systematic Reviews*. John Wiley & Sons, Ltd; 2006:CD001298.pub3. doi:10.1002/14651858.CD001298.pub3

224. Li J, Mooney DJ. Designing hydrogels for controlled drug delivery. *Nature Reviews Materials*. 2016;1(12):16071. doi:10.1038/natrevmats.2016.71

225. Fenton OS, Olafson KN, Pillai PS, Mitchell MJ, Langer R. Advances in Biomaterials for Drug Delivery. *Advanced Materials*. 2018;30(29):1705328. doi:10.1002/adma.201705328

226. Kamaly N, Yameen B, Wu J, Farokhzad OC. Degradable Controlled-Release Polymers and Polymeric Nanoparticles: Mechanisms of Controlling Drug Release. *Chemical Reviews*. 2016;116(4):2602-2663. doi:10.1021/acs.chemrev.5b00346

227. Lynch JR, Tang W, Wang H, Vitek MP, Bennett ER, Sullivan PM, Warner DS, Laskowitz DT. APOE Genotype and an ApoE-mimetic Peptide Modify the Systemic and Central Nervous System Inflammatory Response. *Journal of Biological Chemistry*. 2003;278(49):48529-48533. doi:10.1074/jbc.M306923200

228. Li FQ, Sempowski GD, McKenna SE, Laskowitz DT, Colton CA, Vitek MP. Apolipoprotein E-Derived Peptides Ameliorate Clinical Disability and Inflammatory Infiltrates into the Spinal Cord in a Murine Model of Multiple Sclerosis. *Journal of Pharmacology and Experimental Therapeutics*. 2006;318(3):956-965. doi:10.1124/jpet.106.103671

229. Pane K, Sgambati V, Zanfardino A, Smaldone G, Cafaro V, Angrisano T, Pedone E, Gaetano SD, Capasso D, Haney EF, Izzo V, Varcamonti M, Notomista E, Hancock REW, Donato AD, Pizzo E. A new cryptic cationic antimicrobial peptide from human apolipoprotein E with antibacterial activity and immunomodulatory effects on human cells. *The FEBS Journal*. 2016;283(11):2115-2131. doi:10.1111/febs.13725

230. Tenger C, Zhou X. Apolipoprotein E modulates immune activation by acting on the antigen-presenting cell. *Immunology*. 2003;109:392-297. doi:https://doi.org/10.1046/j.1365-2567.2003.01665.x

231. Osei-Hwedieh DO, Amar M, Sviridov D, Remaley AT. Apolipoprotein mimetic peptides: Mechanisms of action as anti-atherogenic agents. *Pharmacology & Therapeutics*. 2011;130(1):83-91. doi:10.1016/j.pharmthera.2010.12.003

232. Ali K, Middleton M, Puré E, Rader DJ. Apolipoprotein E Suppresses the Type I Inflammatory Response In Vivo. *Circulation Research*. 2005;97(9):922-927. doi:10.1161/01.RES.0000187467.67684.43

233. Azevedo OGR, Oliveira RAC, Oliveira BC, Zaja-Milatovic S, Araújo CV, Wong DVT, Costa TB, Lucena HBM, Lima-Júnior RCP, Ribeiro RA, Warren CA, Lima AÂM, Vitek MP, Guerrant RL, Oriá RB. Apolipoprotein E COG 133 mimetic peptide improves 5-fluorouracil-induced intestinal mucositis. *BMC Gastroenterology*. 2012;12(1):35. doi:10.1186/1471-230X-12-35

234. Sandler AD, Wu X, Srinivasan P, Basu M. Whole cell tumor vaccines and methods of use therof. 2022;(PCTUS2020015583).

235. Rose-John S, Winthrop K, Calabrese L. The role of IL-6 in host defence against infections: immunobiology and clinical implications. *Nature Reviews Rheumatology*. 2017;13(7):399-409. doi:10.1038/nrrheum.2017.83

236. Popko K, Gorska E, Stelmaszczyk-Emmel A, Plywaczewski R, Stoklosa A, Gorecka D, Pyrzak B, Demkow U. Proinflammatory cytokines IL-6 and TNF-α and the development of inflammation in obese subjects. *European Journal of Medical Research*. 2010;15(S2):120. doi:10.1186/2047-783X-15-S2-120

237. Toseland CP. Fluorescent labeling and modification of proteins. *Journal of Chemical Biology*. 2013;6(3):85-95. doi:10.1007/s12154-013-0094-5

238. Atalla A, Coley M, Hamers M, Karodeh N, McGrath J, Minahan E, Nagler M, Nassar Y, Nichols A, Sebastian R, Tiberino M, Wendeu-Foyet K. *Localizing Chemotherapeutic Drug Release Through the Use of Polymer-Based Surgical Sealants to Treat Stage III Colorectal Cancer*. Thesis. 2021. doi:10.13016/uzv7-rcm7

239. Vokes EE. Combined modality therapy of solid tumours. *The Lancet*. 1997;349:S4-S6. doi:10.1016/S0140-6736(97)90011-8

240. Pearce A, Haas M, Viney R, Pearson SA, Haywood P, Brown C, Ward R. Incidence and severity of self-reported chemotherapy side effects in routine care: A prospective cohort study. Ganti AK, ed. *PLOS ONE*. 2017;12(10):e0184360. doi:10.1371/journal.pone.0184360

241. Jones CD, Guiot L, Samy M, Gorman M, Tehrani H. The use of chemotherapeutics for the treatment of keloid scars. *Dermatology Reports*. 2015;7(2). doi:10.4081/dr.2015.5880

242. Bulstrode NW, Mudera V, McGrouther DA, Grobbelaar AO, Cambrey AD. 5-Fluorouracil Selectively Inhibits Collagen Synthesis: *Plastic and Reconstructive Surgery*. 2005;116(1):209-221. doi:10.1097/01.PRS.0000169701.16509.D6

243. Srinubabu G, Rao DP, Sridhar L, Rao JVLNS. Spectrophotometric Method for the Determination of Oxaliplatin in Pure and Dosage Forms. *E-Journal of Chemistry*. 2006;3(1):25-27. doi:10.1155/2006/375721

244. Mortell A, Montedonico S, Puri P. Animal models in pediatric surgery. *Pediatric Surgery International*. 2006;22(2):111-128. doi:10.1007/s00383-005-1593-4

245. Ferland R, Mulani D, Campbell PK. Evaluation of a sprayable polyethylene glycol adhesion barrier in a porcine efficacy model. *Human Reproduction*. 2001;16(12):2718-2723. doi:10.1093/humrep/16.12.2718